

Deliverable 3.4

Case studies for the application of digital-twin

Drafted by: Emil Navntoft Pedersen

Date: 29/10/2026

Grant agreement No: 101069672

Project start date: 1st September 2022

Duration: 54 months

Funded by the European Union

Views and opinions expressed are however those of the author(s) only and do not necessarily reflect those of the European Union or CINEA. Neither the European Union nor the granting authority can be held responsible for them.

BASIC INFORMATION ON THE DELIVERABLE	
DISSEMINATION LEVEL	Public
DUE DATE OF DELIVERABLE	31/12/2025
ACTUAL SUBMISSION DATE	29/10/2026
WORK PACKAGE	WP3 – Advanced technical developments
TASK	T3.4 – Digital-twin based set point optimization for applications with variable loads and off-design operation
TYPE	Report
NUMBER OF PAGES	85

Funded by the European Union

Views and opinions expressed are however those of the author(s) only and do not necessarily reflect those of the European Union or CINEA. Neither the European Union nor the granting authority can be held responsible for them.

Report of Contributors				
	Name	**Org**	**Role/ Title**	**E-mail**
Report leader	Emil Navntoft Pedersen	DTI	Senior Consultant	enp@teknologisk.dk
Contributing Author(s)	Wouter de Vries	TNO	Medior Scientist Integrator	wouter.devries@tno.nl
	Jens Gollasch	DLR	Engineer	jens.gollasch@dlr.de
Reviewer(s)	Jonas L. Poulsen	DTI	Team Manager	jlp@teknologisk.dk
Final review and quality approval	Simon Spoelstra	TNO	Project coordinator	simon.spoelstra@tno.nl

Date	Version	Description
01/06/2026	0.1	**First draft**
29/10/2026	**1.0**	**Final version**

Funded by the European Union

Views and opinions expressed are however those of the author(s) only and do not necessarily reflect those of the European Union or CINEA. Neither the European Union nor the granting authority can be held responsible for them.

DISCLAIMER OF WARRANTIES

This project has received funding from the European Union's Horizon Europe research and innovation programme under grant agreement No. 101069672 (SPIRIT).

This document has been prepared by SPIRIT project partners as an account of work carried out within the framework of the EC-GA contract no. 101069672.

Neither Project Coordinator, nor any signatory party of SPIRIT Project Consortium Agreement, nor any person acting on behalf of any of them:

(a) makes any warranty or representation whatsoever, expressed or implied,

(i). with respect to the use of any information, apparatus, method, process, or similar item disclosed in this document, including merchantability and fitness for a particular purpose, or

(ii). that such use does not infringe on or interfere with privately owned rights, including any party's intellectual property, or

(iii). that this document is suitable to any particular user's circumstance, or

(b) assumes responsibility for any damages or other liability whatsoever (including any consequential damages, even if the Project Coordinator or any representative of a signatory party of the SPIRIT Project Consortium Agreement has been informed of the possibility of such damages) resulting from your selection or use of this document or any information, apparatus, method, process, or similar item disclosed in this document.

Funded by the European Union

Views and opinions expressed are however those of the author(s) only and do not necessarily reflect those of the European Union or CINEA. Neither the European Union nor the granting authority can be held responsible for them.

PROJECT PARTNERS

TNO: NEDERLANDSE ORGANISATIE VOOR TOEGEPAST NATUURWETENSCHAPPELIJK ONDER-ZOEK

DTI: TEKNOLOGISK INSTITUT

DLR: DEUTSCHES ZENTRUM FUR LUFT - UND RAUMFAHRT EV

EHPA: EUROPEAN HEAT PUMP ASSOCIATION

MYK: NV MAYEKAWA EUROPE SA

SINLOC: SINLOC-SISTEMA INIZIATIVE LOCALI SPA

EURAC: ACCADEMIA EUROPEA DI BOLZANO

EHP: EUROHEAT & POWER

DTU: DANMARKS TEKNISKE UNIVERSITET

TVP: TVP Solar

TIS: TIENSE SUIKERRAFFINADERIJ N.V.

TLK: TLK ENERGY GMBH

GEA: GEA Refrigeration Germany GmbH

SPIL: Spilling Project Partner GmbH & Co. KG

SKPS: SMURFIT WESTROCK PAPER SERVICES B.V.

SKC: SMURFIT WESTROCK CZECH SRO

SP: STELLA POLARIS AS

Funded by the European Union

Views and opinions expressed are however those of the author(s) only and do not necessarily reflect those of the European Union or CINEA. Neither the European Union nor the granting authority can be held responsible for them.

TABLE OF CONTENTS

1. Introduction 7

2. Case 1 – Mayekawa & TNO 9

2.1 Case description: Laminate production 11
2.2 Process data: Variable load description 14
2.3 Heat pump integration 17
2.4 Methodology 19
2.5 Results 25
2.6 Discussion 45
2.7 Conclusion 47

3. Case 2 – GEA & DTI 49

3.1 Case description 49
3.2 Heat pump integration 50
3.3 Methodology and goals 52
3.4 Results 53
3.5 Discussion 63
3.6 Conclusion 65

4. Case 3 – Spilling & DLR 67

4.1 Case description 67
4.2 Variable load description 68
4.3 Heat pump integration 71
4.4 Methodology and goals 72
4.5 Results 74
4.6 Discussion 79
4.7 Conclusion 81

5. Conclusion 82

6. References 85

Funded by the European Union

Views and opinions expressed are however those of the author(s) only and do not necessarily reflect those of the European Union or CINEA. Neither the European Union nor the granting authority can be held responsible for them.

1. INTRODUCTION

Industrial process heat accounts for a significant share of final energy demand in Europe and is still largely supplied by fossil fuels. Electrification of process heat through industrial heat pumps is therefore an important pathway for reducing greenhouse gas emissions, improving energy efficiency, and supporting the transition towards climate-neutral industrial production. High-temperature heat pumps are particularly relevant for industrial sectors where useful heat is required above conventional temperature levels and where waste heat streams are available but cannot be used directly without temperature upgrading.

Within the SPIRIT project, several sustainable heat upgrade technologies are demonstrated and evaluated for industrial applications. Work Package 3 focuses on advanced technical developments that support the integration, operation, and optimization of these technologies. Task 3.4 specifically addresses **digital-twin based set-point optimization**, with the aim of investigating how dynamic simulation models can be used to improve the operation of industrial heat pump systems under variable load conditions.

The operation of industrial heat pumps is strongly influenced by the temperature and load profiles of both the heat source and the heat sink. In many industrial processes, these profiles are not constant. Batch production, start-up and shut-down events, changing ambient conditions, fluctuating waste heat availability, and variable energy prices can all affect the optimal operating strategy. In such cases, fixed control set-points may lead to reduced efficiency, limited heat recovery, unnecessary auxiliary energy use, or suboptimal use of thermal storage. Dynamic digital twins provide a way to analyse these interactions in detail by representing the transient behaviour of the heat pump, auxiliary equipment, storage systems, and industrial process.

The objective of this deliverable is to demonstrate how digital twins can support the identification and optimization of relevant control setpoints for different industrial heat pump integration concepts. The focus is not only on the heat pump itself, but also on the surrounding system, including thermal storage, bypass valves, pumps, auxiliary heating systems, and process-side constraints. By evaluating the complete system dynamically, the work aims to quantify the potential performance improvements that can be achieved through improved control strategies.

Three case studies are investigated in this report:

Funded by the European Union

Views and opinions expressed are however those of the author(s) only and do not necessarily reflect those of the European Union or CINEA. Neither the European Union nor the granting authority can be held responsible for them.

- **Case 1 – Mayekawa & TNO:** A cascade high-temperature heat pump originally designed for the Stella Polaris shrimp cooking and freezing process is integrated into an alternative variable-load process for high-pressure laminate production. The analysis focuses on the interaction between the cascade heat pump and hot and cold stratified buffer tanks, and on optimizing the ammonia evaporator and condenser operating conditions.

- **Case 2 – GEA & DTI:** A heat pump is integrated with an autoclave process used for sterilization of beverages. The autoclave has a cyclic heat demand, while useful source heat becomes available later during the cooling phase. The study investigates the effect of steam accumulator sizing and pressure, evaporator source-water temperature glide, and cooling-water return bypass control.

- **Case 3 – Spilling & DLR:** A mechanical vapour recompression system for steam generation in paper drying is combined with solar thermal direct steam generation, thermal storage, and an auxiliary heat pump. The study uses black-box optimization of a dynamic model to investigate price-adaptive storage operation and the influence of flash pressure setpoints.

The three cases differ in technology, temperature level, system layout, and optimization approach. Together, they provide a broad assessment of how digital-twin based methods can be applied to industrial heat pump systems with variable operating conditions. In the first two cases, parameter sweeps are used to evaluate the influence of selected control setpoints. In the third case, the dynamic model is exported as a Functional Mock-up Unit and optimized in Python using black-box optimization methods.

Funded by the European Union

Views and opinions expressed are however those of the author(s) only and do not necessarily reflect those of the European Union or CINEA. Neither the European Union nor the granting authority can be held responsible for them.

2. CASE 1 – MAYEKAWA & TNO

SPIRIT demo 1 involves the demonstration of Mayekawa's HTHP into Stella Polaris' shrimp cooking and freezing process. This demonstration incorporates an industrial heat pump which upgrades the heat rejected from the shrimp freezing plant (~18 °C) to produce steam (~145 °C) for the cooking process. The heat produced by the heat pump covers the full demand of the process under nominal operating conditions (~700 kWth), thereby electrifying the process. Due to the large temperature lift (> 130 K), a cascaded high temperature heat pump was selected, consisting of an ammonia (bottom) cycle and a pentane (top) cycle. The two cycles, illustrated in Figure 2.1, are connected via a heat exchanger, specifically the condenser and evaporator of the ammonia and pentane cycle, respectively. The bottom cycle takes waste heat from the freezing plant while the top cycle produces the steam needed for the shrimp cooker.

The main components of the cascade heat pump were selected for the operational characteristics of the shrimp cooking process of Stella Polaris. The displacement or swept volume of the ammonia compressor is 228 m^3/h at 1450 RPM. For the pentane compressor this is 1600 m^3/h at 3000 RPM. All 3 heat exchangers (ammonia evaporator, ammonia condenser / pentane evaporator and pentane condenser / steam generator) are of the shell & plate type. As mentioned, no intermediate water circuit is present between the ammonia and pentane heat pumps, instead the cycles interface directly within a single heat exchanger. The goal of this section of the report is to investigate the potential integration of the cascade heat pump from SPIRIT Demo 1 into an alternative, more dynamic, process with variable load.

Funded by the European Union

Views and opinions expressed are however those of the author(s) only and do not necessarily reflect those of the European Union or CINEA. Neither the European Union nor the granting authority can be held responsible for them.

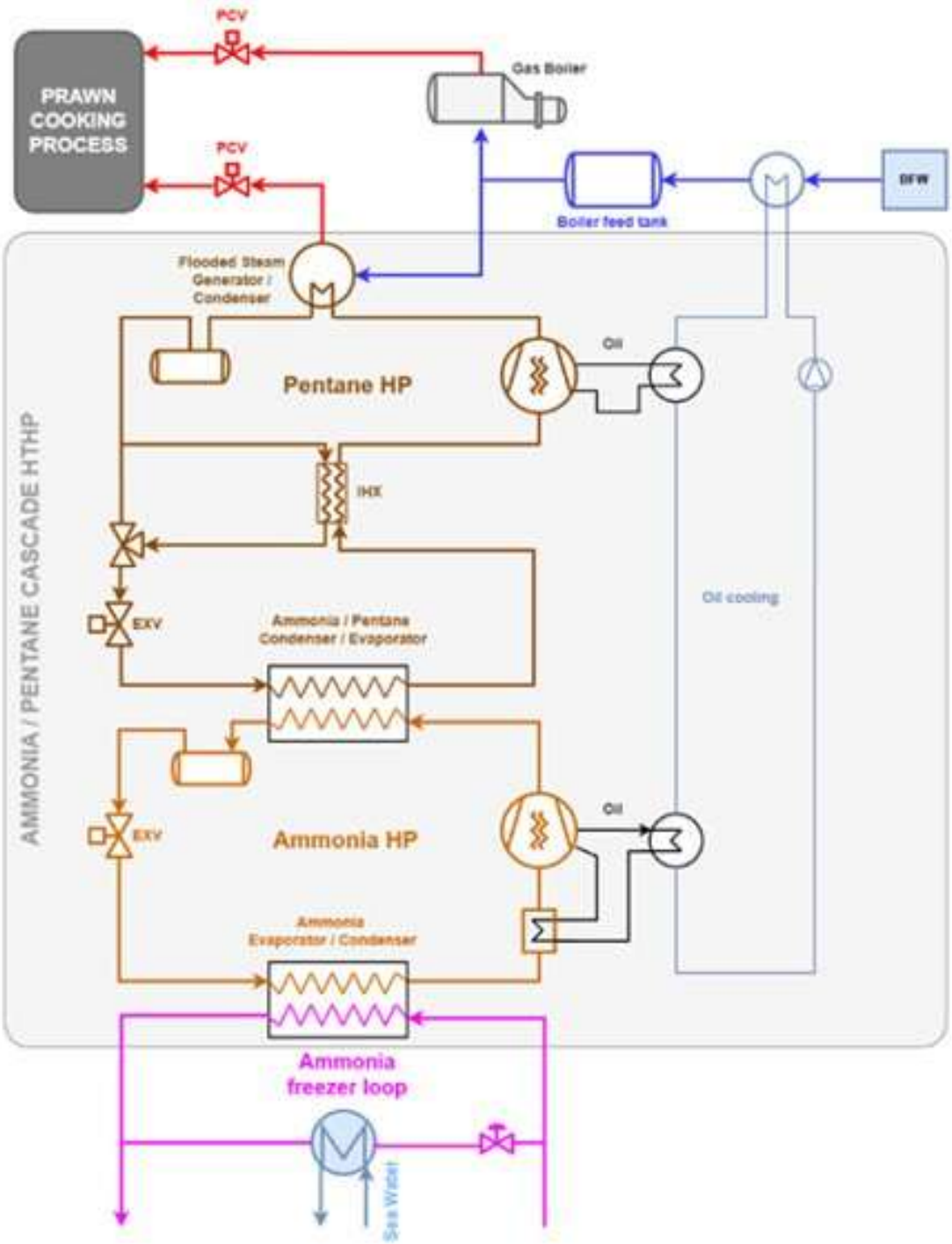


Figure 2.1: Overview of the cascade heat pump of demo 1 integrated at the shrimp cooking process of Stella Polaris.

Funded by the European Union

Views and opinions expressed are however those of the author(s) only and do not necessarily reflect those of the European Union or CINEA. Neither the European Union nor the granting authority can be held responsible for them.

2.1 Case description: Laminate production

The alternative case selected for the cascade heat pump consists of a high pressure laminate production process, located at Trespa, the Netherlands. An example application is shown in Figure 2.2. The process involves curing the resin that binds the laminate. During this process, the laminate is pressed in a mold to get a flat end-product with a good surface quality. On a high level, the process involves 3 steps: (1) heating the mold and laminate up to a certain temperature level where the resin starts to cure, (2) maintaining this temperature for a certain period of time (which could involve both heating and cooling, since the resin cures exothermally), and (3) actively cooling the mold and laminate when the curing is finished. Afterwards, the finalized products are removed from the mold, which is reused for the next production batch. For all 3 steps, pressurized water is used as a heat transfer medium. Pumps supply hot or cold water depending on the process step. The hot water comes from a steam heated storage tank at high temperature, whereas the cooling water is supplied by an ambient cooling system.

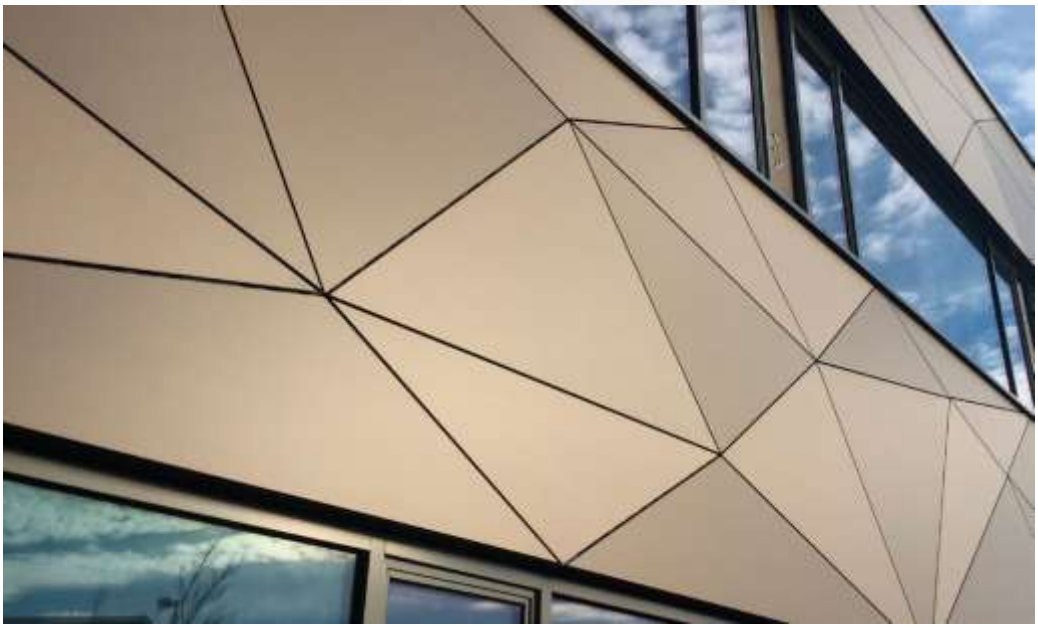


Figure 2.2: Example of the Trespa high pressure laminates used as façade panels (Trespa, 2023).

The aim of the heat pump integration is to reduce the amount of steam required for maintaining the temperature within the steam heated storage tank. Although the temperature of the tank itself is out of reach for the cascade heat pump, the water

Funded by the European Union

Views and opinions expressed are however those of the author(s) only and do not necessarily reflect those of the European Union or CINEA. Neither the European Union nor the granting authority can be held responsible for them.

returning to this tank from the press section is of lower temperature. Replacing this water flow with water of higher temperature, heated by the heat pump, still result in significant energy savings. The cascade heat pump is not expected to have enough capacity to supply the full amount of heat required by laminate production process.

2.1.1 Hot water production, heat sink integration

The return flow from the press is intermittent and varies significantly in temperature and flowrate during a batch. For this reason, an additional hot water storage tank is included for the heat pump integration. Figure 2.3 depicts a schematic overview of the integration on the heat sink side of the cascade heat pump. The tank is fully filled with water, so the volume flowrate entering the scheme, is the same as the volume flowrate leaving the scheme. A 3-way valve is used to regulate the distribution between water that is directly returned to the steam heated storage tank and the water replaced by the hot storage tank.

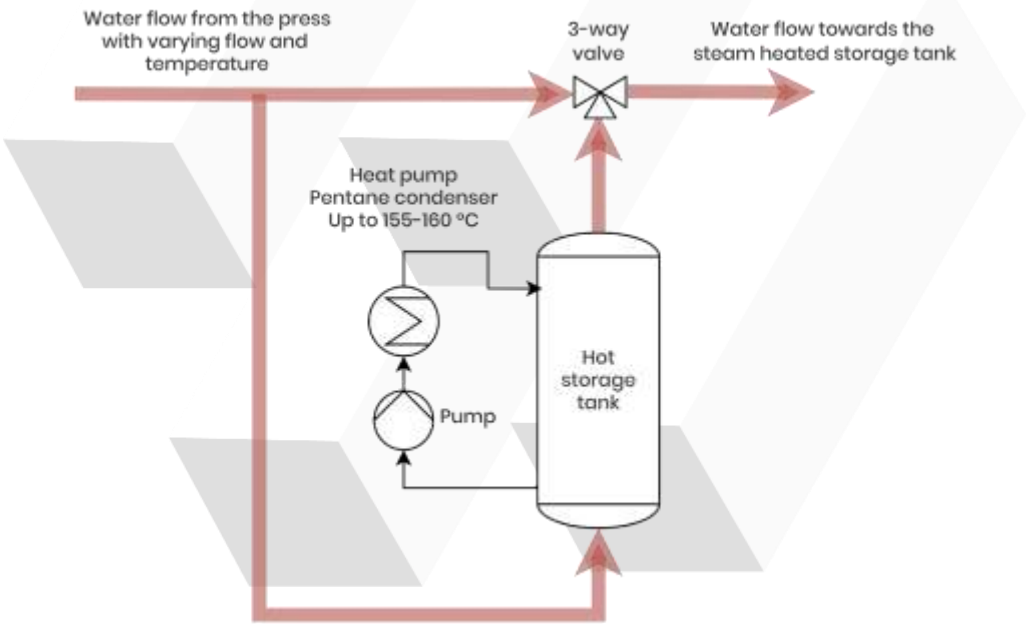


Figure 2.3: Integration scheme on the heat sink side of the cascade heat pump. The indicated temperature at the pentane condenser is the water temperature.

The hot storage tank is designed in such a way that stratification occurs: the hottest water will migrate to the top and the colder water will remain in the bottom. The pentane condenser is fed by cold water from the bottom and the heated water is added to the top of the tank.

Funded by the European Union

Views and opinions expressed are however those of the author(s) only and do not necessarily reflect those of the European Union or CINEA. Neither the European Union nor the granting authority can be held responsible for them.

2.1.2 Waste heat recovery, heat source integration

A similar integration scheme is present on the source or waste heat side of the cascade heat pump, as shown in Figure 2.4. Cooling water coming from the press section can either be added to the cold storage tank or be directly send to the atmospherically cooled storage tank. The distribution is regulated by a 3-way valve. Like the hot storage tank, the tank is assumed to be stratified with the hotter water in the top and cold water in the bottom. The flow from the press is added to the top such that the coldest water is displaced from the tank in a downwards direction, and pushed towards the existing cooling infrastructure. The ammonia heat pump evaporator is fed by the water located in the top of the cold storage tank and reinserted in the bottom by a pump. This assures that the hottest water is used as waste heat, maximizing the potential cascade heat pump efficiency. The heat stored in the tank is effectively waste heat and cannot be used directly within the production process.

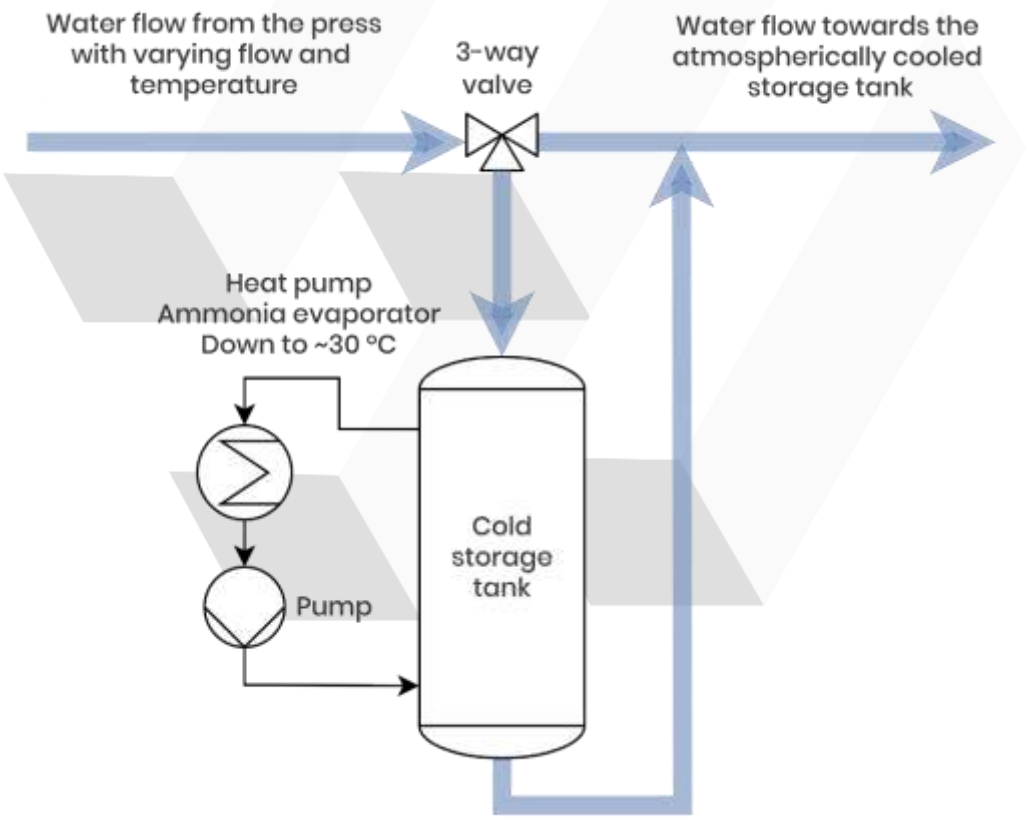


Figure 2.4 Integration scheme on the heat source side of the cascade heat pump. The indicated temperature at the ammonia evaporator, is the water temperature.

Funded by the European Union

Views and opinions expressed are however those of the author(s) only and do not necessarily reflect those of the European Union or CINEA. Neither the European Union nor the granting authority can be held responsible for them.

2.2 Process data: Variable load description

Within this section, we present the data from the laminate production process used for the heat pump integration. Figure 2.5 displays the hot and cold water flow for 3 different production batches of high pressure laminates. At the beginning of the dataset, the hot flow starts, rises and ends after 15 minutes. The cold flow starts 5 minutes after the hot flow ends and lasts for 5 minutes. The wait time until the next batch (after the cold flow ends) is 20 minutes. A full batch has a duration of 45 minutes.

The 135 minutes of available data has been slightly modified such that it can be repeated indefinitely. We selected the down time after the last cold flow such that it matches the time between the other two batches.

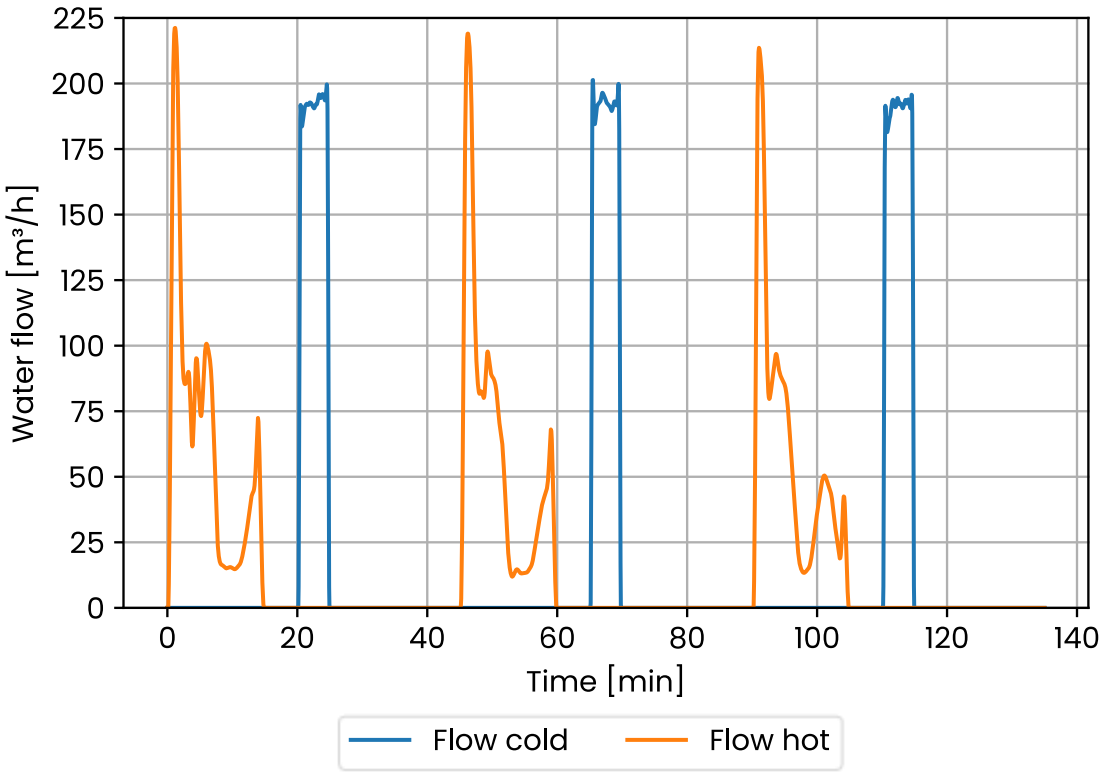


Figure 2.5: Hot and cold water flow rate

Funded by the European Union

Views and opinions expressed are however those of the author(s) only and do not necessarily reflect those of the European Union or CINEA. Neither the European Union nor the granting authority can be held responsible for them.

Figure 2.6 plots the temperature and volumetric flow rate of the hot flow. The flow rate is overlaid to indicate when the sensor measures the water flow temperature, instead of water that is standing still in the pipe. When the flow starts, the temperature dips from 140-150 °C to about 100 °C at the beginning of a batch and then quickly recovers to about 120 °C. Minor differences are visible between the batches, although the general trend is the comparable. From 105 minutes, the temperature has been modified to a linearly increasing trend to match the starting temperature of the available data. This will have no effect on the heat pump performance, since no water flow occurs during this period.

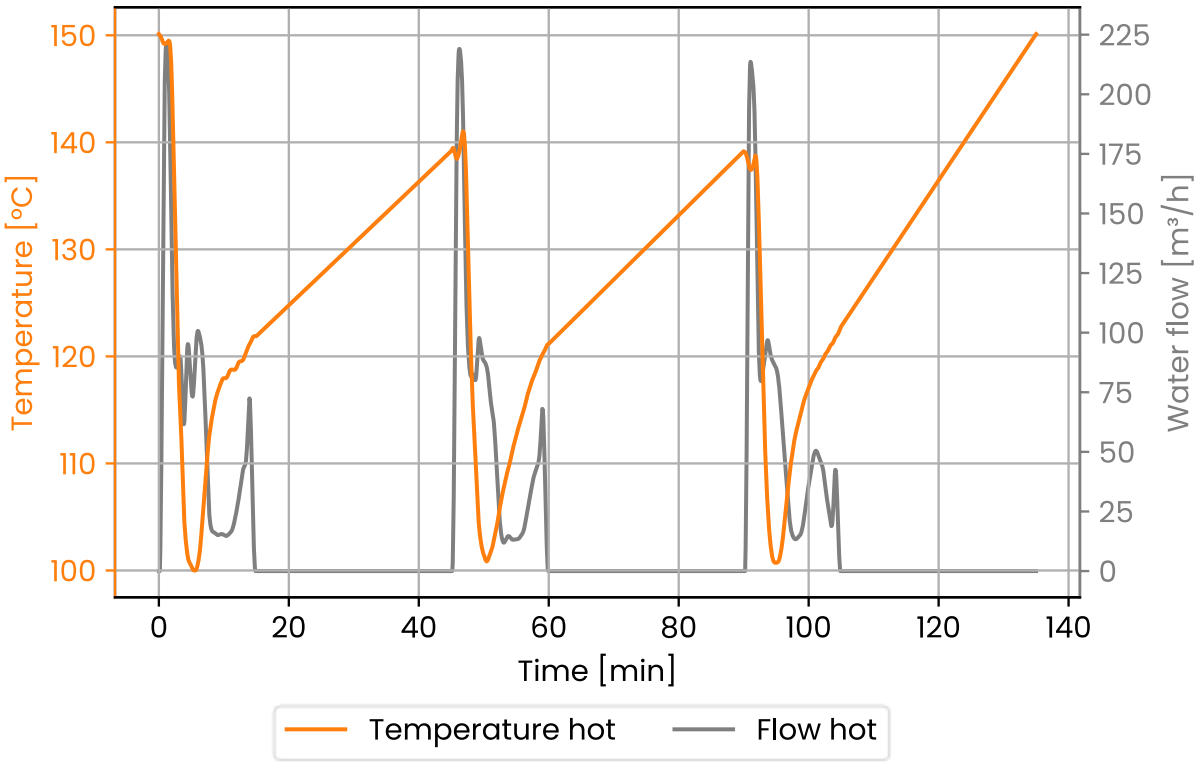


Figure 2.6: Hot temperature in red with the hot water flow overlaid in gray for reference.

Funded by the European Union

Views and opinions expressed are however those of the author(s) only and do not necessarily reflect those of the European Union or CINEA. Neither the European Union nor the granting authority can be held responsible for them.

Figure 2.7 below shows the temperature of the cold flow with the water volumetric flow rate overlaid. Starting from 30-35 °C, the temperature quickly rises to 75-80 °C when the flow starts. For the first and last batch, the temperature displays a peak followed by a downward trend while the flow is still active. For the second batch, the peak coincides with the end of the flow. The temperature profile in the first 20 minutes has been altered such that the temperature at 0 minutes matches the temperature of the final timestamp.

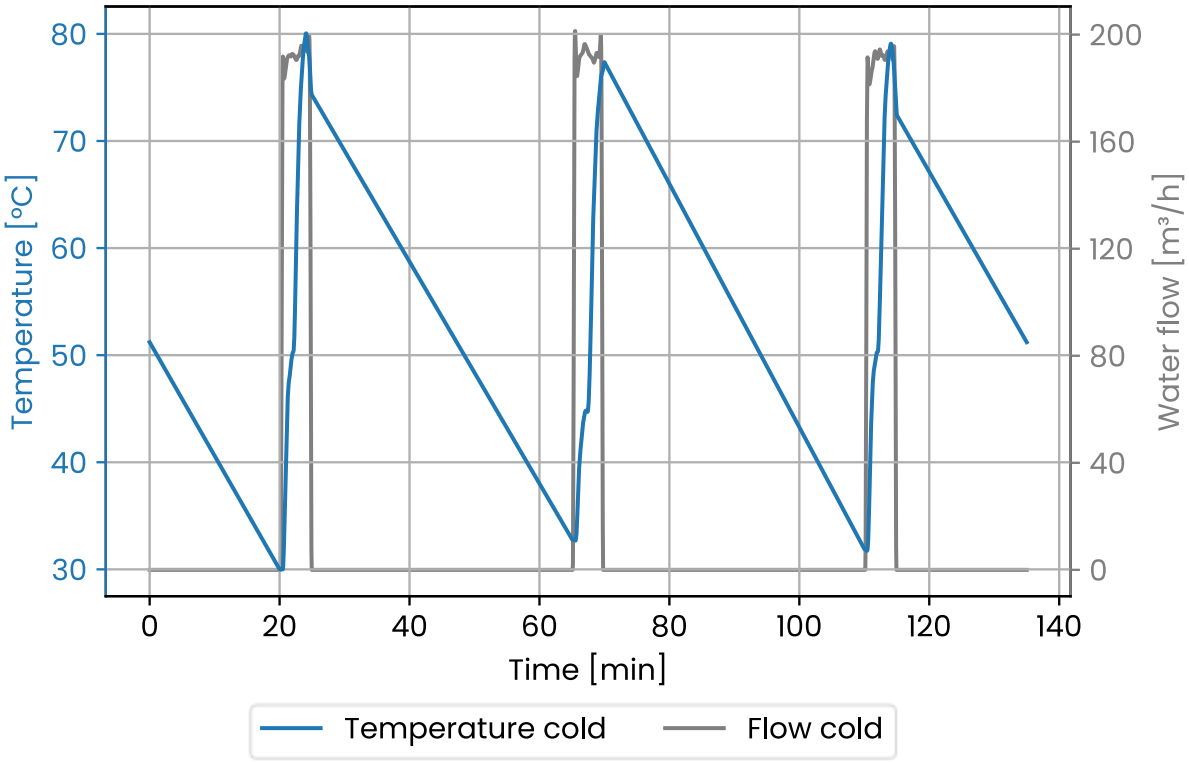


Figure 2.7: Cold temperature in blue with the cold water flow overlaid in gray for reference.

Funded by the European Union

Views and opinions expressed are however those of the author(s) only and do not necessarily reflect those of the European Union or CINEA. Neither the European Union nor the granting authority can be held responsible for them.

2.3 Heat pump integration

For the present analysis we want to keep the modifications of the SPIRIT demo 1 cascade heat pump to a minimum. The sizing of the heat pump, mainly determined by the compressor size, is therefore left unchanged. The identified variable load case has not explicitly been selected as good match with the condenser duty of the heat pump.

The main changes are in the media types on the sink and source side of the heat pump. Instead of condensing ammonia from the shrimp freezing plant, the waste heat now consists of pressurized water. The geometry of the plate & shell heat exchanger is left unmodified, and within the digital twin simulation model, only the media model is changed from ammonia to liquid water. The water is located in between the plates and the ammonia is evaporated from the shell. The heat transfer correlation is not adjusted, even though the mechanism changes from de-superheating and condensation (sensible and latent heat) to purely sensible heat transfer; the liquid water does not undergo any phase change. This yields an overprediction of the heat transfer coefficient, although this effect is considered to be of negligible interest.

The intended purpose of the cascade heat pump is to produce low pressure steam for the shrimp cooking process at Stella Polaris. Within the plate & shell exchanger, pentane condenses between the plates and steam forms on the shell side. This type of heat exchanger is considered to be unsuitable for the integration of the current analysis, where hot water is produced instead of steam. For this reason, an alternative brazed plate heat exchanger (BPHE, also known as a plate/plate heat exchanger) is selected from the manufacturer SWEP using the SSP G8 software (SWEP International AB, 2025). The pentane-side conditions were kept constant as for the original plate & shell heat exchanger, and are shown in Figure 2.8. The water temperature is set 140 °C inlet and 145 °C outlet, which assumes a 5 K approach temperature since there is no subcooling on the pentane side.

Funded by the European Union

Views and opinions expressed are however those of the author(s) only and do not necessarily reflect those of the European Union or CINEA. Neither the European Union nor the granting authority can be held responsible for them.

DUTY REQUIREMENTS		Side 1		Side 2
Fluid		n-Pentane		Water
Flow type			Counter-Current	
Circuit		Inner		Outer
Heat load	kW		740,0	
Inlet vapor quality		1,000		
Outlet vapor quality		0,000		
Inlet temperature	°C	170,0		140,0
Condensation temperature (dew)	°C	150,0		
Subcooling	K	0,0		
Outlet temperature	°C	150,0		145,0
Flow rate	kg/s	2,648		34,52
Fluid condensed	kg/s	2,648		

Figure 2.8: Conditions used for selecting the brazed plate heat exchanger (BPHE) as replacement of the plate & shell heat exchanger. The bold numbers indicate inputs, the others are calculated.

The selected heat exchanger is of type B500TM with 206 plates and has a heat transfer area of 61 m². The empty weight of the heat exchanger is 202 kg and the holdup volume per side is about 59 liters. The dimensions are 304 mm wide, 490 mm deep and 979 mm high. This data will be used to create a representative dynamic model of the BHPE within the overall cascade heat pump model.

2.3.1 Design of auxiliary equipment

For the cascade heat pump integrated with the laminate production process, auxiliary equipment needs to be designed. The water within the hot storage tank, shown in Figure 2.3, expands when heated by the heat pump. This effect is included in the simulation and results in water being pushed out of the tank. A 3-way bypass valve is mounted in such a way that this water comes from the bottom of the tank, and therefore has the lowest temperature, minimizing the thermal losses. We applied a similar approach on the cold storage tank, shown in Figure 2.4, where the water contracts and "sucks" water from the downstream flow direction. Here the water temperature is fixed to 25 °C and it is being added to the bottom of the storage tank, where the water is coldest.

The bypass valves are assumed to be able to respond quickly, without being hindered by long travel times; the valve is assumed to be able to go from 0% to 100% within 1 second.

Funded by the European Union

Views and opinions expressed are however those of the author(s) only and do not necessarily reflect those of the European Union or CINEA. Neither the European Union nor the granting authority can be held responsible for them.

The volume of the storage tanks is estimated once and then kept a constant for all simulations. The aim of the task is the optimize the control for the given system, therefore optimizing the tank volume is outside the scope for this study. The cold storage tank is chosen at a volume of 10 m³ with a height of 7 m, while the hot storage tank is 1.5x the volume at 15 m³ and of the same 7 m height. The tanks are insulated with 10 cm mineral wool with a thermal conductivity of 0.04 W/m-K. The ambient temperature is set to 20 °C. All the required piping is excluded for the sake of simplicity.

2.4 Methodology

The steps taken to adapt the existing digital twin simulation model from SPIRIT task 2.4 to the variable load case of the current task are described in this subsection. This is followed by a description of the control system used as the baseline control.

The main modifications have already been described in the previous subsection; it consists of modifying the source and sink heat exchangers. For the source heat exchanger the ammonia fluid (vapor-liquid equilibrium) is changed to pressurized water (liquid). The BPHE on the sink side is based on the off-the-shelf model for this type of heat exchanger from TIL Suite Modelica library of TLK. The parameters of the model were adjusted to match the weight, internal volume, and heat transfer area of the selected BHPE. A performance comparison between the simulated heat exchanger and the datasheet was performed, resulting in a good agreement.

Similarly, an existing model from the Modelica Buildings Library is used for the hot and cold water buffer tanks. The model simulates a stratified water storage tank by applying a vertical discretization. The 7 m tall tanks are divided into 21 segments of ~0.33 m in height. For the rest of the extra components, i.e. bypass valves and pumps, standard components from TIL Suite were used. Water density changes induced by temperature variations are included for both the TIL components and the Modelica Buildings Library Components. The data from the laminate production process (see Figure 2.6 and Figure 2.7) is added to the model by reading it from file.

To keep track of the overall system performance, integrators or counters are added for the electrical energy consumed by the compressors, the amount of energy added to the cold storage tank and the amount of energy utilized from the hot storage tank. To keep the clutter of the top level model to a minimum, the process data input and energy counters are added to a sub-model titled *TRESPA CONTROL*.

Funded by the European Union

Views and opinions expressed are however those of the author(s) only and do not necessarily reflect those of the European Union or CINEA. Neither the European Union nor the granting authority can be held responsible for them.

Figure 2.9 depicts the source side of the cascade heat pump integrated with the cold buffer storage tank. The measurement data available for the "cold" side is applied to the boundary within the teal colored rectangle (top left of the figure). The cold storage tank is shown in the bottom left of the figure, with the bypass valve located above it. The pump feeding water to the ammonia evaporator is located in the center. Within the bottom right of the figure, the ammonia evaporator is followed by the ammonia heat pump itself, the ammonia/pentane (or cascade) heat exchanger and finally the pentane heat pump. The control systems of the ammonia heat pump, pentane heat pump, and components specific for the Trespa case (i.e. the pumps and bypass valves), are depicted top right. The baseline control is described in the next subsection.

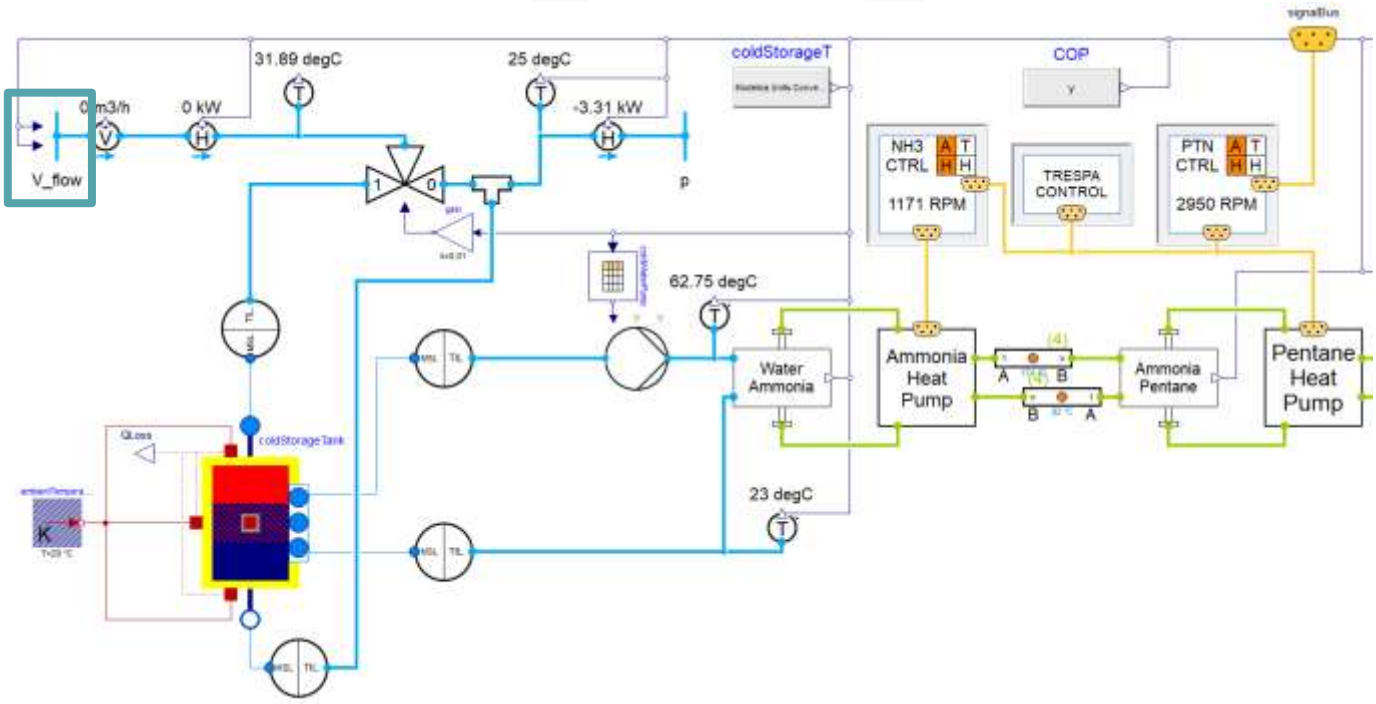


Figure 2.9: Screenshot of the left hand side or source side of the model as implemented in Dymola. The cold storage tank is shown on left, the cascade heat pump is shown on the right. The teal coloured rectangle depicts where the cold side measurement data is used as a boundary condition.

Funded by the European Union

Views and opinions expressed are however those of the author(s) only and do not necessarily reflect those of the European Union or CINEA. Neither the European Union nor the granting authority can be held responsible for them.

Figure 2.10 displays the sink side of the cascade heat pump. The hot side measurement data of section 2.2 is applied to the boundary within the red rectangle (in the centre of the figure). The hot buffer storage tank is shown on the right hand side with the bypass valve located above. Bottom centre shows the pentane condenser and the associated pump.

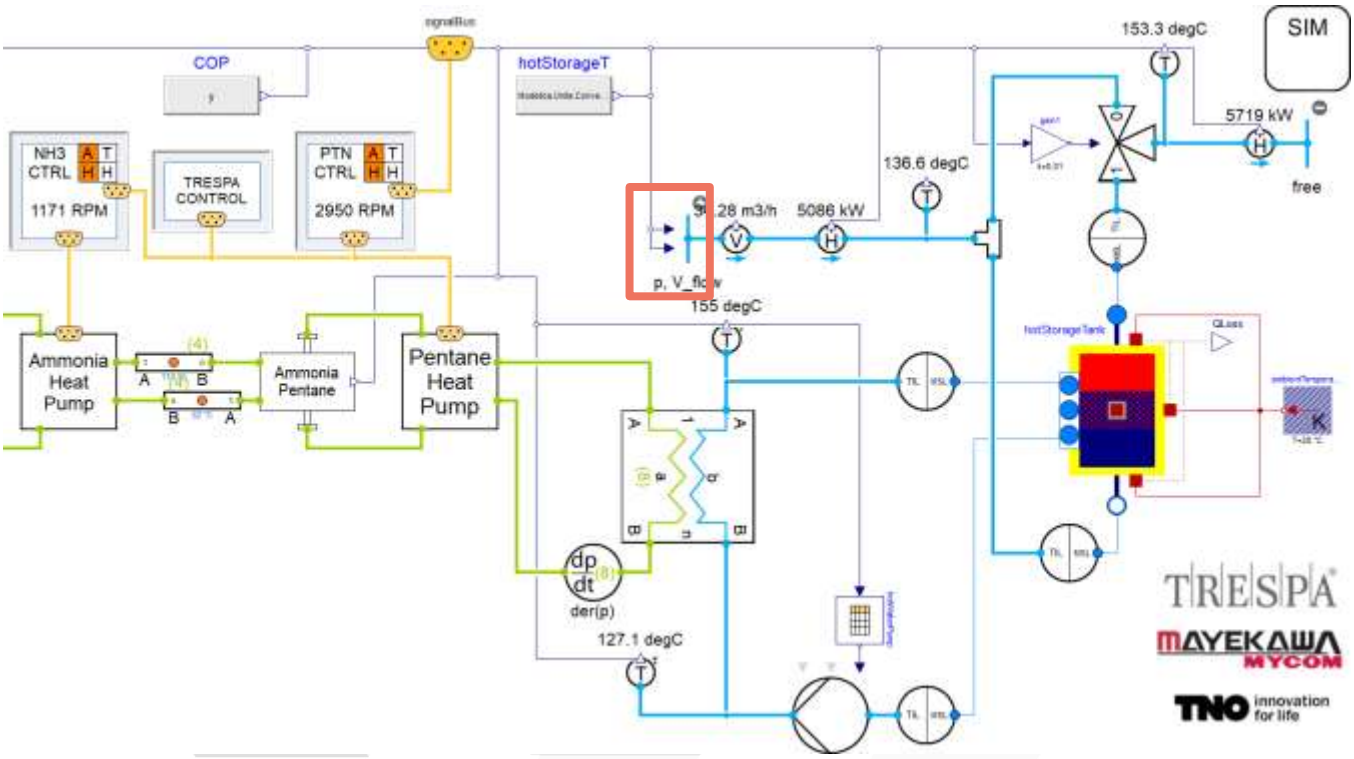


Figure 2.10: Screenshot of the right hand side or sink side of the model as implemented in Dymola. The cascade heat pump is shown on the left, hot storage buffer tank on the right. The red rectangle depicts where the hot side measurement data is used as a boundary condition.

Funded by the European Union

Views and opinions expressed are however those of the author(s) only and do not necessarily reflect those of the European Union or CINEA. Neither the European Union nor the granting authority can be held responsible for them.

2.4.1 Description of baseline control system

In this subsection, we describe the baseline control of cascade heat pump and the auxiliary systems on the source and sink side.

For the cold storage bypass control, the aim is to avoid feeding water into the buffer that is colder than the water already in the buffer. In the baseline control scenario, the control of the bypass valve is based on the average temperature in the top 0.33 m of the tank (the top segment). This is the same segment that feeds the ammonia evaporator. If the bypass valve is at 0%, all water is bypassed and at 100% all water is send to the cold storage tank. Based on this, a reverse acting Proportional integral (PI) controller is used, with the tank temperature as setpoint and the cold flow temperature as process value. If the cold process flow temperature is larger than the tank temperature, then the output of the controller will increase. The initial settings are a gain of 100 and integral time of 10 seconds. The controller is enabled when the flow is above 1e-5 m^3/s and resets to 0% output if disabled.

Similarly, the aim for the hot storage bypass control is to avoid "cooling" the water that comes from the laminate press and the heat recovery system located upstream. In other words, if the upstream temperature of the hot water flow is larger than the temperature in the top of the hot storage tank (~155 °C), then it should be bypassed (0% bypass valve). This is achieved by implementing a forward acting PI controller with the measured tank temperature as setpoint and the hot water flow temperature as process value. Similar to the cold storage control, a gain of 100 is used with an integral time of 10 seconds. The controller is enabled when the flow is above 1e-5 m^3/s and resets to 0% output if disabled.

No major changes are made to the cascade heat pump control system, it is used as designed by Mayekawa for the Stella Polaris integration case. Since the steam header pressure does no longer exist, the pentane heat pump is now controlled by the discharge (or condenser) pressure. The setpoint is 17.5 barg, which corresponds to a saturation temperature of 159 °C.

On the bottom cycle side, the ammonia evaporator water flow control is based on keeping the water outlet temperature at 23 °C. This ensures that the ammonia evaporator pressure is similar to the pressure used in the Stella Polaris application. A forward acting PI controller with a gain of 20 and integral time of 10 seconds is used to control the speed of the pump feeding the ammonia evaporator. The controller gives

Funded by the European Union

Views and opinions expressed are however those of the author(s) only and do not necessarily reflect those of the European Union or CINEA. Neither the European Union nor the granting authority can be held responsible for them.

an output between 0-100% and this is translated to 0.75 – 7.5 kg/s to simulate a real pump. When the cold storage tank is depleted, the pump will go to maximum speed.

On the top cycle, the pentane condenser water flow control is based on keeping the water outlet temperature at 155 °C. This assures that the top of the hot storage tank is always filled with water of the highest temperature, maximizing the usability within the production process. At this sink temperature, the pentane condenser pressure is still within the manufacturer's limits. A reverse acting PI controller with a gain of 20 an integral time of 10 seconds is applied. The controller gives an output between 0-100% and this is translated to 3.0 – 30 kg/s to simulate a real pump. When the hot storage tank is fully charged, the pump will go to maximum speed.

Figure 2.11 on the next page shows a screenshot of the Trespa control system as implemented for the baseline case. At the top is the timetable with the measurement data for the 2 temperature signals and the 2 signals for the volume flow rate. Below that the 2 PI-controllers for the bypass valves are located, with their activation logic and 0% reset values. These are followed by the 3 energy counters for electrical energy, cold energy stored, and hot energy utilized. At the bottom are the 2 PI-controllers for the pumps feeding the ammonia evaporator and pentane condenser.

Funded by the European Union

Views and opinions expressed are however those of the author(s) only and do not necessarily reflect those of the European Union or CINEA. Neither the European Union nor the granting authority can be held responsible for them.

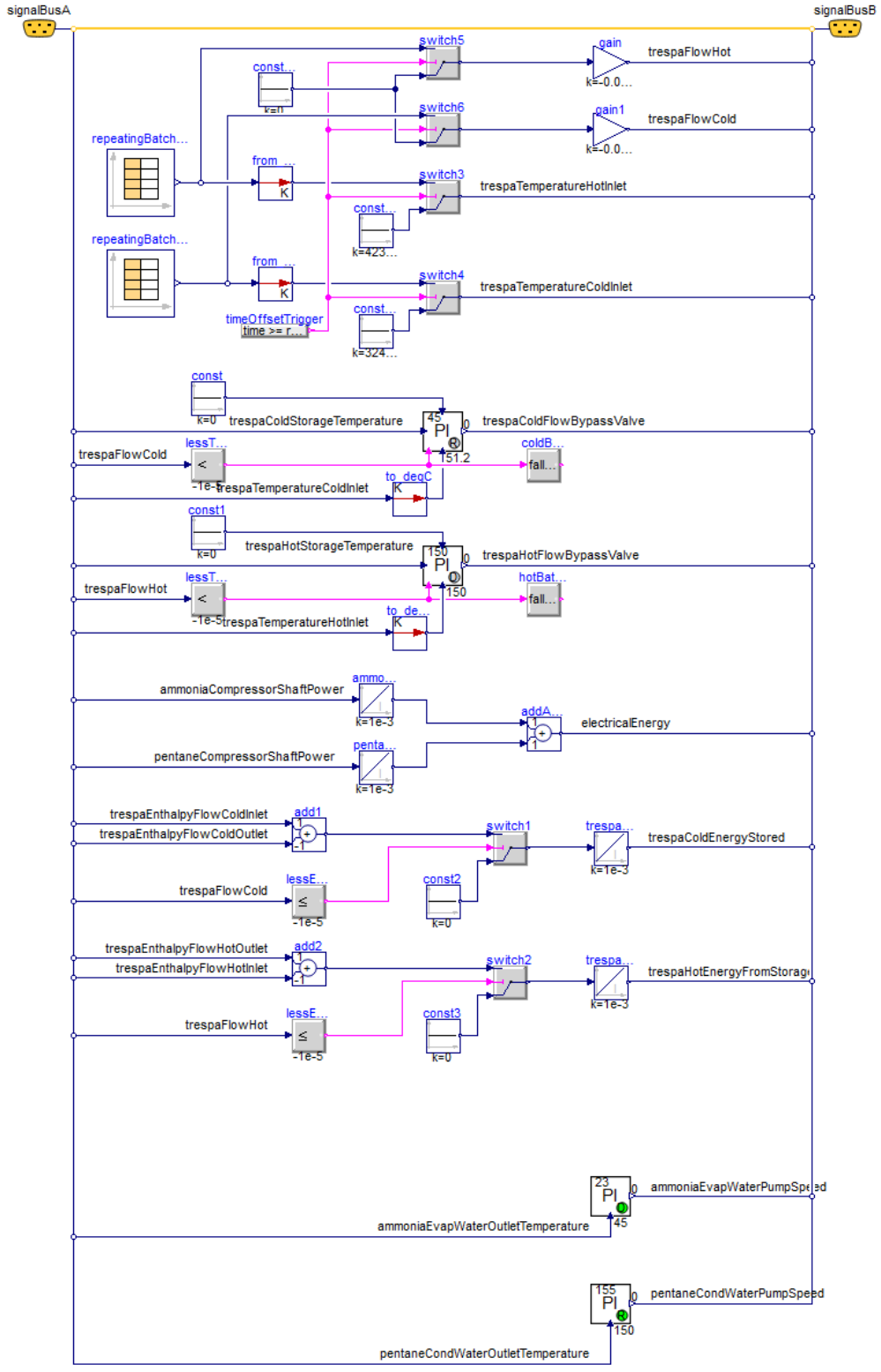


Figure 2.11: Control system for the Trespa integration. Reading of measurement data at the top, bypass valve control below that, followed by the energy flow integrators / counters and the water pump speed control at the bottom.

Funded by the European Union

Views and opinions expressed are however those of the author(s) only and do not necessarily reflect those of the European Union or CINEA. Neither the European Union nor the granting authority can be held responsible for them.

2.5 Results

In this section we present the results from the transient model simulations of the cascade heat pump for the variable load case of Trespa. First, the results of the baseline control system are shown. Based on the insights gained from these, the shortcomings are identified and the parameters to be optimized are selected. The section ends with the results from the optimized control system.

The cold and hot storage tank start at a uniform temperature of 45 °C and 150 °C respectively. Both the ammonia heat pump and the pentane heat pump begin their start sequence at a simulated time of 25 s. The initial conditions within the heat pumps correspond to a cold start scenario: the components with heat tracing are at their setpoint temperature, whereas the other components are at ambient temperature.

The hot flow period of the first batch starts at 800 s and 6 batches with a duration of 45 minutes are simulated (i.e. 2 repetitions of the available measurement data). This brings the total simulated time to 17000 s (~283 minutes). At the end of the simulation, the performance of the cascade heat pump combined with the thermal storage systems is evaluated. Each simulation takes about 2.5 hours to complete and up to 8 simulations can be ran in parallel.

It should be noted that the initial temperatures and the timing of the first batch, as specified in the previous paragraph, are chosen arbitrarily. The selected scenario is assumed to be representative of a typical operating case. Changing the initial conditions and timing of the first batch is considered to be out of scope for the task.

2.5.1 Baseline control system results

In this subsection, the results for the case with the baseline control system are presented. The simulation completes without any trips of the cascade heat pump which implies that none of the temperatures or pressures exceeded their respective limits. The result analysis starts from the hot buffer storage tank, where the “savings” are identified. This is followed by an overview of the cascade heat pump performance, which could be seen as the associated “cost” of the savings. Finally, the behaviour of the cold buffer is investigated briefly.

Funded by the European Union

Views and opinions expressed are however those of the author(s) only and do not necessarily reflect those of the European Union or CINEA. Neither the European Union nor the granting authority can be held responsible for them.

Hot buffer storage tank and bypass valve (heat sink)

The savings are defined as the amount of useful heat added to the water flow coming from the laminate press. The enthalpy (temperature) difference between the water-inlet and outlet, multiplied by the water flow rate and integrated over time yields the amount of heat utilized from the hot storage tank (Q_{hot}). Table 2.1 shows Q_{hot} for each of the 6 batches and the average in the rightmost column. The input data is the same for batch #1 and batch #4, the lower Q_{hot} for the first batch follows from a startup effect of the cascade heat pump.

Table 2.1: Amount of heat utilized from the hot storage tank per batch.

Batch #	1	2	3	4	5	6	*Average*
Q_{hot} [GJ]	1.62	1.75	1.71	1.65	1.71	1.69	1.69

Zooming in on the hot buffer tank itself, Figure 2.12 depicts the water temperature of the buffer at the top, middle and bottom locations over time. The start of each batch is denoted by a sudden drop in the bottom temperature (green). During a batch, the top temperature drops from 155 °C to ~150 °C. In between batches, the heat pump produces enough heat to restore the top temperature to 155 °C (the temperature set-point used for controlling the pentane condenser water pump) and the middle temperature to ~151 °C. For batch 4 at t ≈ 150 min, a temperature inversion can be observed, where the bottom temperature is above the middle temperature. This results in mixing inside the tank and loss of stratification.

Funded by the European Union

Views and opinions expressed are however those of the author(s) only and do not necessarily reflect those of the European Union or CINEA. Neither the European Union nor the granting authority can be held responsible for them.

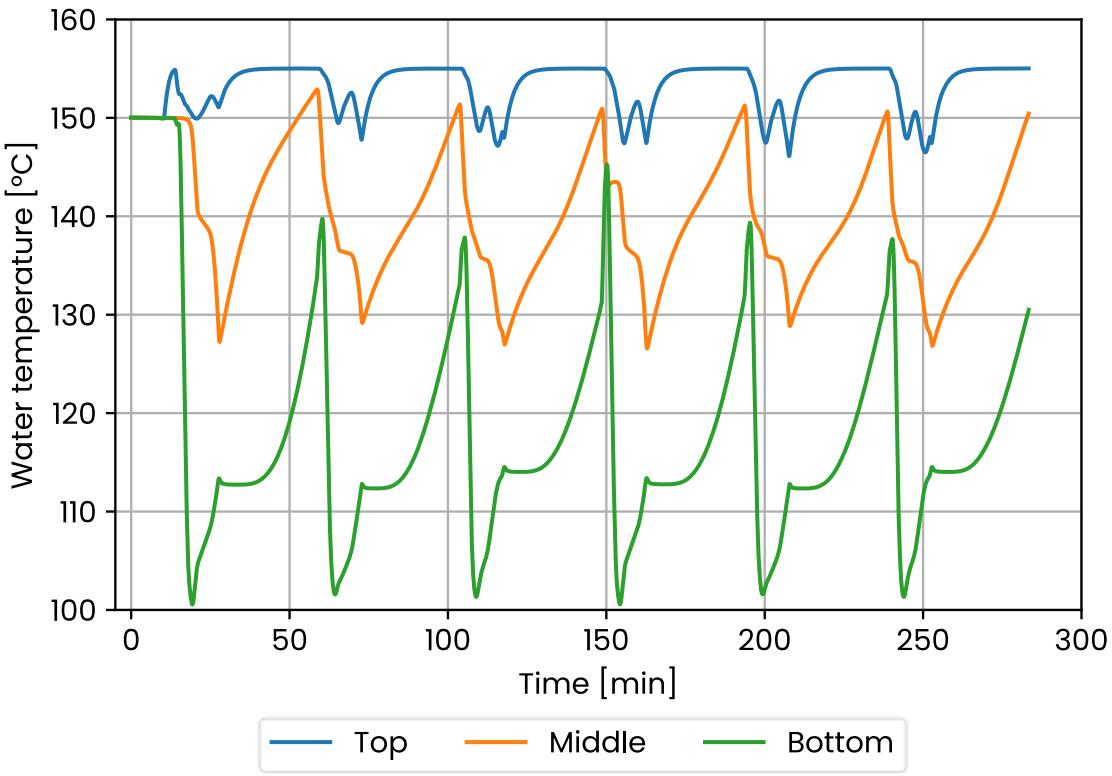


Figure 2.12: Water temperature within the hot buffer storage tank at the top, middle and bottom locations.

Figure 2.13 depicts the water flowrate coming from the laminate press and the bypass valve opening in the top graph, zoomed in on the first batch. The bottom graph shows the top buffer temperature and the hot inlet temperature, both of which are used as a control input for the bypass valve. The bypass valve switches to 100% at the start of the batch, since the top buffer temperature is above the hot inlet temperature ($t \approx 13$ min). In the period that follows, all water coming from the press is added to the bottom of the tank and hot water flows out of the top. This remains until the end of the batch at $t \approx 28$ min. The other 5 batches show very comparable behaviour and for this reason their data is omitted for brevity's sake. The difference in water temperature entering and leaving the tank, multiplied by the flow rate, yields the amount of useful heat that is supplied from the tank. This amount no longer needs to be supplied by alternative, fossil means; it is replaced by heat production from the electrically driven, cascade heat pump.

Funded by the European Union

Views and opinions expressed are however those of the author(s) only and do not necessarily reflect those of the European Union or CINEA. Neither the European Union nor the granting authority can be held responsible for them.

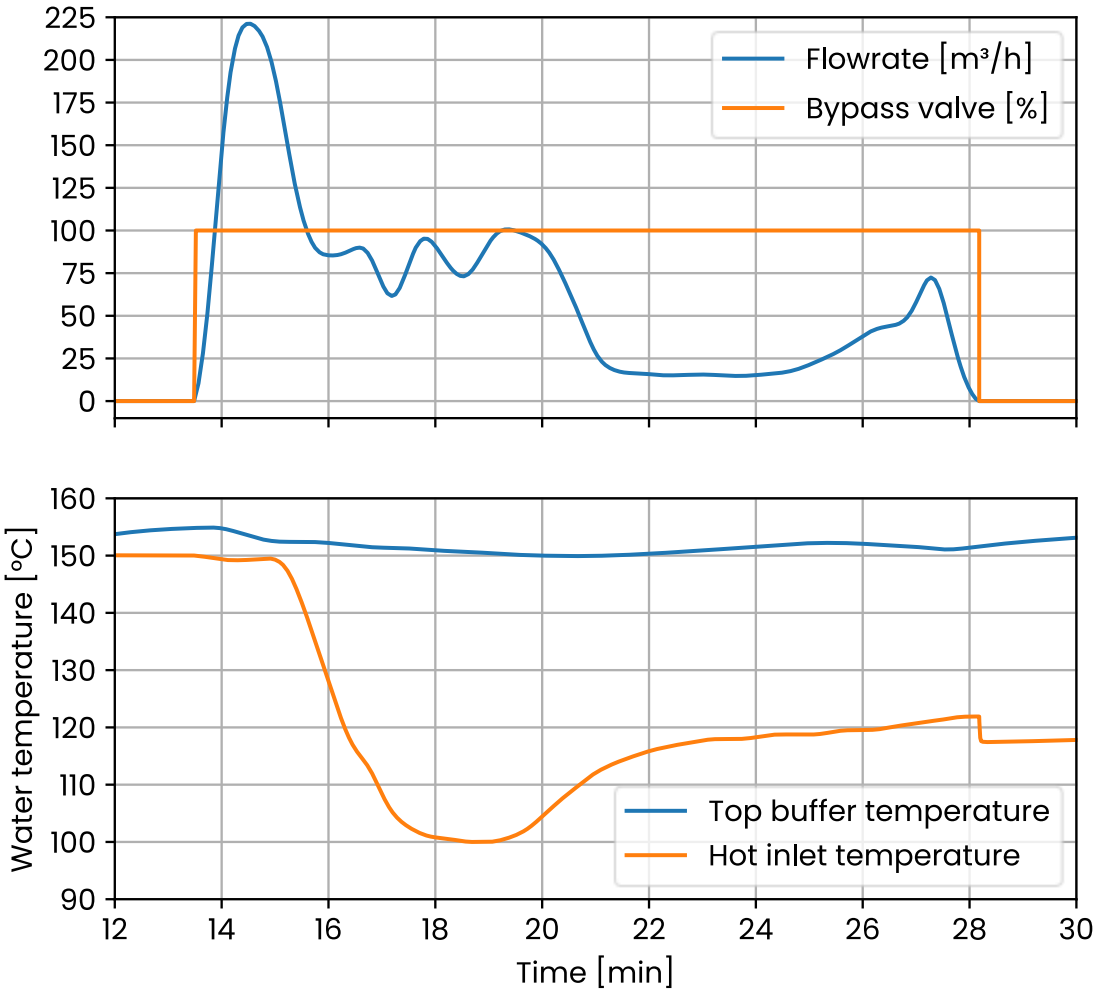


Figure 2.13: The hot water flowrate and bypass valve are shown in the top graph and the bottom graph the top temperature of the hot buffer and the hot water inlet temperature.

Funded by the European Union

Views and opinions expressed are however those of the author(s) only and do not necessarily reflect those of the European Union or CINEA. Neither the European Union nor the granting authority can be held responsible for them.

Cascade heat pump

The analysis of the cascade heat pump begins with the pentane condenser duty and shaft power of the ammonia- and pentane compressor, as depicted in Figure 2.14. During nominal operation, the condenser duty amounts to 670 kW and the ammonia and pentane compressor shaft power to 130 kW and 265 kW, respectively. This makes the instantaneous COP heating of the cascade heat pump equal to 1.70.

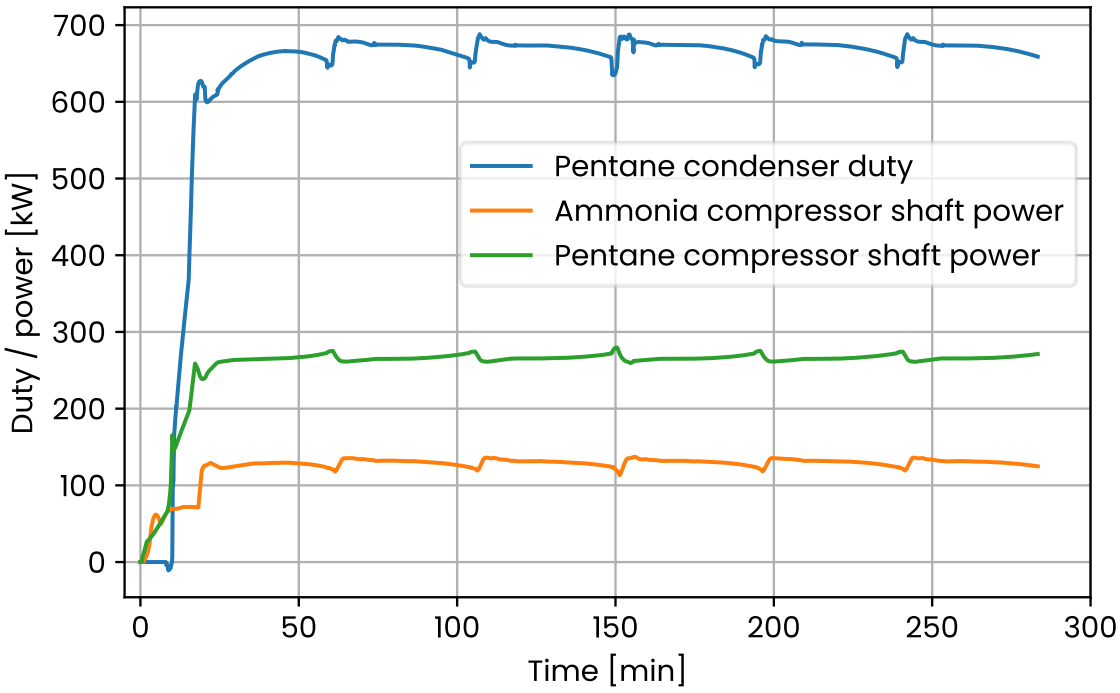


Figure 2.14: Pentane condenser duty, ammonia compressor shaft power and pentane compressor shaft power.

The COP can also be found by evaluating the energy counters for the electrical energy and the amount of heat utilized from the hot storage tank. To compensate for the arbitrary simulation length, the heat required to bring the hot buffer storage tank back to its initial state is included. We want to isolate the heat upgraded by the heat pump and minimize the effect of the initial condition of the hot storage buffer tank. Table 2.2 summarizes the heat utilized from the hot storage (Q_{hot}), electrical energy (E) and COP. A distinction is made between the full simulation, which includes startup of the heat pump, and the last 3 batches, where the system operates nominally.

Funded by the European Union

Views and opinions expressed are however those of the author(s) only and do not necessarily reflect those of the European Union or CINEA. Neither the European Union nor the granting authority can be held responsible for them.

Table 2.2: Heat utilized from storage, compressor electrical energy and COP for the full simulation and the last 3 batches.

	Full simulation (average per batch over 6 batches)	Last 3 batches (average per batch over 3 batches)
Heat utilized from hot storage, Q_{hot} [GJ]	1.66	1.68
Compressor electrical energy, E [GJ]	1.08	1.07
COP	1.54	1.57

The average Q_{hot} of 1.69 GJ per batch of Table 2.1 is slightly higher than the value reported above due to the corrected for the energy content of the hot buffer storage tank. At the end of the simulation, the tanks contains ~147 MJ less internal energy than at the beginning, dividing this difference over 6 batches yields the 1.66 GJ of Table 2.2. The COP of 1.54 is lower than the instantaneous COP (1.70) since startup of the cascade heat pump is included. Considering only the last 3 batches, the averaged Q_{hot} increases to 1.68 GJ. The tank temperature is higher on average, so more heat can be delivered. Moreover, for the last 3 batches the cascade heat pump achieves a COP of 1.57 which is still lower than the instantaneous COP (1.70); this difference is a consequence of water expansion losses (the tank is at constant volume) and heat losses towards the atmosphere. The cascade heat pump supplies 1.80 GJ of heat per batch on average, of which 0.13 GJ is lost due to expanding water being pushed out of the bottom of the tank. The remainder of the difference (~5.7 MJ) is lost towards the atmosphere.

The speed of the ammonia and pentane compressors is shown in Figure 2.15. The pentane compressor reaches full speed (2950 RPM) at ~17 min and maintains this speed throughout the remainder of the simulation. The first batch starts at 800 s (~13 min) and right from the beginning discharging of the hot storage tank commences. This indicates that the first batch comes about 4 min too early, compared to the cascade heat pump reaching full capacity. For a better match, the startup time will have to be reduced, or, if this is not possible, the cascade heat pump will need to start further ahead of the first batch.

Funded by the European Union

Views and opinions expressed are however those of the author(s) only and do not necessarily reflect those of the European Union or CINEA. Neither the European Union nor the granting authority can be held responsible for them.

The ammonia compressor runs at ~1170 RPM in steady state operation (range 750-1450 RPM). This indicates that there is control range available to increase the ammonia evaporator pressure (currently at 7.1 barg / 18 °C saturation), which can result in a rise of overall efficiency. Since density increases with pressure, the ammonia compressor needs to operate at a lower speed for the same mass flowrate of ammonia.

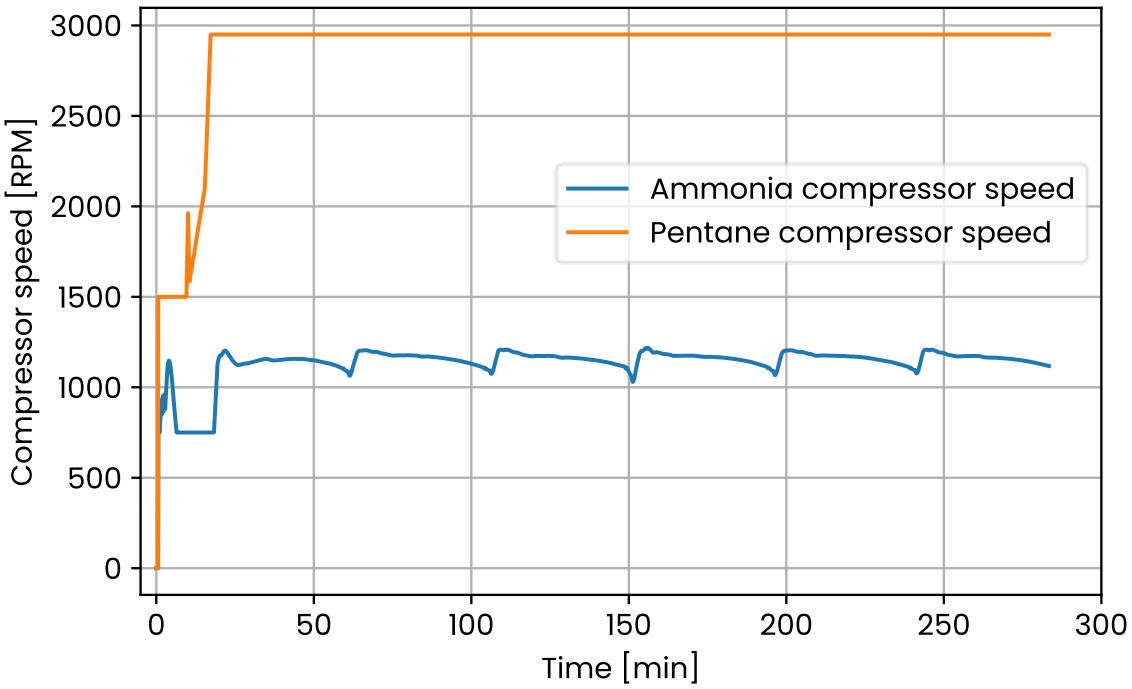


Figure 2.15: Ammonia compressor speed and pentane compressor speed for the full simulation.

The high pressure side of the ammonia heat pump operates at ~42 barg, which corresponds to a saturation temperature of 82 °C. For the pentane heat pump, the evaporator pressure is 2.5 barg (78 °C saturation) and the condenser operates at 15.8 barg (153 °C saturation). Based on these temperatures, the temperature lift of the cascade heat pump is from 18 °C to 153 °C (135 K). The theoretical Carnot COP is 3.16 and considering the instantaneous COP of 1.70, this yields a Carnot efficiency of 54%. The intermediate temperature between the ammonia and pentane heat pump, also known the "cascading temperature", can be chosen freely as long as the heat pump design limits are respected. Increasing this temperature, currently at 82 °C ammonia side / 78 °C pentane side, could yield an improvement in overall heating capacity and efficiency.

Funded by the European Union

Views and opinions expressed are however those of the author(s) only and do not necessarily reflect those of the European Union or CINEA. Neither the European Union nor the granting authority can be held responsible for them.

Cold buffer storage tank and bypass valve (heat source)

The top, middle and bottom water temperature of the cold buffer storage tank are shown in Figure 2.16. The tank starts at a uniform 45 °C and when the ammonia heat pump starts, the bottom temperature quickly reaches 23 °C, corresponding to the temperature control setpoint for the ammonia evaporator water pump. The first batch recharges the tank to 44 °C in the bottom and 80 °C in the top. For the second batch at 80 min, the recharging is less effective since the bottom temperature displays a limited increase to 34 °C. Similarly, the top temperature tops out at 75 °C instead of close to 80 °C. The 3rd, 4th and 6th batches show good behaviour, with temperature increases comparable to the first batch. The 5th batch has the same characteristics as the 2nd batch, displaying only minor temperature increases.

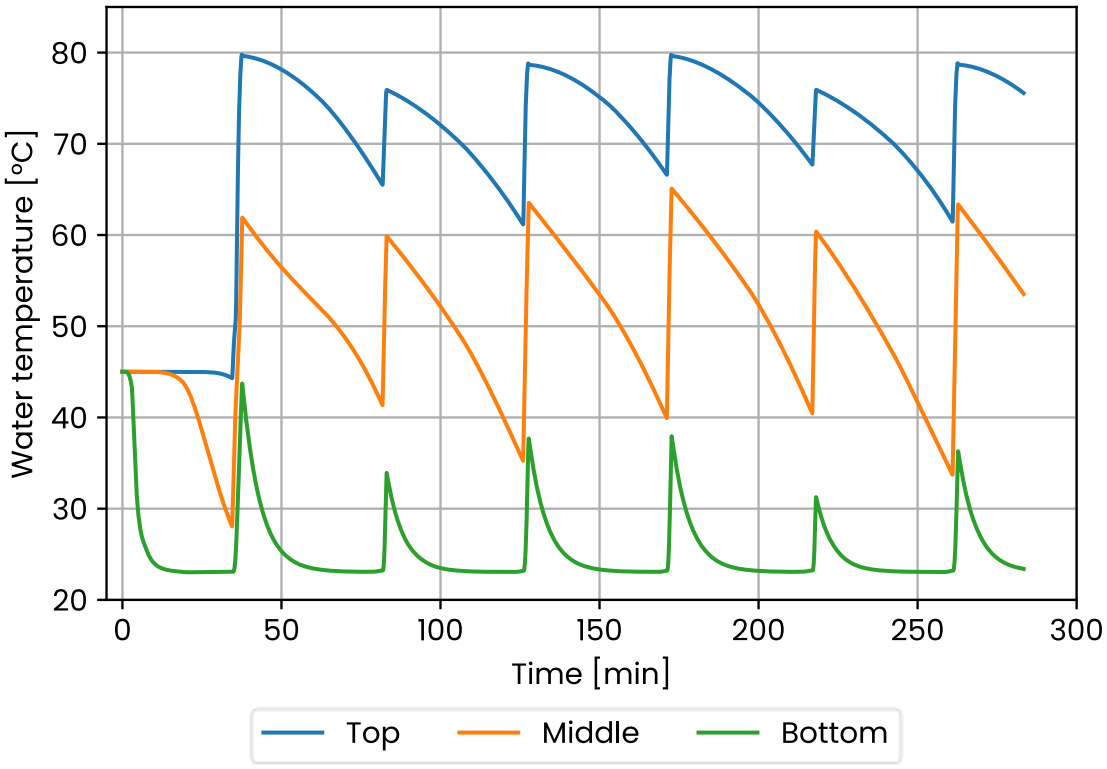


Figure 2.16: Water temperature with the cold buffer storage tank at the top, middle and bottom locations.

Funded by the European Union

Views and opinions expressed are however those of the author(s) only and do not necessarily reflect those of the European Union or CINEA. Neither the European Union nor the granting authority can be held responsible for them.

Figure 2.17 shows the behaviour of the cold storage bypass valve for the 2nd and 3rd batch. During the 2nd batch at 80 min, the bypass valve only opens during the final quarter of the batch, such that only a fraction of the water coming from the laminate press is added to the cold storage tank. Of the 3rd batch at 125 min, about 1/3 is added to cold storage tank (bypass valve at 100% for ~1.7 min). Due to the high water flow rate, this is sufficient time to recharge the buffer. As can be seen in the bottom graph, only the section of the cold flow with the highest temperature is utilized. Excessive depletion of the cold storage buffer due to partially skipped batches, could result in a decrease in ammonia evaporator temperature and loss of performance. This can be avoided by changing the control of the bypass valve.

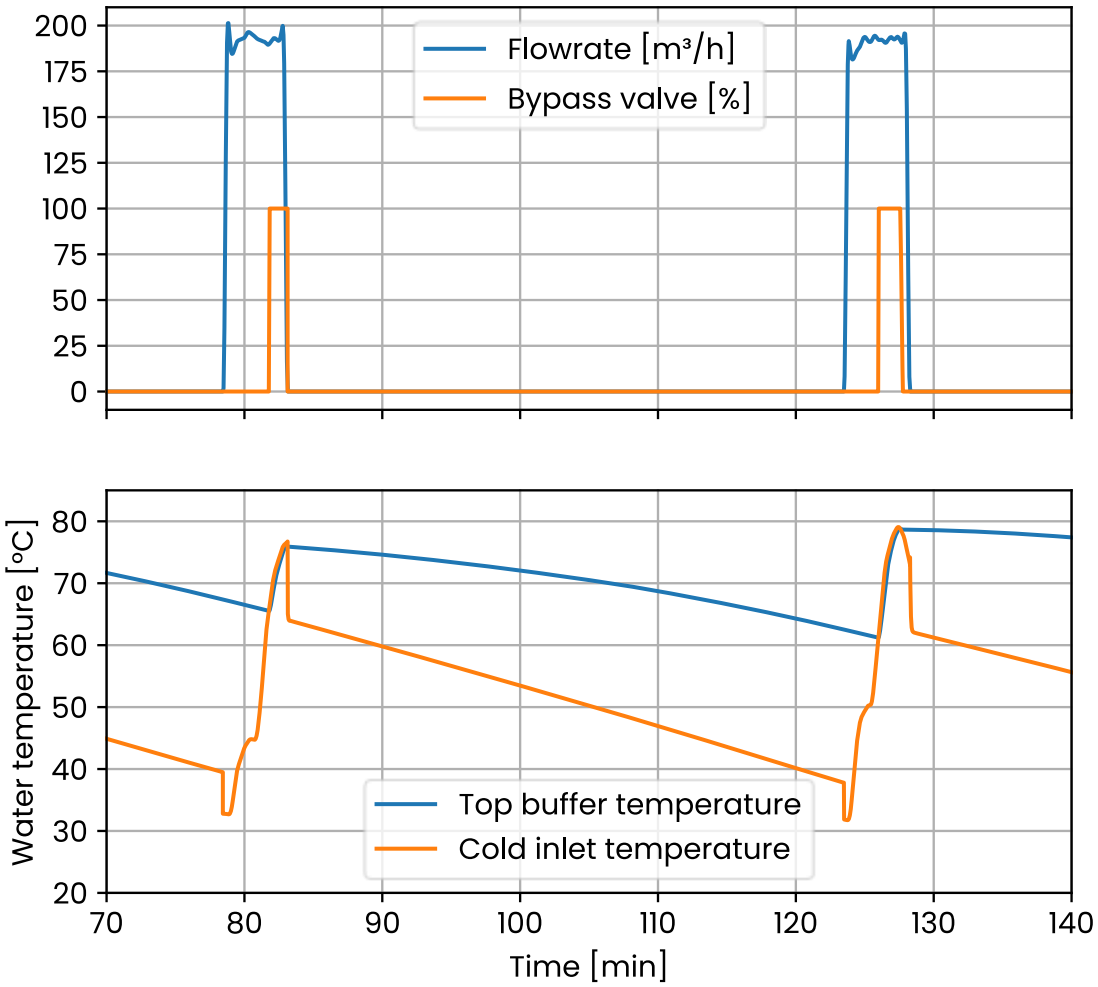


Figure 2.17: The cold water flowrate and bypass valve are shown in the top graph and the bottom graph depicts the top temperature of the cold buffer and the cold water inlet temperature.

Funded by the European Union

Views and opinions expressed are however those of the author(s) only and do not necessarily reflect those of the European Union or CINEA. Neither the European Union nor the granting authority can be held responsible for them.

2.5.2 From baseline control to optimized control

The following paragraphs give an overview of the shortcomings or opportunities identified during the interpretation of the base case results (utilizing the baseline control system). For each of them, the relevant optimization parameters are identified. The combined changes yield an optimized control system with an improved performance of the cascade heat pump. This is followed by the presentation of the results of the optimized case and the differences with the baseline case are highlighted.

Ammonia heat pump evaporator pressure

The ammonia heat pump evaporator pressure is raised by increasing the temperature control setpoint for the water leaving the evaporator. The original setpoint of 23 °C was chosen for the baseline control system to yield an evaporator pressure similar to the integration at Stella Polaris. For the optimized control, the temperature setpoint is increased until one of the limits of the ammonia heat pump is reached (resulting in a trip within the simulation). This can, for example, be a design pressure limit or a lack of suction superheat at the compressor. The latter follows from the design choice to use the cooling water of the compressor as a heat source to fully evaporate and superheat the slightly wet ammonia (about 1% liquid by mass) coming from the flooded evaporator. The cooling water temperature is limited to about 60 °C and the compressors rejects a finite amount of heat; therefore, increasing the evaporator pressure reduces the available driving force (temperature difference) within the suction line superheater.

Cascading temperature

The main effect of raising the cascading temperature, or the temperature transition point between the ammonia heat pump and the pentane heat pump, is an increase the capacity of the pentane heat pump. This follows from the higher pentane evaporator pressure and therefore denser gas entering the compressor, yielding an increase in the working medium mass flow for the same compressor speed. The efficiency effect will depend on the relative performance of the ammonia and pentane heat pumps. Raising the cascading temperature increases the temperature lift for the ammonia heat pump, whereas the lift decreases for the pentane heat pump.

The cascading temperature is set by the discharge pressure setpoint of the ammonia heat pump, which in itself is influenced by the speed of the ammonia compressor. With an elevated evaporator pressure, it becomes possible to increase the discharge

Funded by the European Union

Views and opinions expressed are however those of the author(s) only and do not necessarily reflect those of the European Union or CINEA. Neither the European Union nor the granting authority can be held responsible for them.

ammonia pressure in similar fashion. The change is limited by the design pressure of the ammonia heat pump and the differential pressure over the compressor (max 40 bar). The discharge pressure trip setpoint of the ammonia system is raised to 50 barg, which is 2 bar below the safety valve set by the manufacturer.

Control for hot storage buffer tank at full capacity

With the increase in pentane heat pump capacity, following from the cascading temperature change, the hot storage tank can become fully charged. This is defined as the temperature of the water entering the pentane condenser, which is the same as the bottom temperature of the tank, reaching 150 °C (this leaves a 5 K temperature increase over the condenser). Within the baseline control, the condenser water pump will go to maximum speed, followed by the pentane compressor reducing in speed down due to high condenser pressure. The more elegant solution would be to use information about the state of charge of the hot storage buffer to control the pentane compressor speed and to avoid operating at excessively high condenser pressure with the associated penalty on performance. A straightforward implementation of this concept is to use the water temperature entering the pentane condenser, which corresponds to the temperature within the bottom of the tank, to limit the pentane compressor speed.

For the optimized control system, an additional controller is added, which uses the pentane condenser water inlet temperature as input. When the setpoint is reached, the controller will start to reduce the maximum allowed speed of the pentane compressor. The upper limit of the pentane compressor speed reduction follows from the minimum speed of the ammonia compressor; we want to avoid forcing the ammonia compressor speed to 750 RPM without any available room for control.

Figure 2.18 displays the implementation within Dymola. The top controller activates when the pentane compressor speed reaches 2900 RPM for the first time and stays active indefinitely afterwards. A temperature of 150 °C is used as setpoint for the pentane condenser water inlet temperature. The setpoint for the controller with the ammonia compressor speed as input, is chosen at 800 RPM. By taking the maximum of the 2 controller outputs, it assures that the pentane compressor speed can be reduced based on the condenser water inlet temperature, but lowering the ammonia compressor speed too much is avoided. In other words, when the water temperature reaches 150 °C, the pentane compressor speed is reduced until the ammonia compressor speed reaches 800 RPM.

Funded by the European Union

Views and opinions expressed are however those of the author(s) only and do not necessarily reflect those of the European Union or CINEA. Neither the European Union nor the granting authority can be held responsible for them.

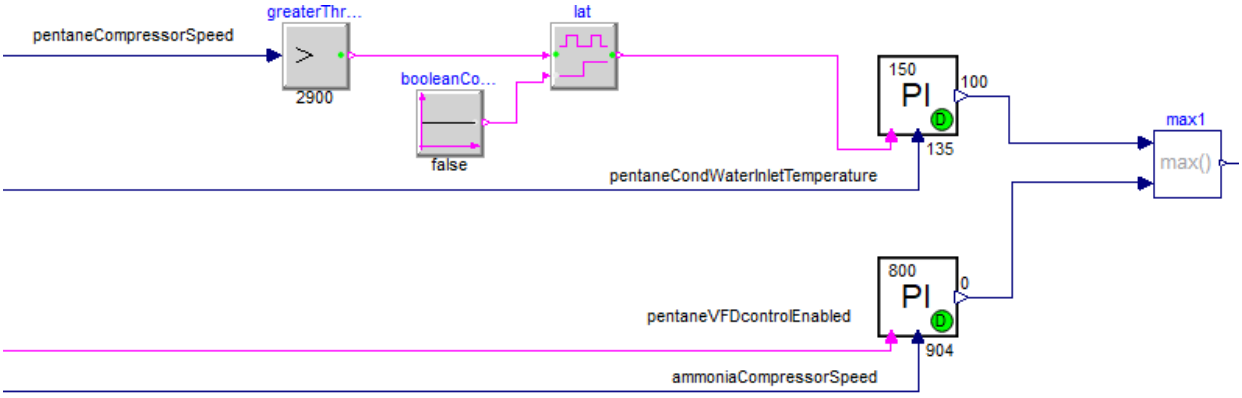


Figure 2.18: The two controllers added to the pentane control system, specifically for the integration with the hot buffer storage tank.

Pentane condenser water outlet temperature / start up speed

In the baseline control system, the water pump feeding the pentane condenser starts at 0% output and increases in speed when the water outlet temperature reaches the setpoint of 155 °C. As a result of this control strategy, the pentane compressor takes a long time to reach full speed. This is due to the speed control of the water pump and the speed control of the pentane compressor interfering with each other. At low water pump speed, the pentane condenser pressure quickly increases, which limits the compressor speed control to a low output value, since it uses the condenser pressure as input.

This is fixed by adding an activation condition based on the speed of the pentane compressor, as presented in Figure 2.19. The pump speed control activates when the compressor speed reaches 2900 RPM, which is just below the maximum speed of 2950 RPM, and stays active indefinitely afterwards. Next to this, the initial output of the controller is changed from 0% to 100%. The pump now starts at maximum speed and ramps down until the temperature setpoint of 155 °C is reached.

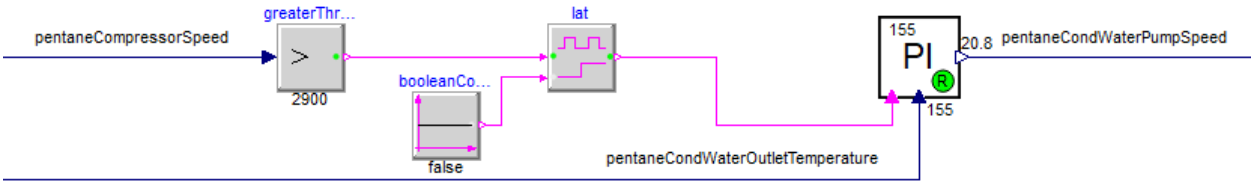


Figure 2.19: The pentane condenser water pump control now waits for the pentane compressor to reach 2900 RPM as an activation condition. The initial output is 100%.

Funded by the European Union

Views and opinions expressed are however those of the author(s) only and do not necessarily reflect those of the European Union or CINEA. Neither the European Union nor the granting authority can be held responsible for them.

Cold storage tank bypass valve

For the baseline case, the control of the bypass valve is based on the top temperature of the cold buffer storage tank. This resulted in water with a higher temperature than most of the tank volume being bypassed, with excessive depletion of the tank as a consequence. The alternative is to allow water to enter the tank even if the temperature is lower than the temperature within the top of the tank. This will result in loss of stratification since the hotter water will "float" back to the top of the tank, mixing along the way upwards.

For the control system, this means changing the temperature sensor used for the bypass valve control to a location lower down the tank. The most extreme case, where the temperature sensor is located within the bottom of the tank, is selected for the optimized control system. Now any water that is hotter than the bottom tank temperature, will be added to the top of the tank, and the water in the bottom, which should be the coldest present in the tank, is pushed out. The average temperature of the cold storage tank, a measure for the energy contents, will always increase as a result of this control scheme, even though the tank is no longer strictly stratified and mixing takes place.

2.5.3 Optimization results

Based on the results with the baseline control system, the two main parameters that determine the performance of the cascade heat pump and associated heat storage system are identified: the ammonia evaporator water outlet temperature and the ammonia heat pump condenser pressure. Increasing the setpoints for these yields a larger amount of useful heat supplied by the cascade heat pump at a better efficiency or COP. The optimum is where the system operates close the limit of tripping, without actually doing so. Due to the computational cost of the model, the optimization is limited to stepwise increments of both parameters. The postprocessing of the simulation results is automated using Python. Figure 2.20 depicts a summary of the results with the modified or optimized control system, as described in the previous section, for different parameter setpoint combinations.

Funded by the European Union

Views and opinions expressed are however those of the author(s) only and do not necessarily reflect those of the European Union or CINEA. Neither the European Union nor the granting authority can be held responsible for them.

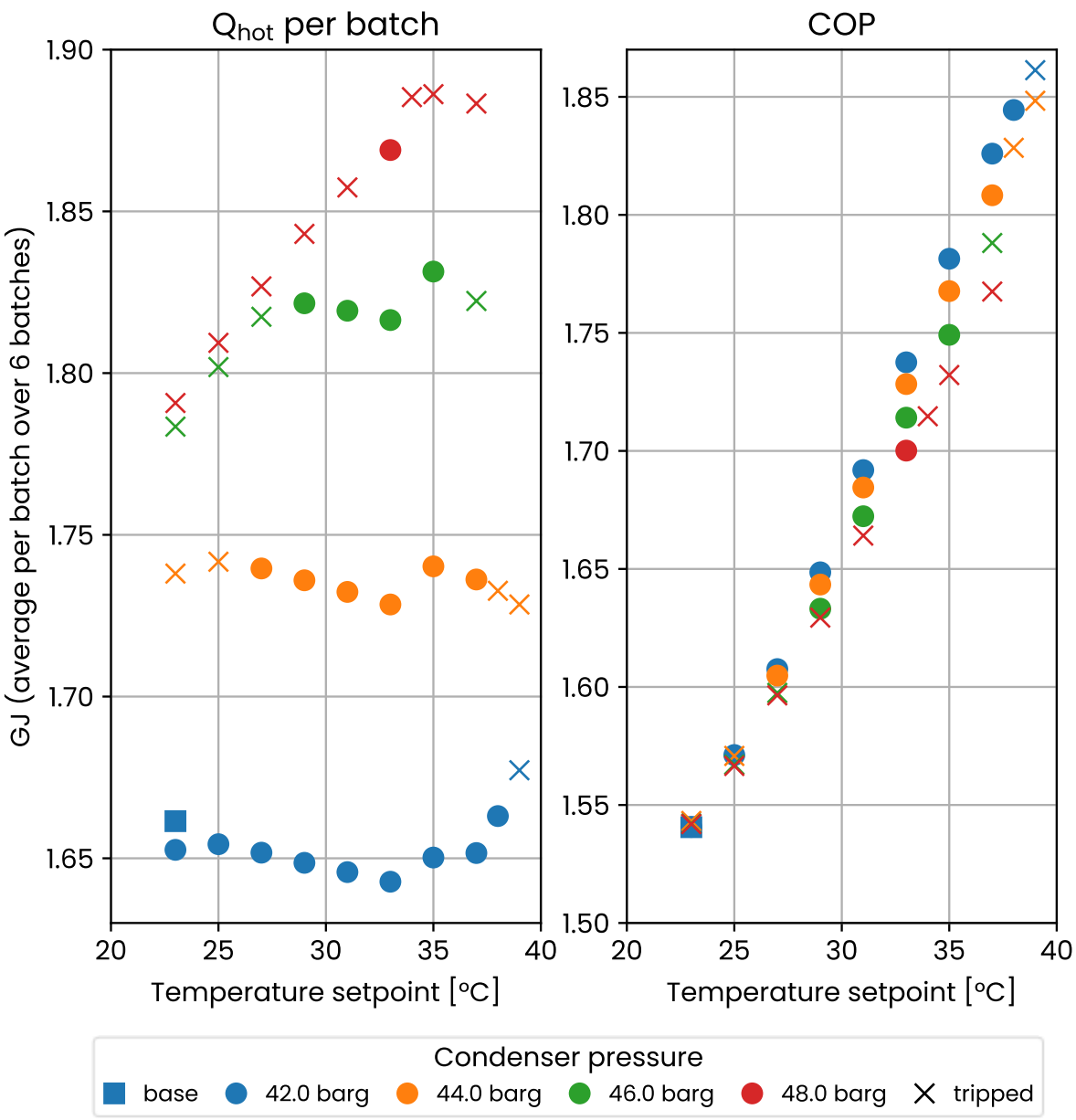


Figure 2.20: Summary of the optimization results. The heat utilized from hot storage (Q_{hot}) per batch is shown in the left figure and the COP in the right figure. The base case is indicated by the square, whereas the colour of the circles indicates the condenser pressure used. An "x" indicates a tripped simulation.

Funded by the European Union

Views and opinions expressed are however those of the author(s) only and do not necessarily reflect those of the European Union or CINEA. Neither the European Union nor the granting authority can be held responsible for them.

In the bottom left, the base case settings of 23 °C water outlet temperature (ammonia evaporator) and 42 barg condenser pressure are applied. For the water outlet temperature, the optimization starts at 23 °C and increases with 2 °C steps up to 37 °C. Similarly, for the condenser pressure, 42 barg is simulated for all water temperatures, followed by 44, 46 and 48 barg. Additional simulations are added at 38 °C and 39 °C water temperature to find the optimum COP. For these simulations, only 42 barg and 44 barg are included, since the higher pressure setpoints did already trip at lower values. In similar fashion, an additional simulation is performed at 34 °C / 48 barg. This brings the total number of simulations to 38, including the base case.

The simulations marked with an "x" instead of a dot contain 1 or more trip occurrences. In practice, the cascade heat pump would have stopped operation; whereas the simulations continue unimpeded. None of the trips were caused by the pentane heat pump. For the ammonia heat pump, the trip was one or multiple of: a too high compressor discharge temperature, a too high condenser pressure, not enough superheat at the suction side of the compressor or a too large differential pressure over the compressor.

The graph on the left hand side of Figure 2.20 shows the heat utilized from the hot storage buffer tank (average per batch over 6 batches). The numbers reported are corrected for the internal energy difference of the tank between the begin and end of the simulation, similar to the baseline control results. Raising just the water outlet temperature setpoint at the ammonia evaporator (blue dots), yields a minor variation in Q_{hot} of about 1%. Incrementing the condenser pressure at the same time (orange, green or red dots), gives a more pronounced increase of ~14% in energy compared to baseline for the simulations without a trip. This indicates that the limiting factor for the heat utilized per batch lies within the pentane heat pump. Only when the capacity of the pentane heat pump is increased by a higher ammonia condenser pressure, yielding a higher pentane evaporator pressure, will Q_{hot} increase significantly.

On the right hand side of Figure 2.20, the associated COP, which includes system startup, is depicted for each of the simulations. A linear relation can be observed when operating at a constant condenser pressure (dots of the same colour). Raising the condenser pressure at similar outlet water temperature setpoint in the ammonia evaporator yields a small penalty on the COP. The difference in COP between the highest and lowest pressure depends on water temperature setpoint used. This follows from the decrease in COP of the ammonia heat pump due to the larger temperature lift. The improvement in efficiency of the pentane heat pump is not enough to fully offset this.

Funded by the European Union

Views and opinions expressed are however those of the author(s) only and do not necessarily reflect those of the European Union or CINEA. Neither the European Union nor the granting authority can be held responsible for them.

The selection of the optimal configuration depends on the intended aim. For the highest Q_{hot} per batch, the simulation with 33 °C as temperature setpoint on the outlet water temperature in the ammonia evaporator and 48 barg condenser pressure is ideal. Alternatively, the highest COP is achieved when setting the outlet water temperature in the ammonia evaporator to 38 °C and leaving the ammonia condenser pressure at the base case setpoint of 42 barg.

The simulation with the highest Q_{hot} (33 °C / 48.0 barg) and the simulation with the best COP (38 °C / 42 barg) are compared with the baseline control in Table 2.3 for the amount of heat utilized from the hot storage tank per batch. As expected, the simulation optimized for this specific purpose (red), outperforms the baseline (black) and the simulation optimized for COP (green) for all 6 batches. During the first 2 batches, Q_{hot} for the COP optimized configuration is above baseline, whereas it is below baseline for the final 4. The cause behind this observation has not been investigated.

Table 2.3: Amount of heat utilized from the hot storage tank per batch. Baseline in black, optimized for Q_{hot} in red and optimized for COP in green.

Batch #	1	2	3	4	5	6	*Average*
Q_{hot} [GJ]	1.62	1.75	1.71	1.65	1.71	1.69	1.69
	1.71	1.83	1.85	1.81	1.90	1.88	1.83
	1.72	1.77	1.70	1.63	1.68	1.66	1.69

Table 2.4 summarizes the cascade heat pump performance for the same three cases as Table 2.3. In similar fashion to Table 2.2, the numbers are corrected for the initial state of the hot buffer storage tank and a distinction is made between the full simulation and second half consisting of the last 3 batches to exclude the effect of startup. Again, the simulation optimized for Q_{hot} outperforms the baseline, even though the compressor electrical energy remains roughly the same. This gives a +0.16 COP improvement over the baseline. Alternatively, optimizing for COP yields an improvement of 0.30-0.33. This does come with a minor penalty on the amount of heat utilized from storage.

Funded by the European Union

Views and opinions expressed are however those of the author(s) only and do not necessarily reflect those of the European Union or CINEA. Neither the European Union nor the granting authority can be held responsible for them.

Table 2.4: Heat utilized from storage, compressor electrical energy and COP for the full simulation and the last 3 batches. Baseline in black, optimized for Q_{hot} in red and optimized for COP in green.

	Full simulation (average per batch over 6 batches)	Last 3 batches (average per batch over 3 batches)
Heat utilized from hot storage, Q_{hot} [GJ]	1.66 1.87 1.66	1.68 1.87 1.65
Compressor electrical energy, E [GJ]	1.08 1.10 0.90	1.07 1.08 0.87
COP	1.54 1.70 1.84	1.57 1.73 1.90

Figure 2.21 shows a comparison to indicate the improved start up speed between the base case and the optimized solutions at 23 °C / 42 barg (similar to the base case), 38 °C / 42 barg (COP optimum) and 33 °C / 48 barg (Q_{hot} optimum). In the top graph, it can observed that it takes until ~17 min for the pentane compressor to reach full speed in the base case (blue line). For the optimized control, this improves to <12 min. for the simulations at elevated water temperature setpoints. The configuration at 23 °C is not as fast, since it takes longer to ramp up the ammonia heat pump capacity at low evaporator pressure. The middle graph indicates that the optimized control reaches the maximum pentane condenser saturation temperature slightly earlier than baseline, with similar behaviour afterwards. The modification on the control of the pentane condenser water pump speed is depicted in the bottom graph. For the optimized configuration, the speed starts at 100% instead of 0% for the baseline. After the occurrence of the first hot batch at ~16 min, the speed drops to below 10%, which is caused by the decrease in condenser water inlet temperature.

Funded by the European Union

Views and opinions expressed are however those of the author(s) only and do not necessarily reflect those of the European Union or CINEA. Neither the European Union nor the granting authority can be held responsible for them.

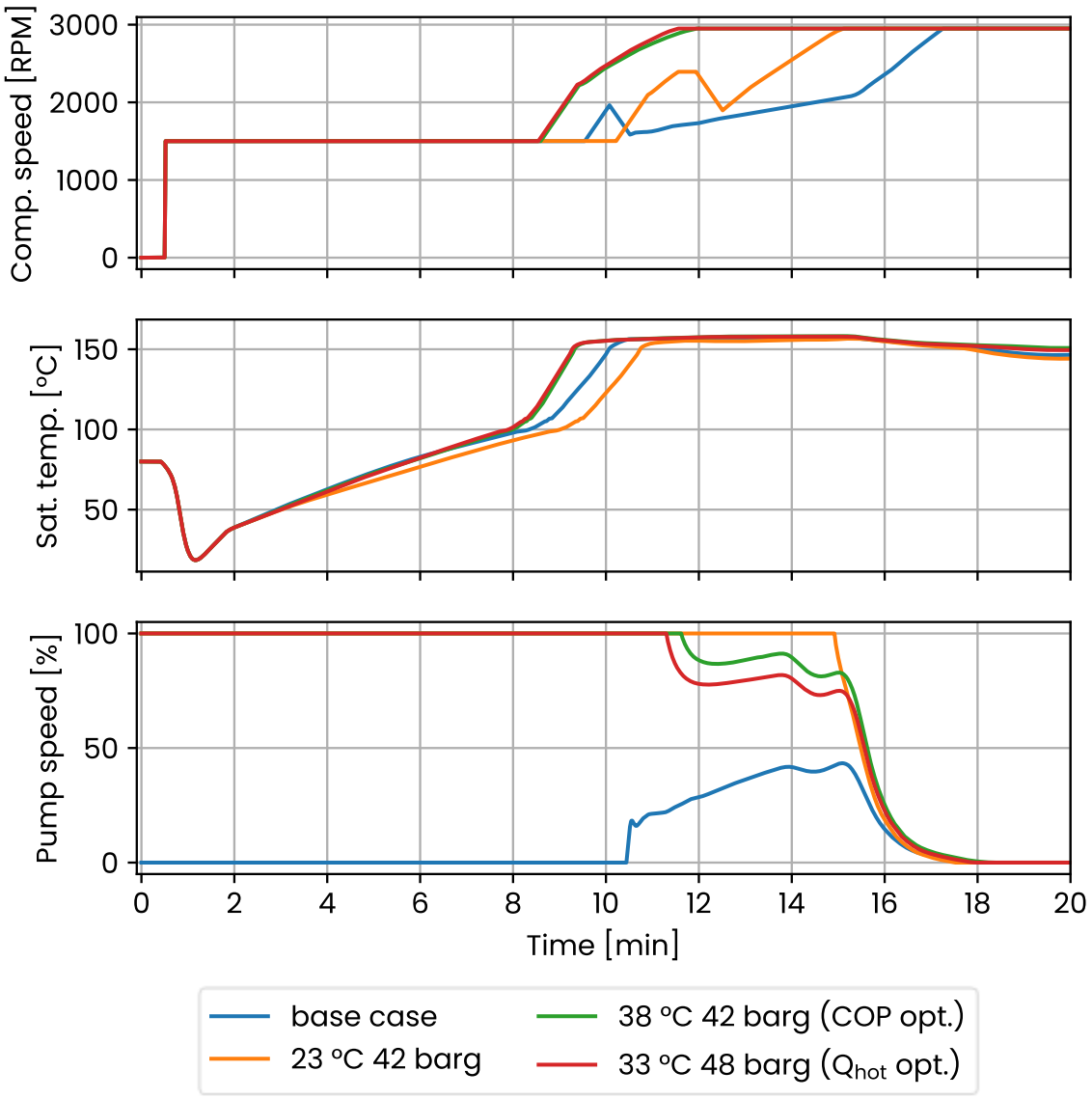


Figure 2.21: Comparison for the first 20 minutes of the simulation between the base case and the 23 °C / 42 barg, 38 °C / 42 barg & 33 °C / 48 barg configurations for the pentane compressor speed (top), pentane condenser saturation temperature (middle) and pentane condenser water pump speed (bottom).

Figure 2.22 depicts the behaviour of the system just before and during the 5th batch for the pentane condenser water in/outlet, the speed of the pentane compressor and the control outputs of the full buffer limiter, ammonia compressor speed control limiter, condenser pressure control and the actual speed control (which is the active output). The hot buffer tank is close to full, as indicated in the top graph by the pentane condenser water inlet temperature (equal to the bottom buffer temperature) reaching

Funded by the European Union

Views and opinions expressed are however those of the author(s) only and do not necessarily reflect those of the European Union or CINEA. Neither the European Union nor the granting authority can be held responsible for them.

150 °C. The pentane heat pump reacts by reducing the compressor speed at ~192 min to 2400 RPM (middle graph). The bottom graph indicates that the full buffer limit controller (blue line) activates, and briefly determines the actual speed control (overlapping red line). The standard speed control based on the condenser pressure (green line) reacts slightly slower and catches up about 1.5 min later. The limiter for the ammonia compressor speed does activate (orange line), but it's never directly of influence on the actual compressor speed.

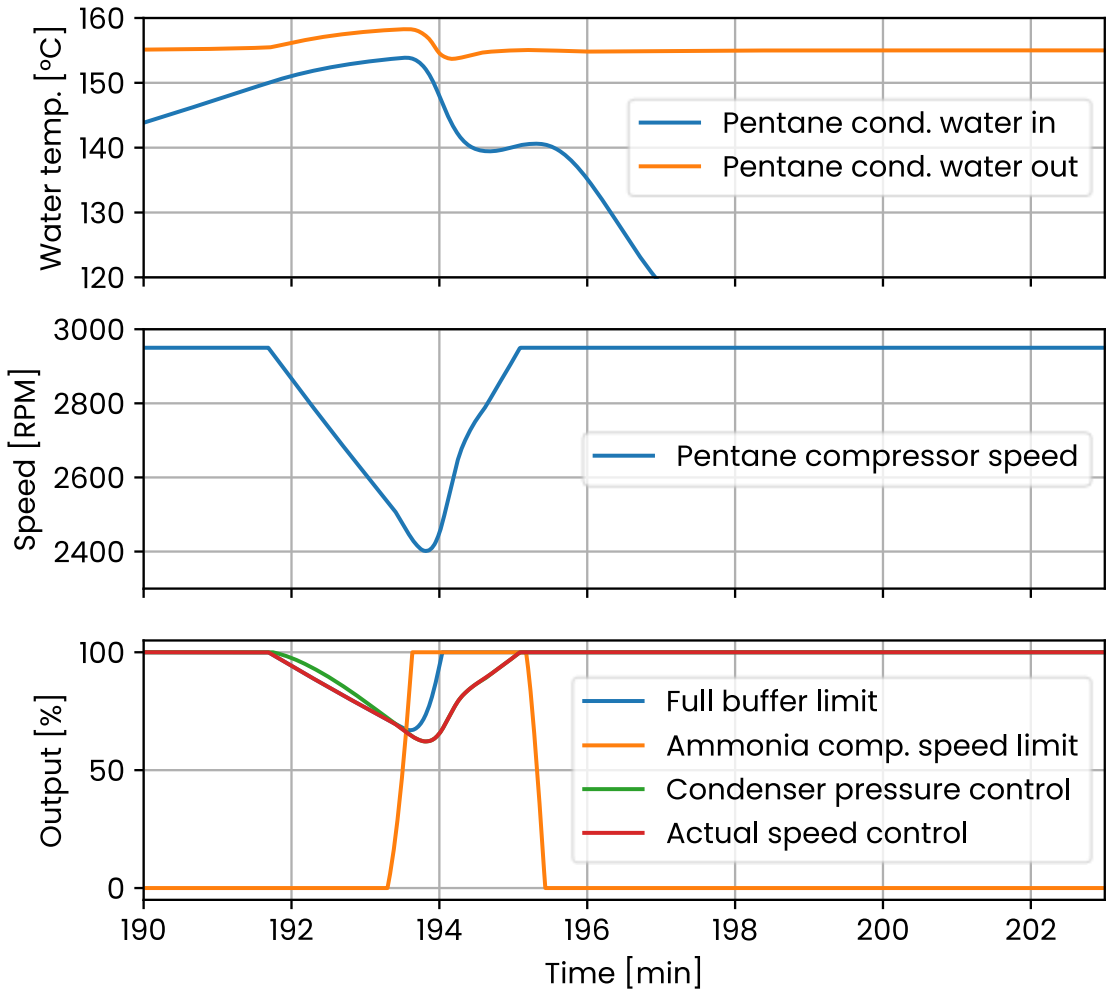


Figure 2.22: Simulation results between 190 and 203 minutes for the 33 °C / 48.barg configuration. The inlet and outlet water temperature of the pentane condenser (top), the pentane compressor speed (middle), and the control outputs of the full buffer limiter, ammonia compressor speed control limiter, condenser pressure control and the actual speed control (bottom).

Funded by the European Union

Views and opinions expressed are however those of the author(s) only and do not necessarily reflect those of the European Union or CINEA. Neither the European Union nor the granting authority can be held responsible for them.

Figure 2.23 depicts the effect of changing the control of the cold buffer storage tank bypass valve from the top to the bottom tank temperature for the 2nd and 3rd cold batch. The second batch at 80 min is no longer mostly skipped and the bottom temperature rises from 23 °C to 51 °C, compared to 34 °C for the base case. The downside is the effect on the top buffer temperature (blue line), which drops significantly during the batch. The water pump feeding the ammonia evaporator responds quickly enough, avoiding significant changes in the ammonia evaporator pressure. Where the original strategy maintained a level of stratification, the new control yields a nearly isothermal temperature profile over the tank during a batch (the blue, orange and green lines are on top of each other). This is of no consequence for the performance of the cascade heat pump, as long as the average tank temperature is well above the temperature setpoint used for the ammonia evaporator water outlet.

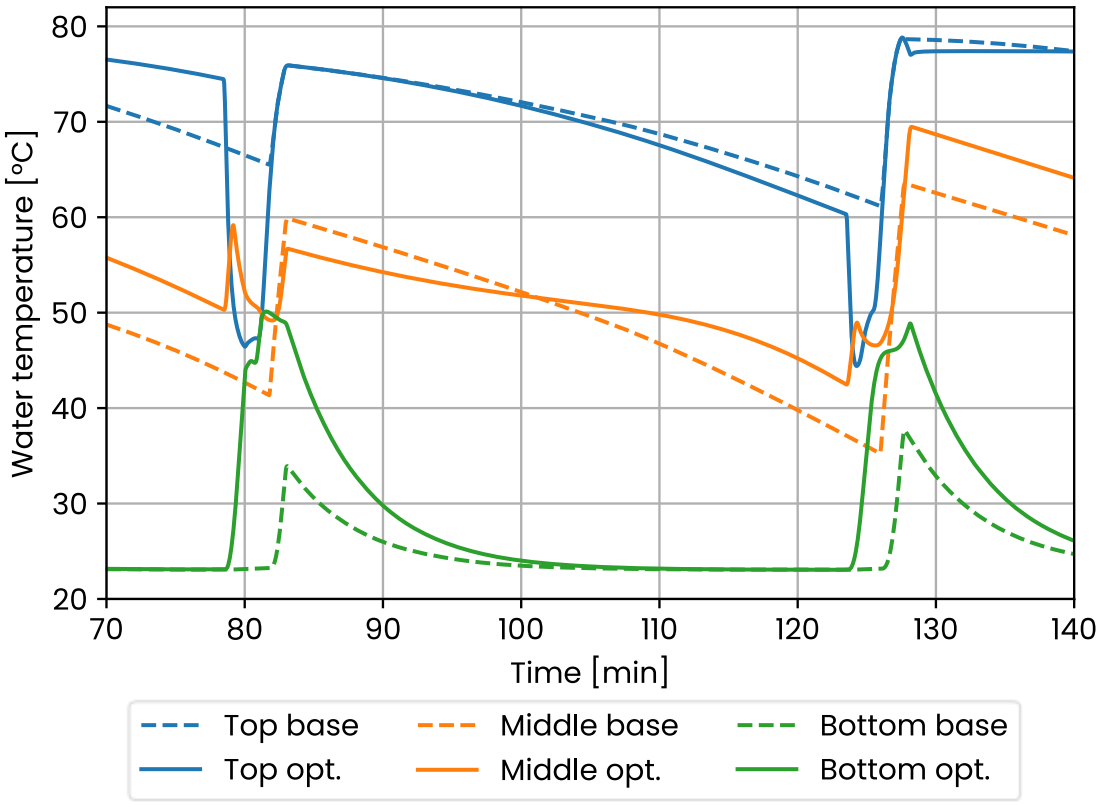


Figure 2.23: Cold buffer storage tank top, middle and bottom temperatures for the baseline and optimized configuration (23 °C / 42 barg). The baseline configuration is depicted by the dashed lines, whereas the optimized configuration is shown in continuous lines.

Funded by the European Union

Views and opinions expressed are however those of the author(s) only and do not necessarily reflect those of the European Union or CINEA. Neither the European Union nor the granting authority can be held responsible for them.

2.6 Discussion

The parameters identified for the optimization, the ammonia evaporator water outlet temperature and the ammonia condenser pressure, have a strong influence on both the amount of useful heat produced and the COP. For the baseline control system, the water temperature setpoint is chosen to reflect the operating conditions at Stella Polaris. Optimization of this setpoint yields a clear improvement of the COP. At 23 °C water temperature setpoint, the ammonia evaporates at about 18 °C (7.1 barg). The optimization raises this to ~32 °C (11.4 barg) for the simulation with the highest COP or ~27 °C (9.7 barg) for the variant with the highest heat output. On the condenser side, the base case saturation temperature of 82 °C changes to ~88 °C for the Q_{hot} optimized variant. For the simulation with the highest efficiency this stays the same.

The volume of 10 m³ chosen for the cold storage tank is proven to be adequate. Sufficient waste heat coming from the press section is buffered to avoid a reduction in ammonia evaporator pressure due to a depleted storage. A larger volume could be beneficial for higher water temperature setpoints, since the difference with the maximum waste heat temperature coming from the press decreases, which reduces the amount of sensible heat that the heat pump can be utilized. The topmost water temperature setpoint investigated is 39 °C, although all the simulations resulted in a trip. At the setpoint below of 38 °C, only the simulation with the lowest condenser pressure setting of 42 barg finishes successfully. The sudden increase in water temperature entering the ammonia evaporator during a batch, when the cold storage tank is recharged, is identified as a common cause for the trips. Figure 2.24 depicts how this could be alleviated by adding a three-way valve between the cold storage and the pump feeding the ammonia evaporator. Instead of directly coupling the top of the tank to the ammonia evaporator water inlet, the temperature entering the evaporator is controlled at a fixed setpoint by the 3-way valve. This should allow for sufficient damping of the temperature changes.

Funded by the European Union

Views and opinions expressed are however those of the author(s) only and do not necessarily reflect those of the European Union or CINEA. Neither the European Union nor the granting authority can be held responsible for them.

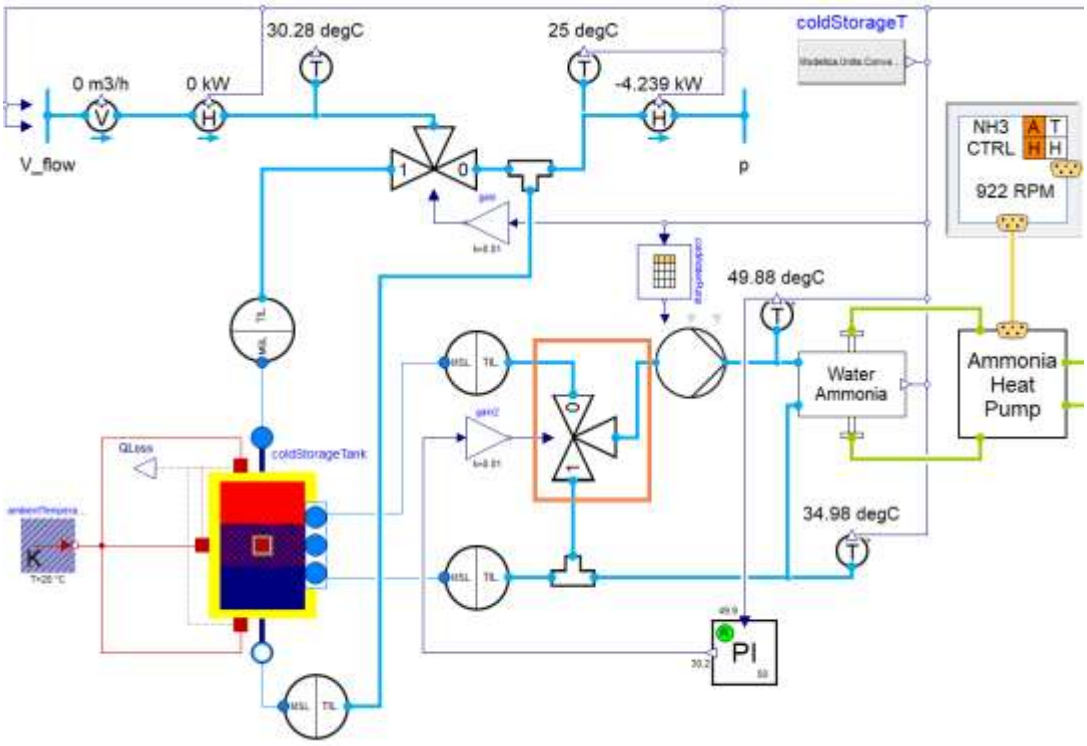


Figure 2.24: An additional 3-way valve (orange rectangle) is added between the cold storage tank and the pump feeding the ammonia evaporator. The control is based on the water temperature entering the evaporator.

The sizing of the hot buffer storage tank at 15 m³ matches well with the base case configuration. The top temperature of the buffer shows a decline of about 5-8 °C when heat is utilized during a batch. A too small buffer would show a larger temperature decline. For the optimized cases, a larger buffer size would be of interest. The pentane heat pump has to reduce its output during some parts of the simulation due to a fully charged buffer. Further investigation will be needed on this front, since the increasing buffer size comes with economic implications.

In the current topology, the hot buffer has the water inlet at the bottom of the tank. As observed in Figure 2.12, this results in a temperature inversion and loss of stratification during some parts of the simulation, which negatively impacts the efficiency. A potential fix would be to add an additional water inlet, for example at the middle of the tank, and to control the inlet being used based on the temperature of the water being fed to the tank. If the water temperature is above the bottom tank temperature, then the inlet higher up the tank should be used for the water entering the tank. The optimal location of one or more additional inlets and to quantify the benefits of this configuration, is the subject of further study.

Funded by the European Union

Views and opinions expressed are however those of the author(s) only and do not necessarily reflect those of the European Union or CINEA. Neither the European Union nor the granting authority can be held responsible for them.

For the cascade heat pump, it was shown that the unmodified baseline control system was sufficiently robust to be integrated with the variable load case. The simulation completed without any trips and the performance could be analysed. From the start, it was clear that the pentane heat pump would not able to satisfy the full amount of heat required by the press. Up to the maximum temperature of 155 °C, the cascade heat pump has enough capacity. Providing heat above this temperature would require a redesign of the cascade heat pump with alternative working media. For example, switching from pentane to cyclopentane would increase the temperature limit to 173 °C at the same pressure level. For the bottom ammonia cycle, a similar analysis will determine if it makes sense to switch to a different working medium for further increasing the cascading temperature.

With respect to the initial conditions, the starting temperature of the hot and cold buffer tanks has been chosen arbitrarily. Similarly, the relative timing between the first hot batch and startup of the cascade heat pump, for which only a cold start scenario is investigated, has not been varied. Alternative scenarios would be a hot (re)start of the cascade heat pump with changed buffer temperatures. Although no significant effect on the performance is expected, the robustness of the control system could be investigated for the different starting conditions.

2.7 Conclusion

The digital twin simulation model of the Demo 1 cascade heat pump was successfully integrated with a variable load case. The batch process of high pressure laminate production proved to be an adequate match with the operating limits of the cascade heat pump. Minor adjustments were required within the heat pump model itself for the integration with the hot and cold buffer storage tanks that feed the laminate production process. The main change was to replace the plate & shell heat exchanger used for producing steam, with a plate & plate heat exchanger for producing hot water.

The baseline control system of the cascade heat pump, as designed by Mayekawa for the Stella Polaris case, could be used as is for the variable load case, and yielded an overall COP of 1.54. The new control system designed for the water pumps feeding ammonia evaporator and pentane condenser, proved to be sufficiently robust. A similar conclusion can be drawn for the control of the bypass valve of the hot and cold buffer storage tanks.

The optimization was mainly focused on the ammonia heat pump, since both the evaporator pressure, determined by the water temperature setpoint, and the

Funded by the European Union

Views and opinions expressed are however those of the author(s) only and do not necessarily reflect those of the European Union or CINEA. Neither the European Union nor the granting authority can be held responsible for them.

condenser pressure setpoint were changed. This effectively resulted in the ammonia heat pump operating in off-design conditions. For the pentane heat pump only minor differences in operating conditions were observed. The increased cascading temperature, set by the ammonia condenser pressure setpoint, raises the evaporator pressure of the pentane heat pump, which also improves the maximum capacity (i.e. pentane condenser duty).

Due to the computational cost for each simulation, a limited combination of parameter settings was investigated, with 38 variants in total. Two different optima were identified, the first showing the highest COP and the second providing the most useful heat from the hot buffer storage tank. In case of the first, the COP improves to 1.84 (+0.30 or 19% above the baseline performance), whereas the amount of useful heat remains similar. For the second optimum, 0.21 GJ of additional useful heat is provided per batch, an improvement of 13% over the baseline amount of 1.66 GJ. The COP for this optimum still shows an increase to 1.70, although the efficiency is not as good as the first optimum. It should be noted that the performance observed is specific for the 3 batches for which measurement data was available, the initial conditions chosen and the timing of the first batch relative to startup of the heat pump. Further study is needed to vary these, although the expectation is that the improvements shown as a result of the optimization process, will be upheld.

Funded by the European Union

Views and opinions expressed are however those of the author(s) only and do not necessarily reflect those of the European Union or CINEA. Neither the European Union nor the granting authority can be held responsible for them.

3. CASE 2 – GEA & DTI

3.1 Case description

The chosen case introduces an autoclave as the consumer on the sink side and uses the autoclave cooling water as the heat source.

The autoclave load is cyclical in its nature, as it is a batch process where cold beverages enter the autoclave and are subsequently heated up to the required temperature and then cooled down again. There is also a discrepancy in time between when the source heat is available and the sink heat is needed, as the source heat is provided by the cooling of the autoclave, which happens after the heating is finished.

The hypothetical use case of the autoclave is to sterilize dairy beverages in cans and glass bottles. This means that the autoclave is required to reach a temperature of around 110 °C for the sterilization to be effective. The case is based on a representative case from actual operating data from a plant. The data is however anonymized and altered due to confidentiality.

Figure 3.1 shows the temperature profile used for the beverages. This is the temperature profile that the beverages must follow for the sterilization process to be effective. The cycle time is relatively long, at 80 minutes in total, with a heating phase of 20 minutes, a constant temperature holding phase of 20 minutes, and a cooling phase of 30 minutes, followed by 10 minutes of recharging the autoclave with product.

Funded by the European Union

Views and opinions expressed are however those of the author(s) only and do not necessarily reflect those of the European Union or CINEA. Neither the European Union nor the granting authority can be held responsible for them.

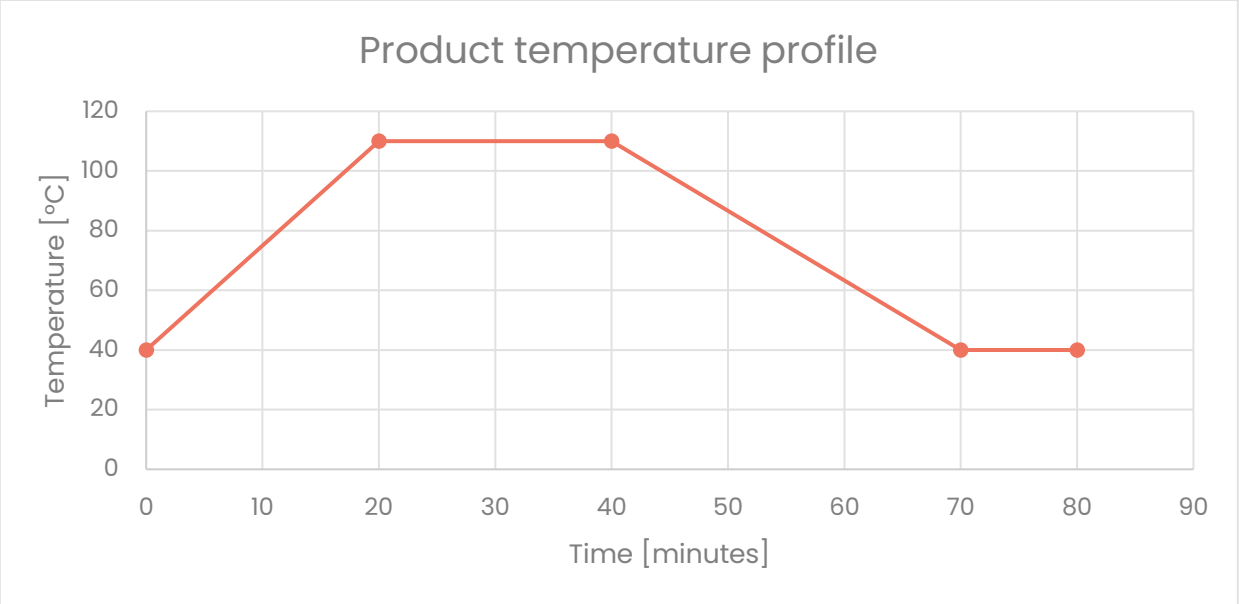


Figure 3.1 - Temperature profile that the beverages must follow.

The autoclave is sized such that the peak heating load is larger than the capacity of the heat pump. The autoclave is modelled to have a heat capacity of roughly 80.000 kJ/K, and it must be heated from 40 °C to 110 °C over 20 minutes, meaning an average heating load of around 4.7 MW during the heating phase. Meanwhile the heating capacity of the heat pump varies with the operating conditions, but peaks during the conditions of this case at 2.2 MW. This means that the steam accumulator must be charged sufficiently high enough, to provide the excess heating needed that cannot be covered by the heat pump.

3.2 Heat pump integration

A diagram of the integration is shown in Figure 3.2.

On the sink side a steam accumulator is placed, to balance out the load of the autoclave. A pump circulates the condensate from the bottom of the accumulator through the condenser of the heat pump. A thermosyphon setup could also have been employed. During the heating phase the steam is injected into the autoclave, heating the autoclave and its contents up, and, in the process, condensing the steam which is then returned to the steam accumulator.

On the source side a stratified hot water tank is placed. During the cooling phase, water from the cold side of the tank is pumped to the autoclave, heating the water up

Funded by the European Union

Views and opinions expressed are however those of the author(s) only and do not necessarily reflect those of the European Union or CINEA. Neither the European Union nor the granting authority can be held responsible for them.

and cooling the autoclave, before it is returned to the top of the hot water tank. A cooling tower with a bypass valve is added to the forward line, to be able to cool the water down further during the coldest part of the cooling phase. The cooling tower bypass controls are set to ensure that the water temperature going to the autoclave is at least 20 K lower than the desired autoclave temperature profile at any given time.

A bypass valve is added on the return side of the cooling water. This allows for controlling the temperature that the hot water tank is charged with.

On the evaporator side of the source water loop a three-way control valve is placed after the evaporator. This valve controls where the return water is injected into the tank, either into the middle or at the bottom. This is controlled based on the temperature of the return water from the evaporator. At above 50 °C the water is sent to the middle of the tank, and below 50 °C it is sent to the bottom. This helps to prevent mixing the temperature levels in the tank.

Funded by the European Union

Views and opinions expressed are however those of the author(s) only and do not necessarily reflect those of the European Union or CINEA. Neither the European Union nor the granting authority can be held responsible for them.

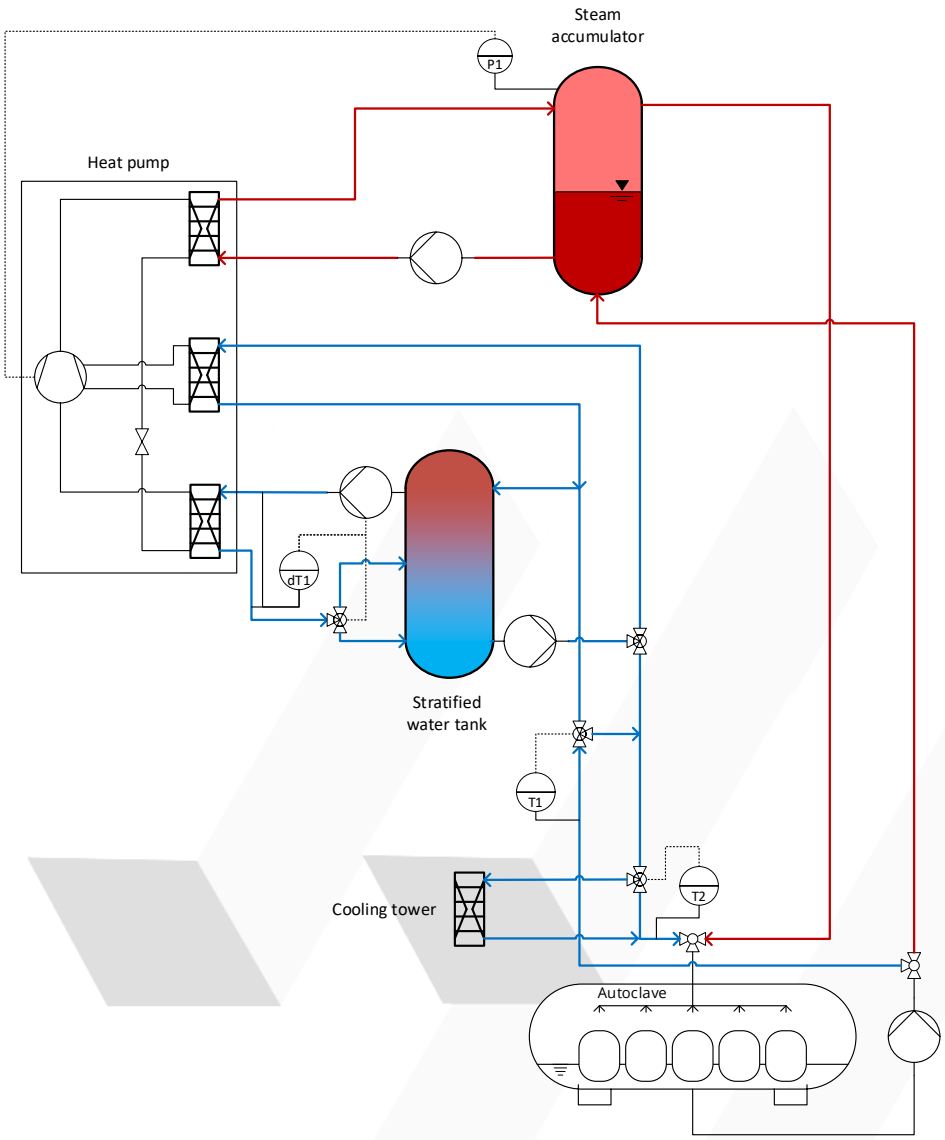


Figure 3.2 A diagram of the heat pump integration with the autoclave

3.3 Methodology and goals

3.3.1 Optimization parameters and goal

The goal of the optimization is to reduce total energy consumption of the heat pump.

On the source side, two parameters for optimization have been identified. The first is the temperature difference setpoint of the pump that feeds water from the hot water tank to the evaporator. This is illustrated in Figure 3.2 by the sensor dT1. A smaller

Funded by the European Union

Views and opinions expressed are however those of the author(s) only and do not necessarily reflect those of the European Union or CINEA. Neither the European Union nor the granting authority can be held responsible for them.

temperature difference will result in a higher evaporation temperature for a given water inlet temperature. On the other hand, it also increases mixing in the storage tank, potentially leading to lower inlet temperatures on average. The pump power will also increase, but this has not been included in this analysis.

The second parameter on the source side is the setpoint for the bypass valve on the cooling water return side. This is shown in Figure 3.2 by the sensor T1. Increasing the setpoint increases the minimum temperature of the return water, but it will also decrease the total flow of water to the storage tank.

The final parameter is the pressure setpoint of the steam accumulator. This is shown in Figure 3.2 by the sensor P1. For a given size of the steam accumulator it is desired to have as low a pressure as possible while still being able to store enough energy to heat up the accumulator.

3.3.2 Methodology

Running 15 cycles of the autoclave in the model, takes around 30 minutes. This means that the model is not suitable for optimization using optimization algorithms within a reasonable timeframe, as the number of calculations they require would lead to very long running times. The time required to trouble shoot and fix potential errors combined would also be extensive. For this reason, a parameter sweep method has been employed instead.

The parameter sweep method means that the calculation is run for a number of different setpoints for each of the chosen parameters, after which the results for each calculation are compared. This gives an overview of the impact of changing each parameter in isolation.

3.4 Results

3.4.1 Accumulator size and pressure setpoint

This analysis seeks to determine the minimum pressure setpoint for the steam accumulator for three different sizes of steam accumulators and to compare the performances of the three optimums.

The minimum required setpoint is for this task defined as the setpoint that results in the system being able to bring the autoclave up to the required max temperature of

Funded by the European Union

Views and opinions expressed are however those of the author(s) only and do not necessarily reflect those of the European Union or CINEA. Neither the European Union nor the granting authority can be held responsible for them.

110 °C at a maximum of 200 seconds after the time defined by the temperature set profile. Figure 3.3 shows the temperature profile of the last autoclave cycle out of 15 for the case of a 70 m^3 steam accumulator.

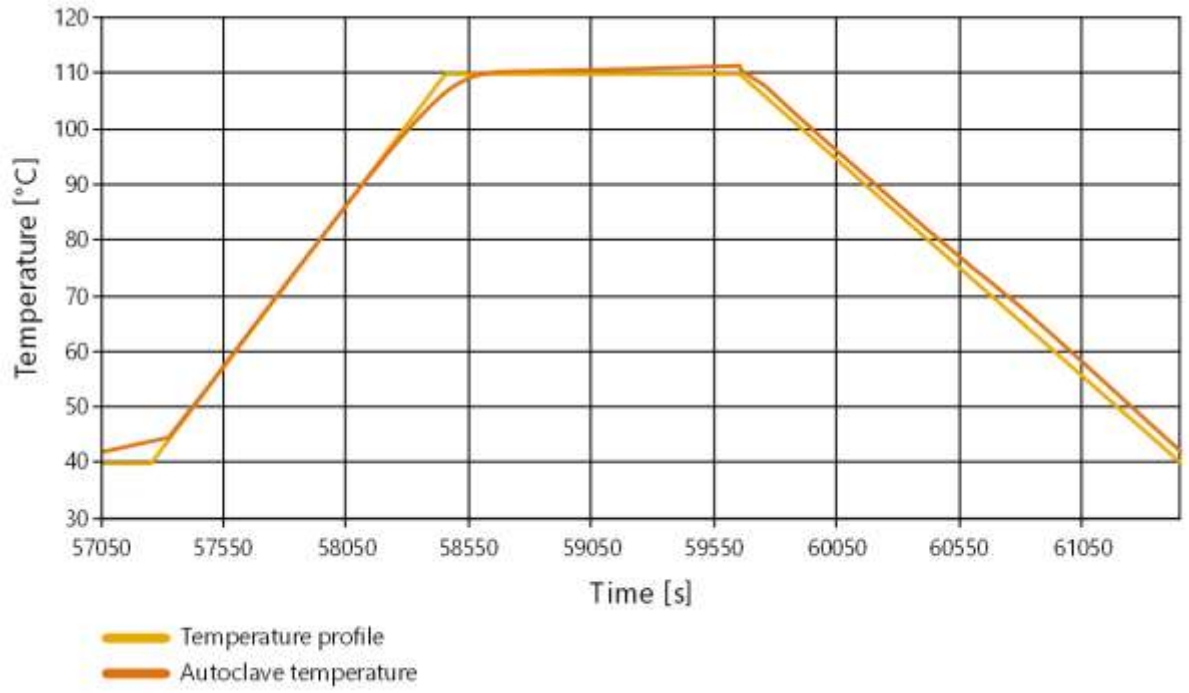


Figure 3.3 The autoclave temperature profile with the actual autoclave temperature for the 70 m^3 case overlaid.

Figure 3.4 shows a graph of the energy use of the compressor and the heat transferred to the condenser during the last of the autoclave cycles for each of the three different cases.

Funded by the European Union

Views and opinions expressed are however those of the author(s) only and do not necessarily reflect those of the European Union or CINEA. Neither the European Union nor the granting authority can be held responsible for them.

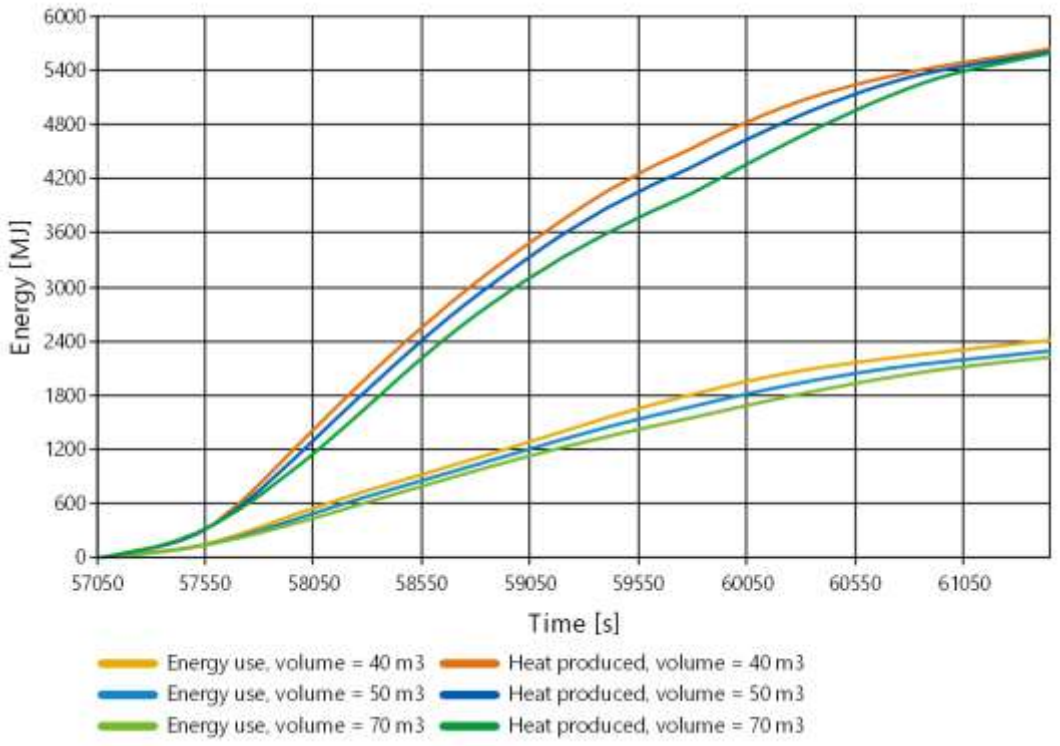


Figure 3.4 Energy use and heat production over time for the 15th autoclave cycle

The results are further summarized in Table 3.1. There is a trend of noticeably higher COP for a larger accumulator size, although this comes at a trade-off of increased CAPEX.

Table 3.1 Results for the three cases

Accumulator size [m³]	Pressure setpoint [bar]	Heat produced [MJ]	Energy use [MJ]	COP
40	3.7	5650	2420	2.33
50	3.2	5620	2302	2.44
70	2.85	5602	2230	2.51

Funded by the European Union

Views and opinions expressed are however those of the author(s) only and do not necessarily reflect those of the European Union or CINEA. Neither the European Union nor the granting authority can be held responsible for them.

3.4.2 Evaporator source pump setpoint

The pump on the source side determines the temperature glide of the water across the evaporator. For an evaporation process, the smaller the temperature glide the better, especially in a flooded evaporator with no superheating as is the case for this system. This is because the evaporation temperature is determined by the outlet temperature of the water and thus a smaller glide results in a higher evaporation temperature. On the other hand, an increased flow rate will result in more mixing in the stratified water tank, potentially leading to lower average temperatures going to the evaporator.

The area under investigation is shown in Figure 3.5. To investigate the optimal temperature glide, four different setpoints for dT1 have been analysed for the 70 m^3 steam accumulator case. These setpoints are 2.5 K, 5 K, 10 K and 20 K. The three-way valve controls are not changed between cases.

The energy use and heat produced over the 15th autoclave cycle for each case is shown in Figure 3.6. It is clear that the 20 K temperature difference setpoint results in a noticeably worse COP, as the heat production is lower and the energy use is higher than for the 5 K and 10 K glide setpoints.

Funded by the European Union

Views and opinions expressed are however those of the author(s) only and do not necessarily reflect those of the European Union or CINEA. Neither the European Union nor the granting authority can be held responsible for them.

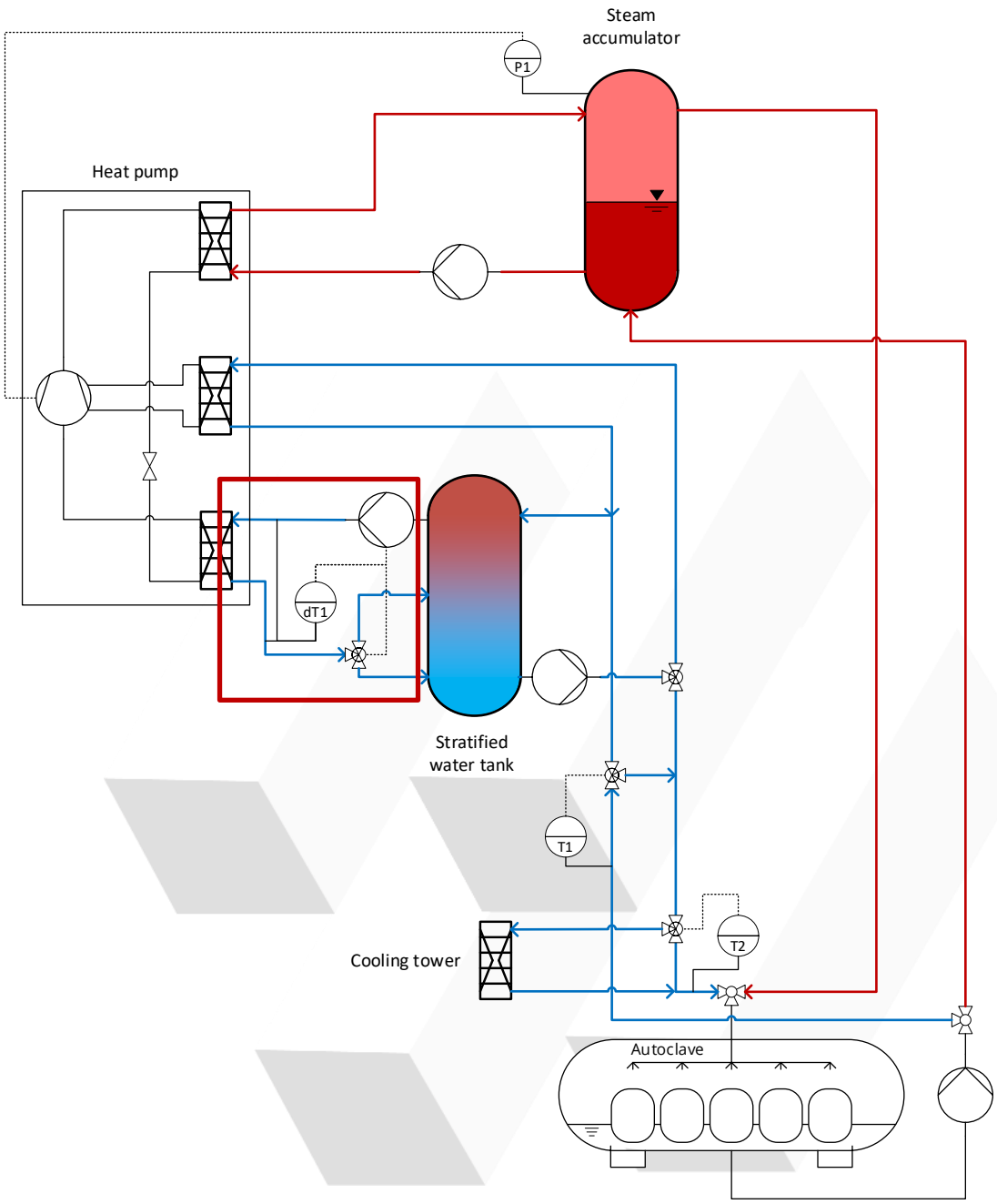


Figure 3.5 The evaporator pump and temperature difference sensor are highlighted in the red box

Funded by
the European Union

Views and opinions expressed are however those of the author(s) only and do not necessarily reflect those of the European Union or CINEA. Neither the European Union nor the granting authority can be held responsible for them.

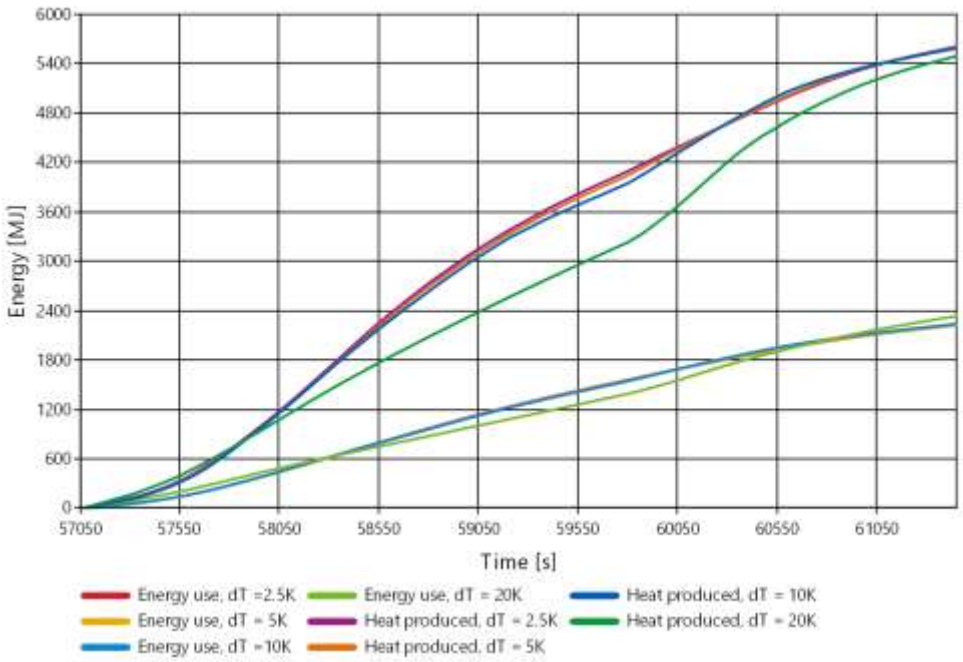


Figure 3.6 Energy use and heat production for the four cases

Table 3.2 shows the resulting energy use, heat production and COP, for the time-period. The COP is highest for the 5 K glide setpoint, but with only a slight improvement over the 10 K setpoint. Meanwhile the 20 K setpoint performs far worse.

Table 3.2 Summarized results for the four cases

Source dT [K]	Heat produced [MJ]	Energy use [MJ]	COP
2.5	5616	2234	2.51
5	5606	2231	2.51
10	5598	2246	2.49
20	5508	2343	2.35

Funded by the European Union

Views and opinions expressed are however those of the author(s) only and do not necessarily reflect those of the European Union or CINEA. Neither the European Union nor the granting authority can be held responsible for them.

Figure 3.7 shows the temperature at the top of the stratified water tank, where the outlet to the evaporator is placed. Generally, there is a trend of lower temperatures at the top of the tank for a lower temperature glide setpoint. On its own this should result in a worse COP for the heat pump, but it must seemingly be counteracted by the decreased temperature glide to a large enough extent for this case where it does not result in a lower COP for a lower temperature glide.

The effects of mixing may also have been more pronounced if it were not for the three-way control valve on the evaporator return water side, as this prevents high temperature water from being injected at the bottom of the tank and keeps a relative high-temperature zone at the top of the tank, despite a high water-flow.

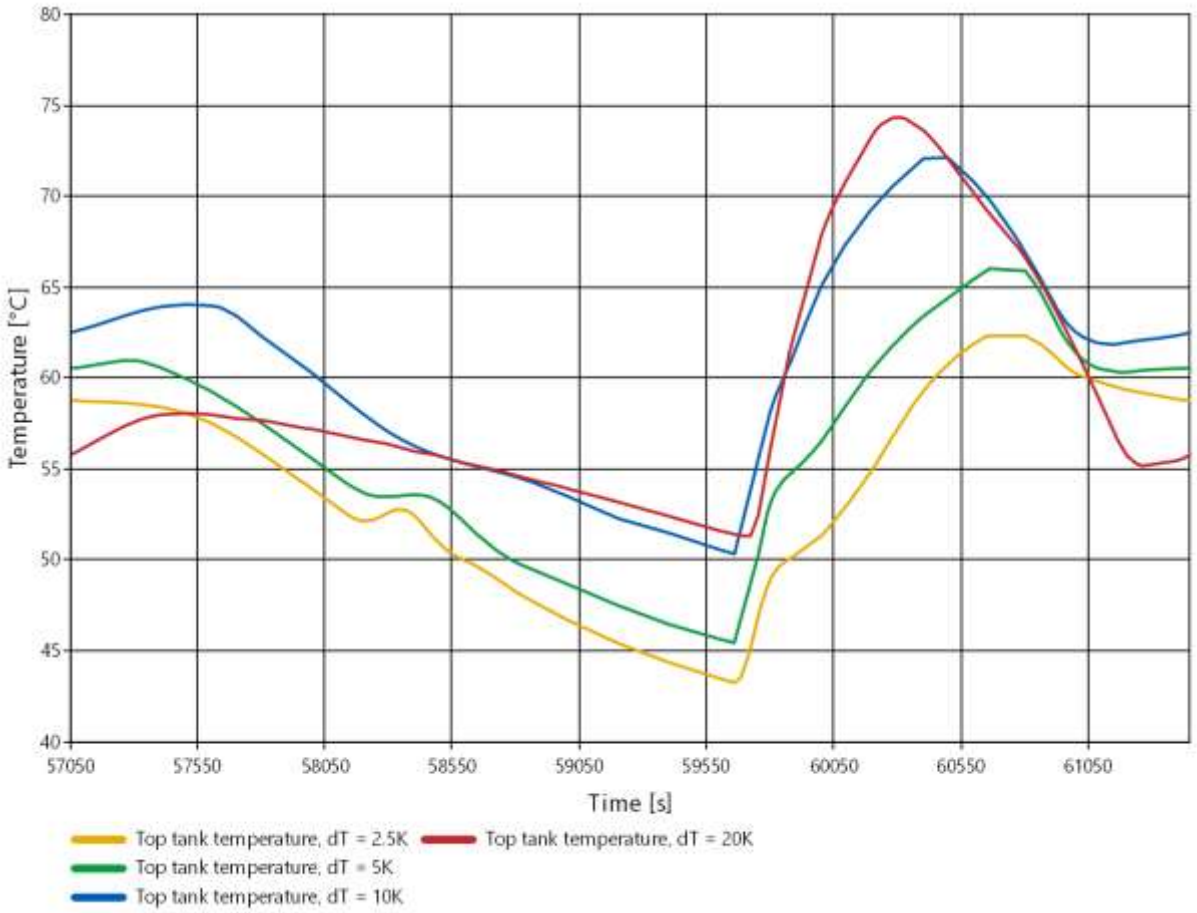


Figure 3.7 - Temperature at the top of the stratified water tank.

Funded by the European Union

Views and opinions expressed are however those of the author(s) only and do not necessarily reflect those of the European Union or CINEA. Neither the European Union nor the granting authority can be held responsible for them.

3.4.3 Cooling water return-bypass setpoint

The return water bypass helps to control the temperature at which water is returned to the hot water tank. With an optimal setting this reduces the amount of heat that is wasted in the cooling tower and increases the average temperature in the stratified water tank. The area under investigation is marked in Figure 3.8.

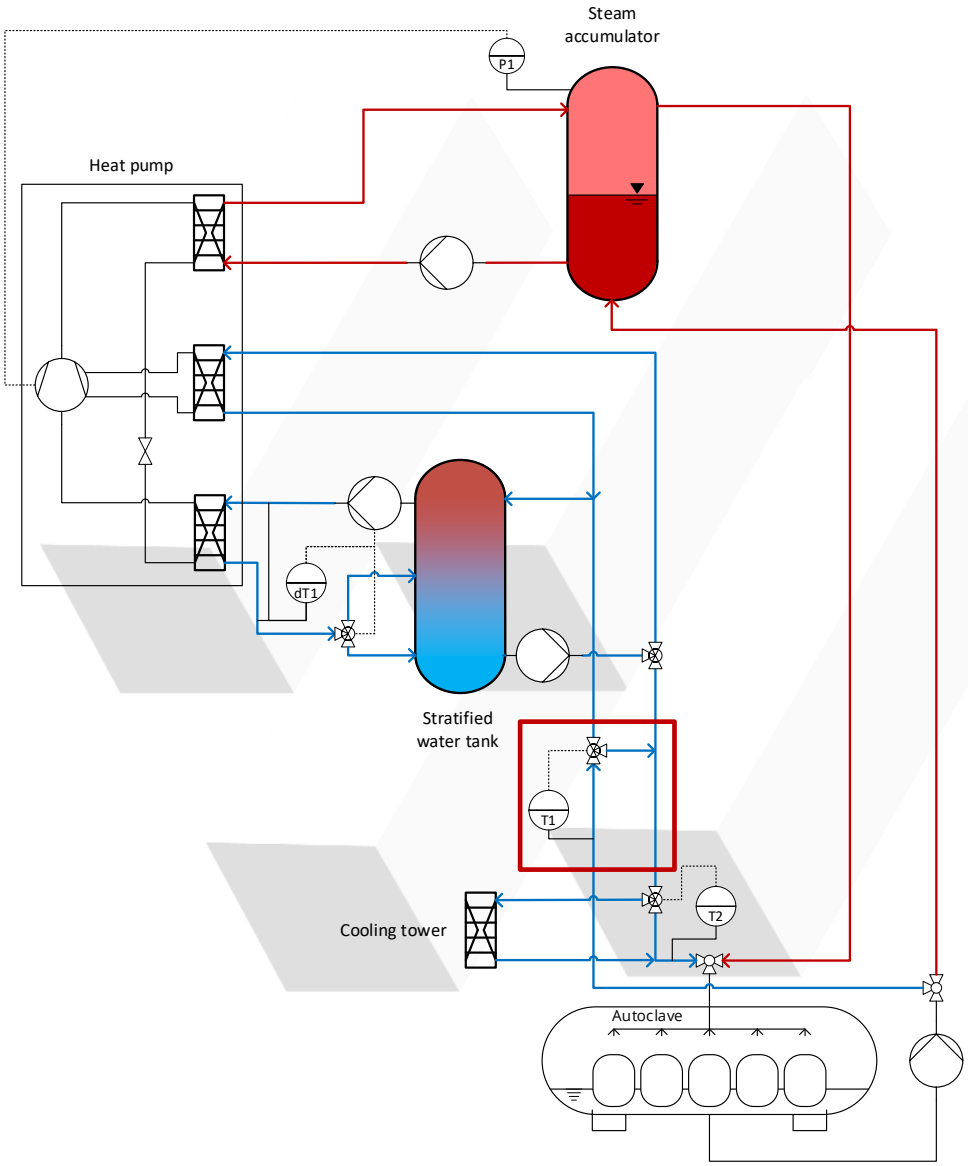


Figure 3.8 Diagram of the integration. The cooling water return bypass is highlighted

Four different setpoints activation of the three-way valve have been investigated in this analysis, 40 °C, 50 °C, 60 °C and 70 °C. For all the setpoints, the source temperature

Funded by
the European Union

Views and opinions expressed are however those of the author(s) only and do not necessarily reflect those of the European Union or CINEA. Neither the European Union nor the granting authority can be held responsible for them.

glide setpoint is set to 10 K. The resulting energy use and heat production for the 15th cycle is shown in Figure 3.9.

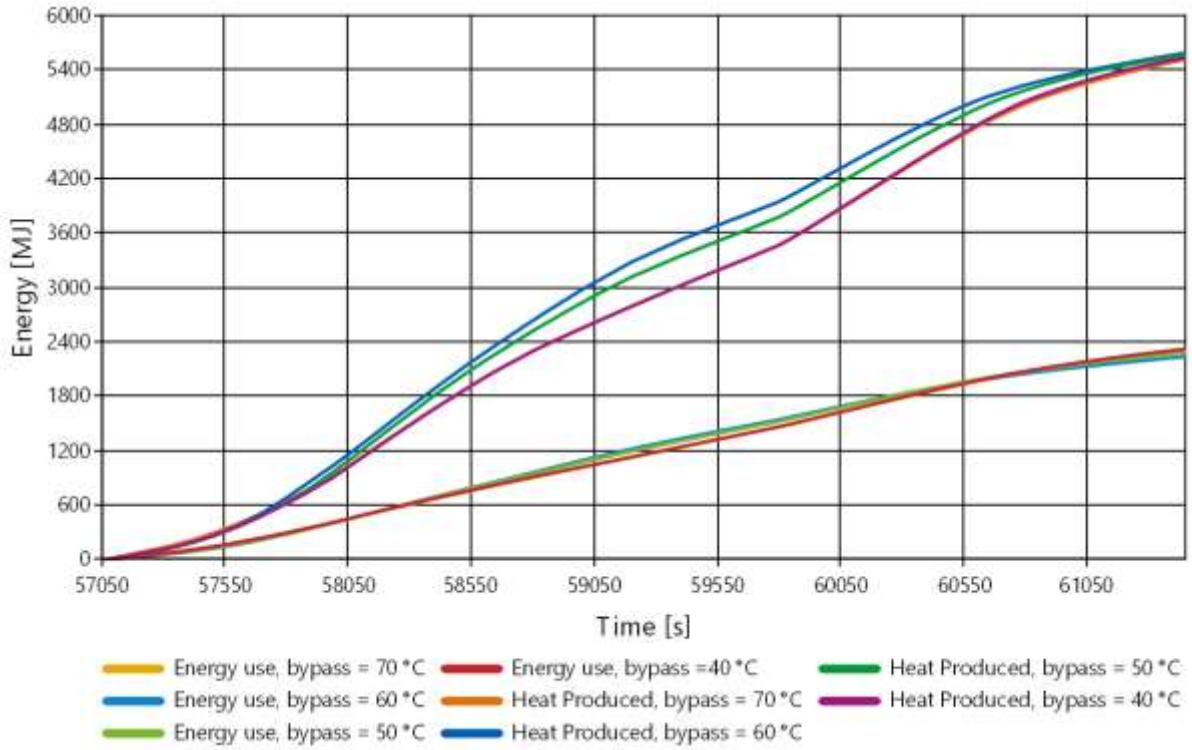


Figure 3.9 - Energy use and heat production for the 15th cycle.

Table 3.3 shows the results in tabular form. Here it can be seen that the 60 °C setpoint results in the highest COP, 4.6 % higher than the lowest of the modelled setpoints.

Table 3.3 Summarized results for the four bypass setpoint cases

Return bypass setpoint [°C]	Heat produced [MJ]	Energy use [MJ]	COP
70	5529	2325	2.38
60	5598	2248	2.49
50	5574	2290	2.43
40	5544	2333	2.38

Funded by the European Union

Views and opinions expressed are however those of the author(s) only and do not necessarily reflect those of the European Union or CINEA. Neither the European Union nor the granting authority can be held responsible for them.

Table 3.4 shows the energy lost in the cooling tower for the 15th autoclave cycle. A higher bypass setpoint temperature results in less heat being lost.

Table 3.4 - Energy lost in the cooling tower for the 15th autoclave cycle.

Return bypass setpoint [°C]	Heat lost in cooling tower during the 15th cycle [MJ]
70	27.1
60	122
50	151
40	217

Figure 3.10 shows the temperature at the top of the hot water tank for the four setpoints. Here it is clear that the temperature is largest for the most optimal setting of 60 °C.

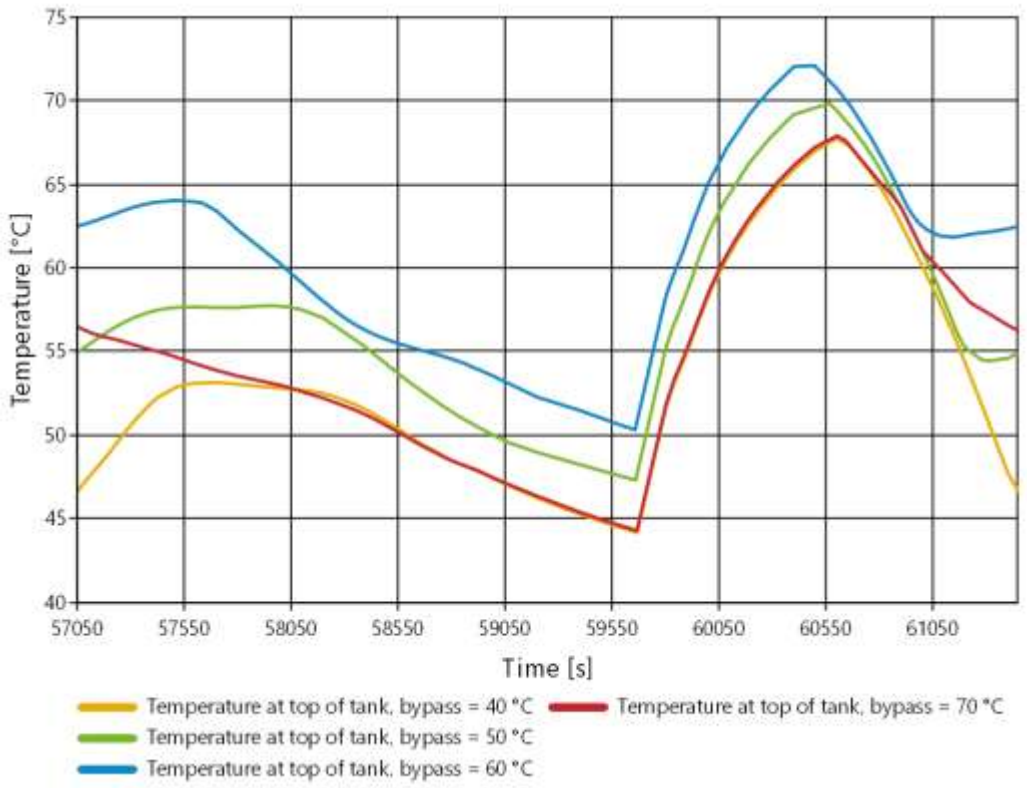


Figure 3.10 - Temperature at the top of the hot water tank for the four setpoints.

Funded by the European Union

Views and opinions expressed are however those of the author(s) only and do not necessarily reflect those of the European Union or CINEA. Neither the European Union nor the granting authority can be held responsible for them.

3.5 Discussion

The analysis performed for this demo case show that there are significant energy efficiency gains to be achieved by optimizing the controls of a variable load energy source. The controls of the heat pump itself have not been investigated, except for controlling the compressor speed to reach the desired steam accumulator pressure setpoint, as the heat pump is relatively simple in its control design, and as such there is not much room for changing parameters. Instead focus has been placed on the controls related to the external heat source and heat sink.

For this case, where a stratified hot water tank is used on the source side to feed the evaporator, it is evident that a larger water flow from the hot water tank is preferable, as it results in a smaller temperature difference on the source side of the evaporator leading to higher evaporation temperatures. This is despite the fact that a larger flow results in more mixing in the hot water tank, because this mixing does not result in consistently lower evaporation temperatures for cases that have been analysed. The fact that mixing is not more of a problem is possibly because of the use of a three-way control valve on the return water side from the evaporator that helps to maintain the stratification within the hot water tank.

The analysis shows that controlling a bypass on the return side of the heat source allows for controlling the temperature at which the hot storage tank is charged. The bypass leads back through a cooling tower to reach the desired temperature and then back to the autoclave. This ensures that the autoclave can be sufficiently cooled, while also controlling charging temperature of the hot water tank.

The model results show that there are inherently no issues with operating the heat pump under a variable sink and source load. The temperatures chosen in this case did however prove to not be ideal for the heat pump. The suction and discharge pressures for the final autoclave cycle is shown in Figure 3.11. The suction temperature nearly goes below atmospheric pressure, added a higher risk of air entering the system with the chosen refrigerant.

The pressure ratio is shown in Figure 3.12. At certain points the pressure ratio peaks at above 9, which is in the high end for a single screw compressor. This could however be solved by using two compressors in series or cascade mode, providing similar results of this study.

Funded by the European Union

Views and opinions expressed are however those of the author(s) only and do not necessarily reflect those of the European Union or CINEA. Neither the European Union nor the granting authority can be held responsible for them.

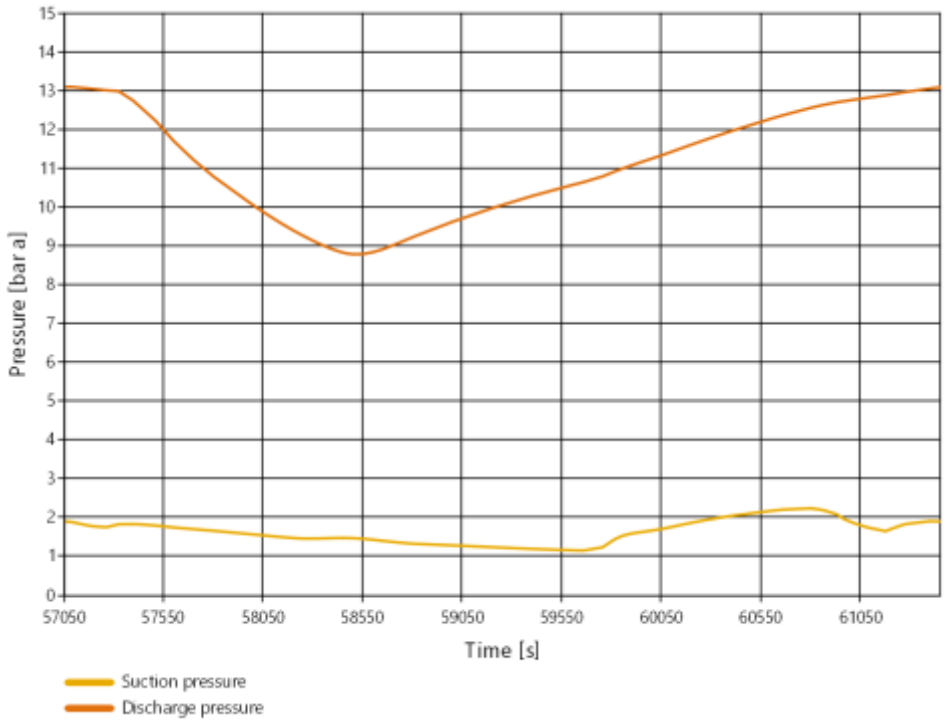


Figure 3.11 Suction and discharge pressures for the 15th autoclave cycle

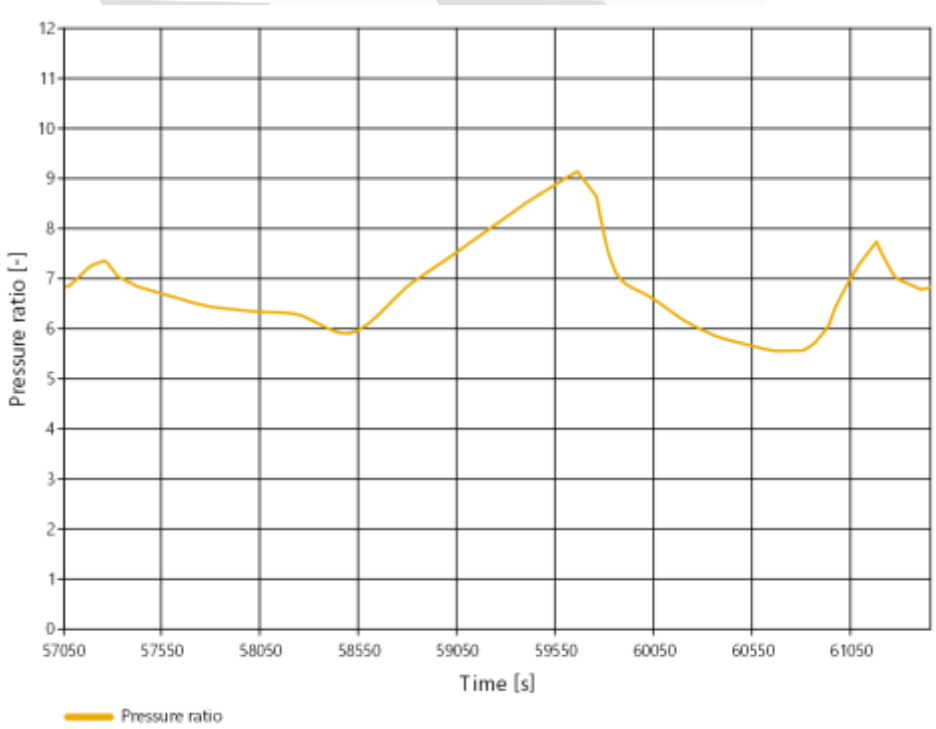


Figure 3.12 Pressure ratio for the 15th autoclave cycle

Funded by the European Union

Views and opinions expressed are however those of the author(s) only and do not necessarily reflect those of the European Union or CINEA. Neither the European Union nor the granting authority can be held responsible for them.

3.6 Conclusion

This case study investigated the operation and optimization of a heat pump integrated with a variable autoclave process. The autoclave represents a cyclic batch load, where heat is required during the heating and holding phases, while useful source heat becomes available later during the cooling phase. To manage this mismatch, the heat pump system was integrated with a steam accumulator on the sink side and a stratified hot water tank on the source side. A cooling tower and bypass arrangement were included to ensure sufficient cooling of the autoclave while recovering as much useful heat as possible.

Three main control parameters were investigated: the steam accumulator size and associated pressure setpoint, the temperature difference setpoint across the evaporator source-water loop, and the return-water bypass temperature setpoint on the autoclave cooling circuit. The optimization was carried out using parameter sweeps, as the simulation time of the dynamic model made algorithm-based optimization impractical within the scope of the study.

The results show that all three parameters have a clear influence on the heat pump performance. Increasing the steam accumulator size allowed the system to operate at a lower pressure setpoint while still meeting the autoclave heating demand. This reduced the average sink temperature and improved the COP. Among the investigated accumulator sizes, the 70 m³ accumulator achieved the best performance, with a COP of 2.51 compared to 2.33 for the 40 m³ case.

For the evaporator source-water pump, lower temperature glide setpoints generally improved performance by increasing the evaporation temperature. The best performance was obtained for the 2.5 K and 5 K setpoints, both resulting in a COP of approximately 2.51. However, further reductions in temperature glide may lead to very high flow rates and increased pump energy consumption, which was not included in this analysis. Therefore, a 5 K setpoint appears to be a reasonable compromise between heat pump performance and expected practical operation.

The return-water bypass setpoint also had a significant effect on system performance. The best result was obtained with a bypass setpoint of 60 °C, giving a COP of 2.49. At lower setpoints, more water was returned to the storage tank but at a lower temperature, reducing the usefulness of the stored heat. At higher setpoints, less heat was transferred to the storage tank, which also reduced performance. This

Funded by the European Union

Views and opinions expressed are however those of the author(s) only and do not necessarily reflect those of the European Union or CINEA. Neither the European Union nor the granting authority can be held responsible for them.

demonstrates the importance of controlling not only the amount of recovered heat, but also the temperature level at which it is stored.

Overall, the study shows that the heat pump can be operated under the strongly variable source and sink conditions of the autoclave process, provided that suitable thermal storage and control strategies are implemented. The investigated optimizations resulted in meaningful COP improvements, with differences of approximately 0.11–0.18 between the least and most favourable settings for the individual parameters. The results therefore confirm that digital-twin based analysis can be an effective tool for identifying suitable setpoints and storage configurations for industrial heat pump systems exposed to variable loads.

Some limitations remain. Pump power was not included in the analysis, and this may affect the optimal source-water temperature glide in practice. In addition, the selected refrigerant and operating temperatures led to very low suction pressures and high pressure ratios at certain points in the cycle, which may require design adjustments such as an alternative refrigerant or two-stage compression.

Nevertheless, the overall system concept was shown to be technically feasible, and the analysis provides useful guidance for improving the operation of heat pumps in cyclic industrial processes.

Funded by the European Union

Views and opinions expressed are however those of the author(s) only and do not necessarily reflect those of the European Union or CINEA. Neither the European Union nor the granting authority can be held responsible for them.

4. CASE 3 – SPILLING & DLR

4.1 Case description

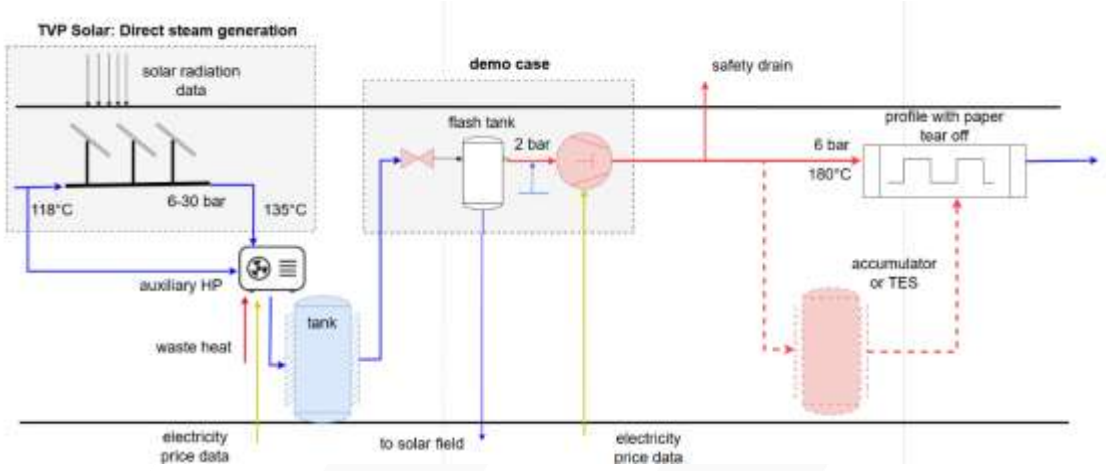


Figure 4.1 Layout of the use case: The demo case is combined with solar thermal for direct steam generation

Demo case 3 is a mechanical vapor compression (MVR) heat pump producing steam for paper drying. Steam is condensed in drying cylinders, transferring heat to the paper material on the outside. For this process, 180 °C steam at 6 bar pressure is required. The condensate is flashed to 2 bar and saturated steam is led to the piston compressor provided by Spilling. With a pressure ratio of 3, the steam is compressed to the required level while condensate injection is used to control the outlet temperature. This demo case is combined with a direct steam generation concept using solar thermal as suggested by TVP Solar. Weather data from the demo location in Czech Republic are used to produce hot pressured water at 135 °C that is flashed to 2 bar to match the demo case. Condensate is returned to the solar field where the mass flow is controlled to achieve the target temperature. If there is not enough solar energy, the auxiliary heating system is activated to ensure that the steam supply is available at all times. This represents a conceptual study matching direct steam generation with the demos case. It must be noted, that the solar field is operating at rather high temperature with regard to the solar radiation at the present location. Alternative concepts are discussed that integrate solar thermal with heat pumps. Figure 4.1 shows the layout of the adapted demo case: Data for a whole year simulation with fluctuating availability of solar thermal depending on time of day and seasonal weather is used. To compensate for these fluctuations, a storage tank is applied together with a heat pump that provides hot water in periods with low availability of solar energy. This

Funded by the European Union

Views and opinions expressed are however those of the author(s) only and do not necessarily reflect those of the European Union or CINEA. Neither the European Union nor the granting authority can be held responsible for them.

auxiliary heat pump utilizes waste heat, which is the humid air from the drying cylinders with a temperature of 70-80 °C. A steam accumulator can potentially be applied to further adapt to variable loads, weather effects or prices. In this study, a configuration without the steam accumulator is used as a proof of concept to use detailed dynamic models for dynamic set point optimizations.

4.2 Variable load description

Paper drying using steam networks usually doesn't invoke a wide range of load requirements for the steam compressor. Paper tear-off represents events where the drying process is interrupted and the steam demand of the paper machine is drastically reduced instantaneously. In the present case study, this is considered using a load profile of the steam demand.

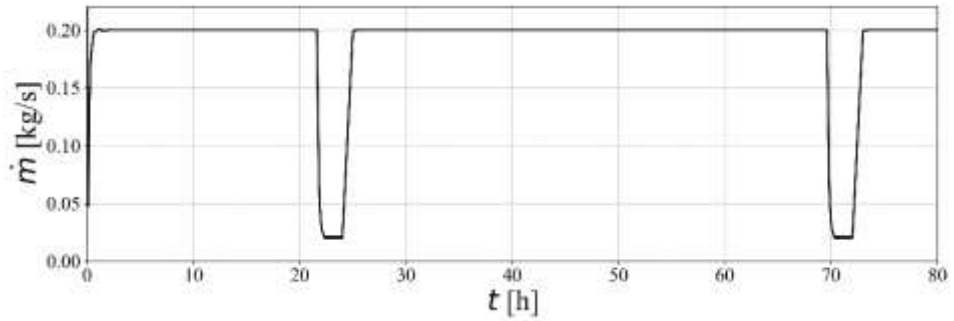


Figure 4.2 Paper tear-off events in steam demand profile

Figure 4.2 shows these events with tear-off appearing multiple times a week while lasting for several hours. In these periods, a safety control strategy is used that interrupts steam production: Pressurized water from solar thermal is stored while the steam compressor is shut down and run at low rotational speeds. A safety draining valve is used to release surplus steam. The compressor is rapidly ramped up when production is starting again. The start-up strategy was studied in (Gollasch, et al., 2025) with the result that the MVR system can be safely ramped up in a time span of approximately 10 minutes.

Funded by the European Union

Views and opinions expressed are however those of the author(s) only and do not necessarily reflect those of the European Union or CINEA. Neither the European Union nor the granting authority can be held responsible for them.

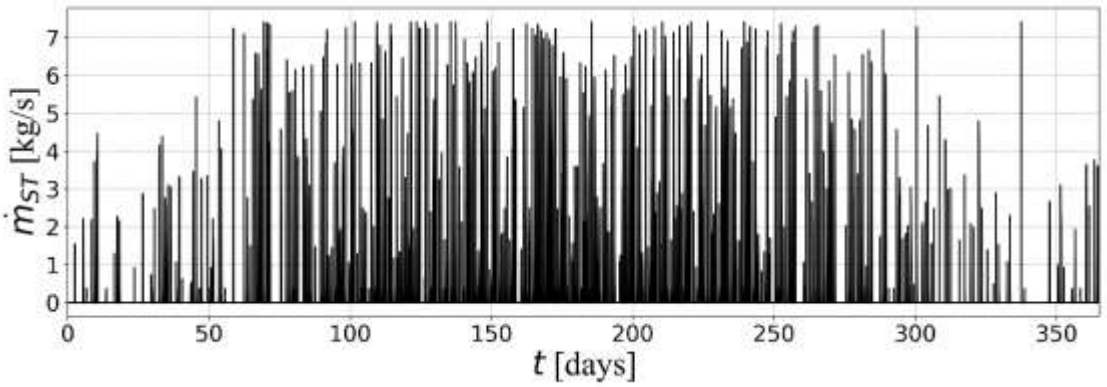


Figure 4.3 Mass flow rates from solar field throughout the year.

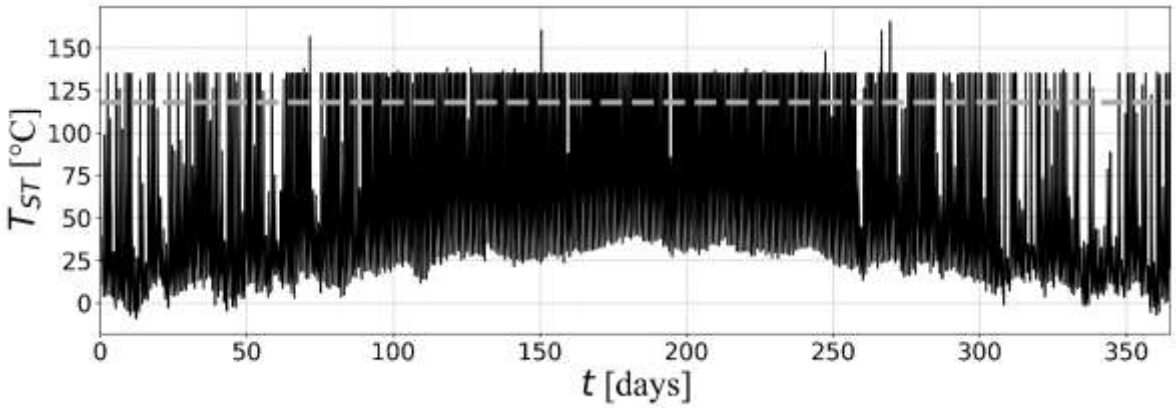


Figure 4.4 Temperature yield from solar thermal.

Another aspect of part load operation in this study is weather effects and variable waste heat availability. The seasonal and weather effects can be seen in Figure 4.3 and Figure 4.4. Because of the demo location, solar energy is only high enough during summer months to directly produce steam at the 2 bar pressure level. In cases where the solar field cools down the return flow ($T_{ST} < 118°C$), the supply flow is switched off. In Figure 4.5 this occurs in winter months and only low output from the solar plant is achieved with gaps in mass flow supply.

Funded by the European Union

Views and opinions expressed are however those of the author(s) only and do not necessarily reflect those of the European Union or CINEA. Neither the European Union nor the granting authority can be held responsible for them.

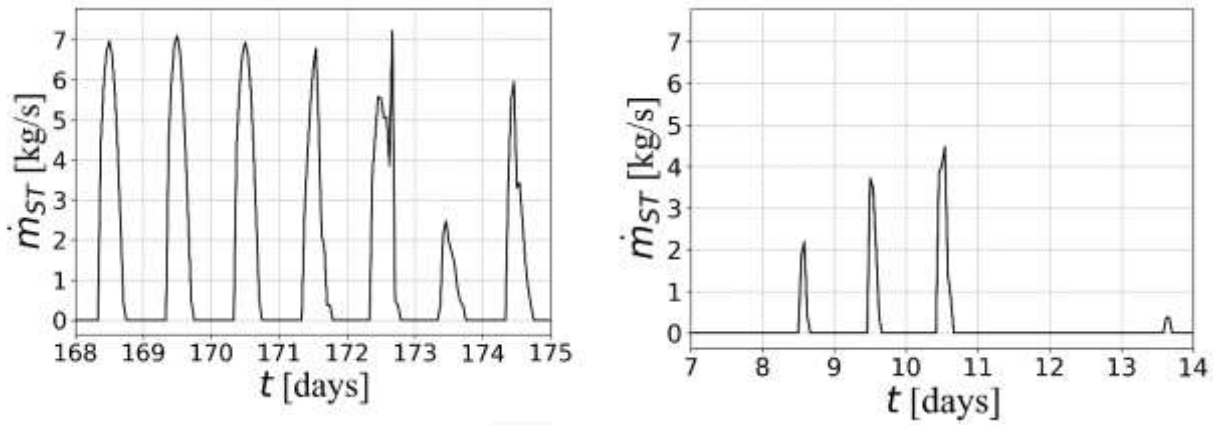


Figure 4.5 Comparison of solar thermal output for a week in summer (left) and in winter (right)

As a consequence, a week during summer was chosen with daily yield from the solar thermal plant, which is highlighted in Figure 4.6. During winter, there is a very low thermal output with the present concept.

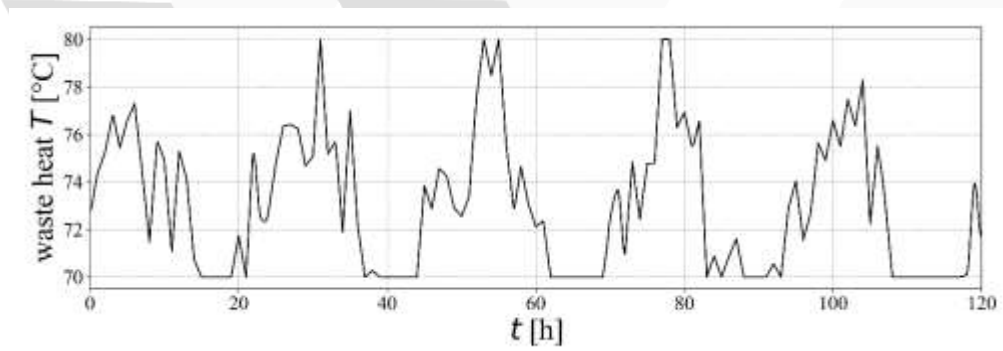


Figure 4.6 Waste heat profile with assumed stochastic fluctuations

The system also has to adapt to a varying profile of waste heat, which fluctuates between 70 °C and 80 °C. This can be caused by process loads, ambient temperatures and heat losses. The auxiliary heat pump needs to be operated in part load to adapt to the temperatures, which enables additional potential for dynamic set-point optimization. The operation of the use case is optimized for minimal operating costs based on an energy price profile. The hot water storage needs to be controlled to store energy in periods of high waste heat and solar energy.

Funded by the European Union

Views and opinions expressed are however those of the author(s) only and do not necessarily reflect those of the European Union or CINEA. Neither the European Union nor the granting authority can be held responsible for them.

4.3 Heat pump integration

The operating conditions of the solar thermal plant are matched with the demo case. This means, instead of receiving saturated steam from flashing condensate of the drying cylinders, the steam is delivered by the solar thermal field. The innovative compressor design of the demo can be directly used in this way. The use case was developed with the purpose to combine the direct steam generation of solar thermal with the MVR system. Other integration concepts would invoke a large disruption to the demo concept, its design and operating conditions. The integration concept is therefore not necessarily the most efficient but represents a case study with the focus on the operational optimization of such a system using a detailed dynamic model.

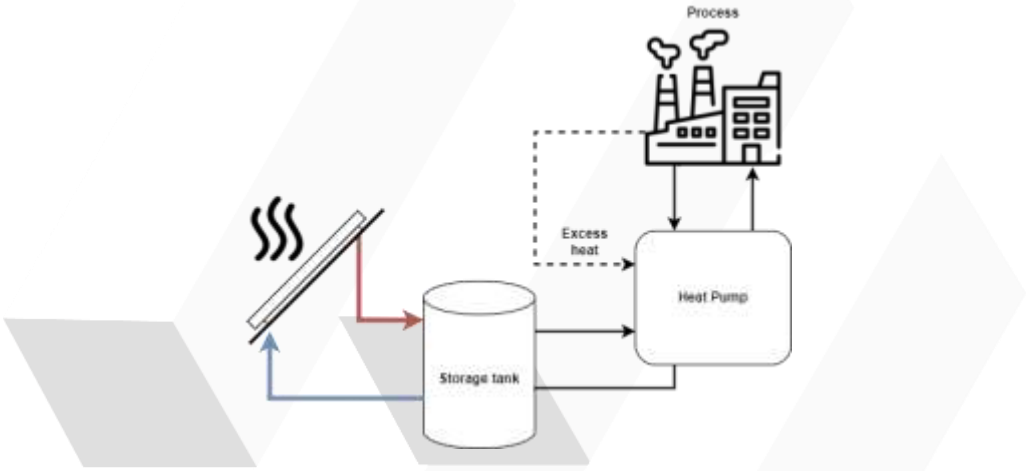


Figure 4.7 Integration concept using solar thermal as the heat source

An alternative integration concept would be to use solar thermal as a heat source. This allows to operate the solar plant at lower temperatures with higher yield in regions of northern Europe. Together with a storage tank and additional waste heat, a heat pump can be integrated to provide process heat. The transfer of this concept is discussed in Section 4.6 but not directly investigated in this work, as it would require compressor designs far off from the demo case.

Funded by the European Union

Views and opinions expressed are however those of the author(s) only and do not necessarily reflect those of the European Union or CINEA. Neither the European Union nor the granting authority can be held responsible for them.

4.4 Methodology and goals

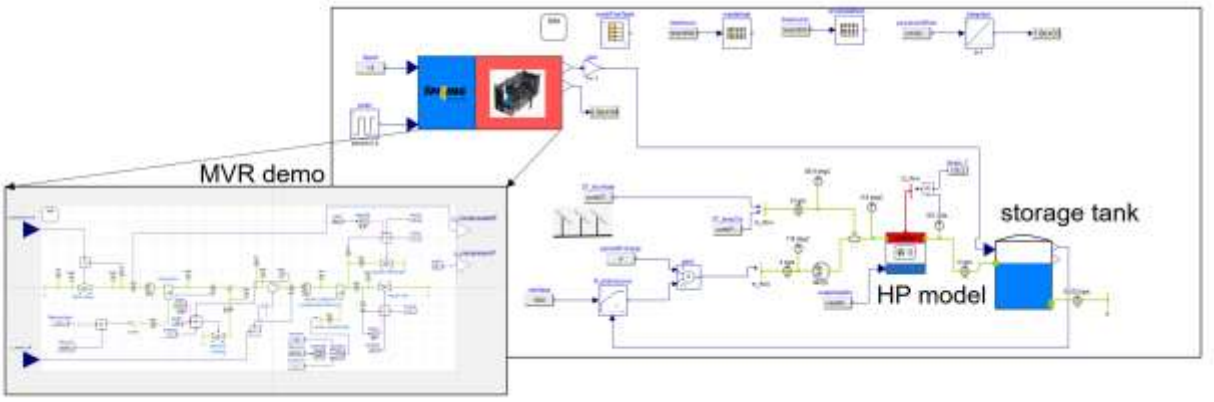


Figure 4.8 Dynamic model of MVR demo and integration with solar thermal, storage tank and auxiliary heat pump

Figure 4.8 shows the model, which consists of the demo case model embedded with solar thermal data, an auxiliary HP and the storage tank. The MVR demo is using TIL (Modelica library for thermal system simulation) classes that are extended for part load and heat transfer effects as described in (Gollasch, et al., 2025).

The heat pump is a reduced order model based on the Carnot efficiency:

$$\eta_{Carnot} = \frac{COP_r}{COP_{id.}} = 0.5$$

$$COP_{id.} = \frac{T_H}{T_H - T_C} \qquad COP_r = \frac{\dot{Q}}{P_{el}}$$

The Carnot efficiency is set to a constant value of 50%. With that assumption, the real COP_r can be computed based on the heat pumps sink and source temperatures. As a last step, the electric energy to drive the compressor can be calculated. This generic heat pump model is suitable for the present case because it represents a study focused on demonstrating the dynamic set point optimizations with transient models.

$$\frac{d\,m_{mix}}{dt} = \dot{m}_{in} + \dot{m}_{out} \text{ with } m_{mix,0} = 1000kg$$

$$\frac{dT_{mix}}{dt} = \dot{m}_{in}\frac{T_{in}-T_{mix}}{m_{mix}+0.001} \text{ for } m_{mix} > 0$$

Funded by the European Union

Views and opinions expressed are however those of the author(s) only and do not necessarily reflect those of the European Union or CINEA. Neither the European Union nor the granting authority can be held responsible for them.

The storage model is set up with a new class using TIL fluid ports and energy and mass balances. In this way, the liquid mass stored in the tank is computed as well as the mixing temperature based on the energy balance. When solar thermal delivers a surplus of mass flow relative to the demand, the excess flow is directed to the tank. If the tank is emptied to a threshold value, a control logic is applied to keep the tank at this level. For this, a PI controller activates the auxiliary HP to ensure a constant supply temperature of 135 °C and heats up additional water in periods where the storage level is low.

The solar thermal data is integrated using table interpolation with spline smoothing. The input signal $\boldsymbol{u}(t)$ represents a set of decision variables for the optimizer regarding whether the tank is charged or discharged. The signal is updated every hour and steps are smoothed using first order filters. The set point optimizations are performed for different time horizons ranging from 24 h to 5 days. The CPU-time to evaluate the model ranges from 6 seconds for 24 h to >20 s for five days. Applied PI controllers have been tuned and the number of events was reduced in order to decrease computational effort and model stiffness.

$$min\, C(\boldsymbol{u}(t)) = \int_{t_0}^{5d} c(\boldsymbol{x}(t),\, \boldsymbol{u}(t), t)dt$$

$$s.t. V_l(\boldsymbol{x}(t),\, \boldsymbol{u}(t), t) \leq V_{t,\,max}$$

The general formulation of the optimization problem is based on minimizing the operational costs C resulting from the inputs $\boldsymbol{u}(t)$ and system states $\boldsymbol{x}(t)$. A single input is chosen as the optimization variables: $\boldsymbol{u}(t) = \dot{\boldsymbol{m}}_{\boldsymbol{ch.}}(t)$. With this input the optimizer can decide whether to charge or discharge the storage tank. The maximum allowable stored liquid volume V_l can be formulated as a constraint to consider storage tank sizing. The optimizer defines a time series of set points that are cost optimal based on input data like the load profile, solar radiation, energy prices and waste heat availability. Optimizations are performed using a functional mockup unit (FMU) and optimizers in Python. This concept represents a black-box optimization problem where the optimizer has no access to the model equations. As the evaluation of detailed transient models can be time consuming, two optimization approaches are considered: First, a combined approach between differential evolution and a gradient based local optimization (SLSQP) is applied. Both algorithms are imported from the scipy.minimize library. Differential evolution as a global approach is executed for a small number of generations to find feasible start values for the gradient based local solver SLSQP. The gradients are computed using finite differences requiring n+1 function evaluations

Funded by the European Union

Views and opinions expressed are however those of the author(s) only and do not necessarily reflect those of the European Union or CINEA. Neither the European Union nor the granting authority can be held responsible for them.

depending on the dimensions of $\boldsymbol{u}(t) \in R^n$. For large time horizons, gradient based methods become computationally expensive. For this reason, a surrogate assisted Bayesian optimization (BO) is comparatively investigated as a second approach. This represents an efficient global method based on exploring surrogate models that approximate the objective function. These surrogates are explored using acquisition functions that are based on compromises between improvement of the objective and exploration of regions with high uncertainty. Gaussian process regression (GPR) from the scikit-learn library is used as the surrogate method here.

In addition to the algorithm to solve the optimization problem, the problem statement is of major importance. The decision variable is set up in a robust way, so that it is avoided that the model runs into infeasible states. Additionally, dimensionality reduction is performed. The input variables of the optimizer are set every 6 hours and Akima spline interpolation calculates the actual hourly model inputs. This reduction was chosen based on the input frequencies of the solar thermal output, which has the highest impact on the decision making.

The optimization studies are performed with the following focus:

1. Investigation of the performance of dynamic set point optimizations with detailed transient models (digital-twins)
2. Identification of suitable black-box optimization approaches using Python and evaluation of computational effort
3. Discussion of potential applications for transient digital twins in the field of optimization
4. Analysis of the application of direct steam generation with solar thermal in comparison with alternative integration concepts.

As a last step, the set point of the pressure level of the flash tank is varied in order to investigate its impact. Reducing the flash pressure means, that less pressured hot water is required but also invokes higher pressure ratios in the steam compressor.

4.5 Results

In a baseline approach, a simple control logic is applied that ensures sufficient supply of hot water to be flashed, depending on the demand of saturated steam. The compressor speed is set with a PI controller to meet the required mass flow based on the load profile. Condensate injection is controlled to reduce the temperature at the compressor outlet to a setpoint of 180 °C. As the yield from the solar thermal plant is

Funded by the European Union

Views and opinions expressed are however those of the author(s) only and do not necessarily reflect those of the European Union or CINEA. Neither the European Union nor the granting authority can be held responsible for them.

dependent on solar radiation, there are fluctuations depending on time of day and weather conditions.

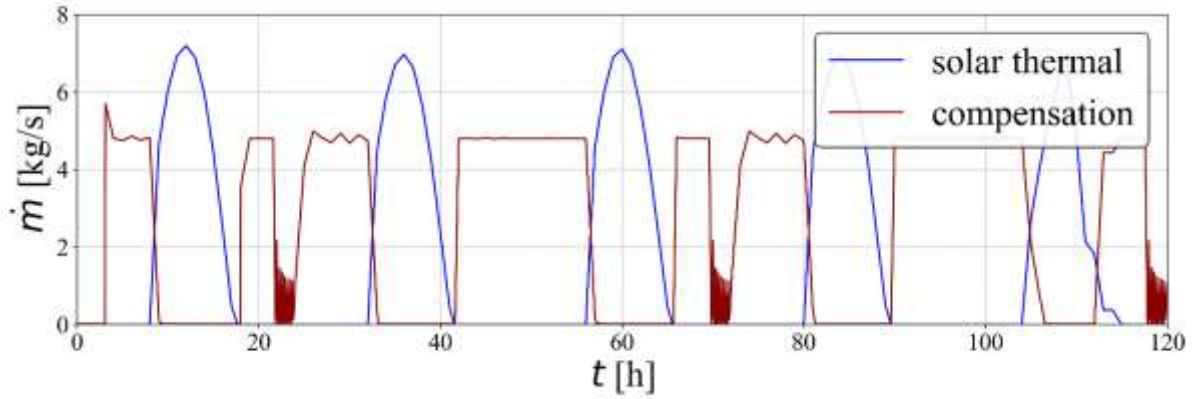


Figure 4.9 Mass flow rates with baseline control logic.

Figure 4.9 shows the periodic mass flow delivered by solar thermal. In periods with low availability, the auxiliary system is activated for compensation to ensure safe supply. Surplus water is stored in the tank.

Figure 4.10 shows the driving power of the auxiliary HP. When the solar thermal plant provides sufficient mass flows and temperatures, the HP is deactivated. It is adapting its operating point to always reach a delivery temperature of 135 °C. The fluctuations are caused by variable temperatures of the solar thermal mass flow as well as the variable waste heat profile and paper tear-off events.

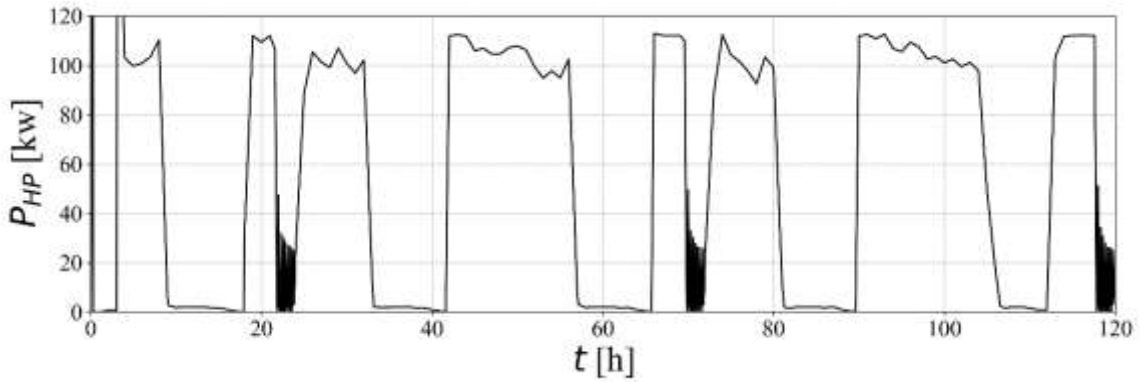


Figure 4.10 Auxiliary HP drive power in baseline operation.

Funded by the European Union

Views and opinions expressed are however those of the author(s) only and do not necessarily reflect those of the European Union or CINEA. Neither the European Union nor the granting authority can be held responsible for them.

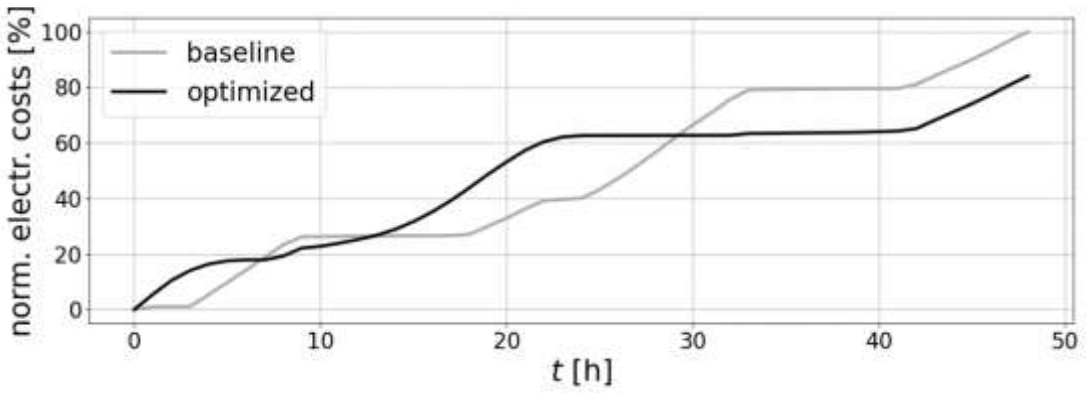


Figure 4.11 Accumulated operational costs for a 48h horizon.

The optimization result is a series of set points setting the auxiliary mass flow to charge or discharge the storage tank. The accumulated costs in Figure 4.11 are the integrated value of overall energy costs for the time horizon of 48 h. The costs consist of the electric energy to drive the steam compressor as well as the energy to drive the auxiliary heat pump. The gray line represents the baseline control logic. Comparing the black line of optimized spendings shows that there are savings of 16 % at the final time.

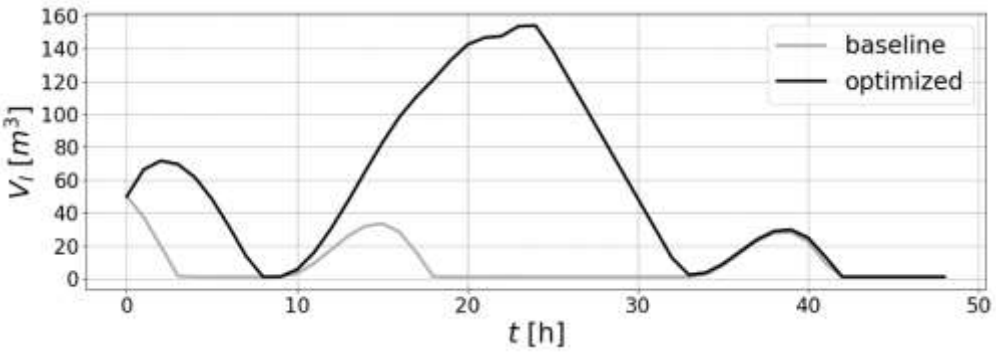


Figure 4.12 Storage operation in a 48h horizon

The savings result from the storage operation, which is charged in a period with low energy prices and discharged in the following hours to avoid high spendings with increased prices. The baseline control logic does not adapt to prices and ensures safe supply only. As a consequence, only the surplus mass flow from the solar plant is stored. In the last third of the considered time horizon, these setpoints are not changed by the optimizer. This can be explained with the fact, that at these times there is high output from the solar thermal plant and there is no need to activate the auxiliary heating system. It can be concluded, that investing in a larger storage and using price-adaptive control logic shows the potential to increase the economic

Funded by the European Union

Views and opinions expressed are however those of the author(s) only and do not necessarily reflect those of the European Union or CINEA. Neither the European Union nor the granting authority can be held responsible for them.

performance of such concepts. The optimization problem with a single control variable $\boldsymbol{u}(t)$ is of simple nature to investigate the potential of using detailed digital twins for black box optimizations. The analysis of the results indicates, that the approach is feasible and very similar results are produced in repeated runs. The results of all performed optimizations are summarized in Table 4.1. Three time horizons (24 h, 48 h and 5 days) are optimized with gradient based local optimization (SLSQP) and global surrogate assisted Bayesian optimization (BO). The relative savings $\boldsymbol{C^*/C_{base}}$ compared to the baseline results are analyzed as well as the CPU time and the number of required function evaluations. For all cases, the operating costs can be reduced [10, 16] % with minor deviations between the optimization algorithms. This indicates that the globally initialized local solver does not tend to converge into local minima, which would require multi-start approaches. The gradients need to be computed for each input variable in each iteration step, which can lead to high computational effort in dynamic optimization problems with high dimensions. In this work, the control trajectory is approximated using Akima spline interpolation. Based on the frequency of the fluctuation inputs, the optimizer sets a spline sample every six hours. The model is evaluated with updated inputs every hour that are interpolated from the spline. This results in only 4 optimization variables for the 24 h case and both optimization approaches require a moderate number of function evaluations. The evaluation time of the model for 24 h real time is 5-7 s, which results in a low CPU time of only five minutes for SLSQP. With larger time horizons, the number of variables increases as well as the model evaluation time. As a consequence, the optimization of a 5 day horizon with SLSQP is already very time consuming and lasts 45 min. in a single core setup. For high model effort and a moderate number of variables (e.g. < 100) BO might be beneficial as it produces similar results with a lower number of function evaluations. The CPU time can be reduced to 30 min. As a downside, BO requires surrogate training for each iteration and evaluation of the acquisition function, which is the optimization of expected improvement in the present case. This results in additional CPU effort but can be advantageous for models with high computational costs. In summary, it can be stated that the detailed transient model can be optimized with real time capability specifically for time horizons < 48 h.

It is assumed that the return flow of hot water after flashing is directly led to the solar plant to be heated up again. As an exemplary study, the flash pressure is varied, which has significant impact on the required hot water flow rate as well as the steam compressors pressure ratio. The effect on the return temperature of separated water to the solar field is not considered, as solar thermal evaluation is based on external data and remains unchanged. The exemplary results highlight the high sensitivity of the flash pressure set point.

Funded by the European Union

Views and opinions expressed are however those of the author(s) only and do not necessarily reflect those of the European Union or CINEA. Neither the European Union nor the granting authority can be held responsible for them.

Table 4.1 – Optimizations

time horizon	algorithm	C^*/C_{base}	CPU time	evaluations
24h	SLSQP	90.4%	5 min.	45
48h	SLSQP	85%	15 min.	85
5d	SLSQP	84%	45 min.	205
24h	BO	90.4%	9 min.	62
48h	BO	85.2%	17 min.	74
5d	BO	86.5%	30 min.	86

Figure 4.13 shows the costs with the 2.2 bar pressure level and baseline control logic (gray line) in comparison to 1.5 bar pressure and optimized control. Lowering the flash pressure set-point means that a higher steam fraction is achieved. Consequently, the auxiliary system needs to deliver lower flow rates which saves energy (Figure 4.14). In a trade-off, the pressure ratio of the steam compressor is increased. It can be concluded, that this set-point is of major importance for design as it impacts the temperature level of solar thermal, sizing of the storage tank and the auxiliary system as well as the design of the steam compressor.

Funded by the European Union

Views and opinions expressed are however those of the author(s) only and do not necessarily reflect those of the European Union or CINEA. Neither the European Union nor the granting authority can be held responsible for them.

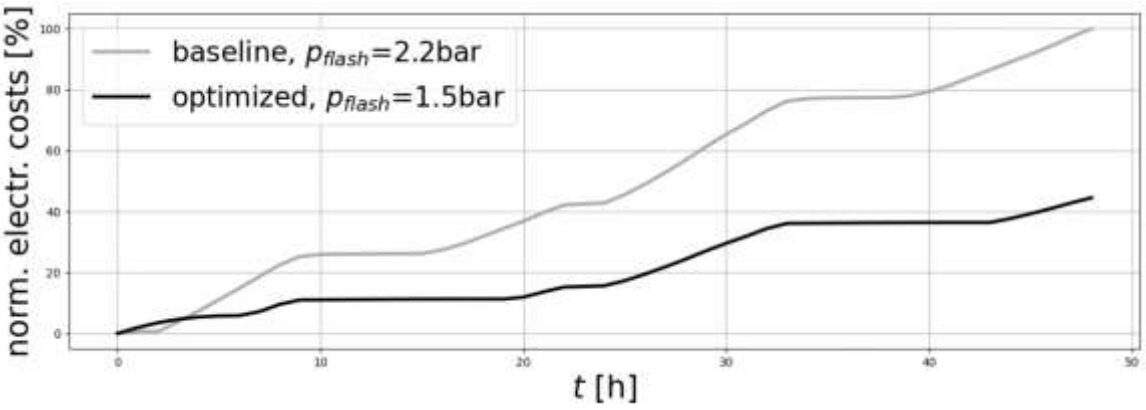


Figure 4.13 Accumulated costs with impact of flash pressure set-point.

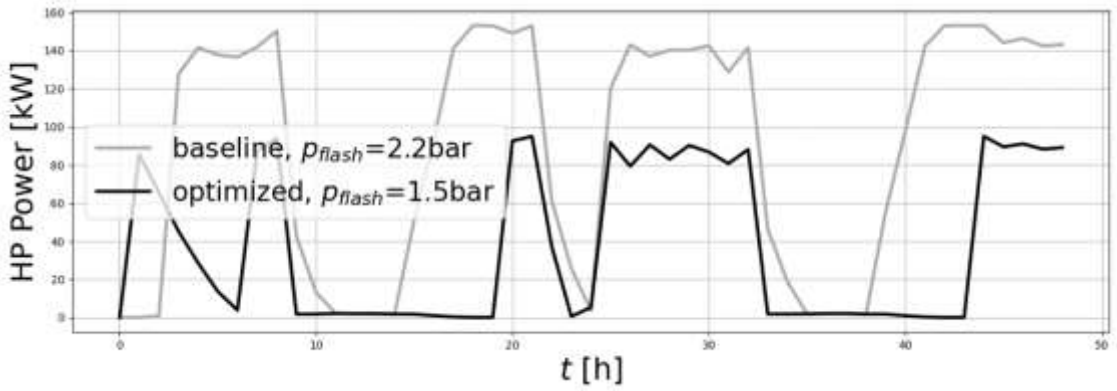


Figure 4.14 Auxiliary HP driving power impacted by flash pressure set-point.

4.6 Discussion

The results indicate that detailed transient models are suitable for dynamic set point optimization enabling the full potential of heat pumps by evaluating the performance in full system context with other utility. It has to be mentioned, that the present case study delivers exemplary results for a use case combining solar thermal with the demo case steam compressor. A detailed investigation of integration concept, system design and optimized operational strategy for specific locations is required. After system layouts are defined in conceptual design phases, more detailed transient digital twins can be used to study its operation and set points. The modelling approach can be improved as the present study is based on externally performed evaluations of the solar thermal plant. The solar field is matched to the demo use case and the designs and component sizes are not optimized. The operating temperatures of the solar plant are directly dependent on the pressure level of saturated steam at the steam

Funded by the European Union

Views and opinions expressed are however those of the author(s) only and do not necessarily reflect those of the European Union or CINEA. Neither the European Union nor the granting authority can be held responsible for them.

compressor inlet, which is why solar thermal simulation should be integrated in the model. Additionally, the modelling depths of the heat pump or storages can be increased.

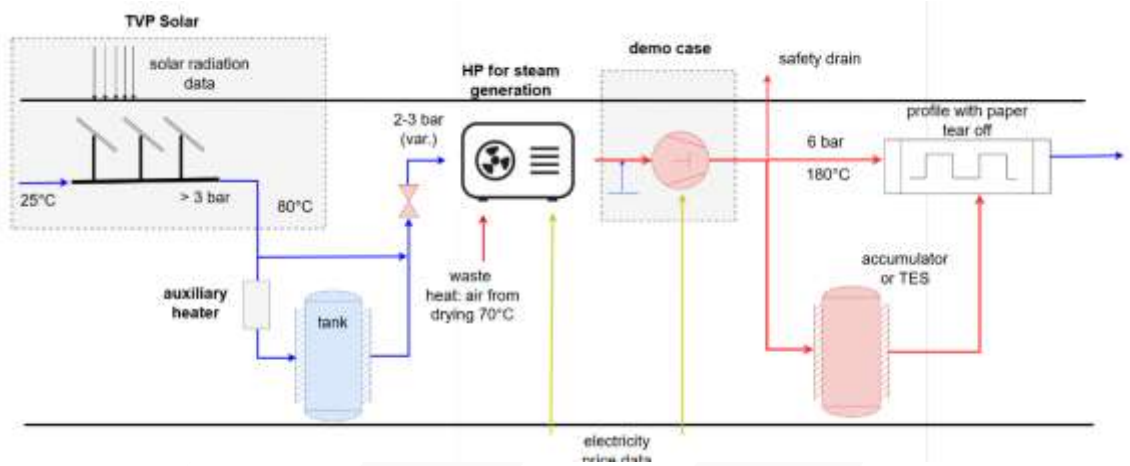


Figure 4.15 System layout using solar thermal as heat source for a steam generating heat pump with an additional compressor stage.

An alternative integration concept and its system layout is shown in Figure 4.15. Solar thermal operates at lower temperatures providing hot water to be used as heat source in a steam generating heat pump. This overcomes two shortcomings: The yield from solar thermal will increase for locations with lower solar radiation and for winter months. Secondly, using ST as the heat source does not require flashing and the steam output can be significantly increased with a heat pump in permanent operation. An additional steam compressor stage can be used to set the target pressure, similar to a scaled-up version of the demo compressor. Comparative studies of the integration concept together with system design show potential for further research. As the investigation of the flash pressure set point has shown, a combined design strategy that also considers the operation is required. There are strong interactions between sizing of the solar plant, the storage tank, the heat pump as well as the design point of the steam compressor. The results of the study underline, that optimized operation can significantly decrease operating costs. A further application of digital twins could be in early phases of design to improve decision making.

Black box optimizations for a time series of set points are straightforward to implement using FMUs in Python but cannot be solved as efficiently compared to white box approaches with direct access to the equations. This means, there are many options to perform complex optimizations with digital twins with a high potential for

Funded by the European Union

Views and opinions expressed are however those of the author(s) only and do not necessarily reflect those of the European Union or CINEA. Neither the European Union nor the granting authority can be held responsible for them.

research. Well-posed Modelica models as well as the problem statement together with the optimization approach are crucial challenges for the functionality of the optimizations. Also, model reduction (or decomposition) and dimensionality reduction techniques are important, as indicated with the applied spline trajectories in this study. Concerning optimal control, there a various alternatives compared to the present study of black-box dynamic optimizations. As an example, optimizations could be used for training of controller logics instead, which would enable real time capability even if very fast response times are required.

4.7 Conclusion

The present study shows that by embedding the detailed transient model into a black-box optimization framework, a 10–16 % reduction in operating costs is achieved compared to a baseline control logic. This mainly results from price- and state-adaptive storage charging and discharge. Furthermore, the optimization reveals a strong dependency between flash pressure set points and the energy consumption of the auxiliary system. The results highlight the strong interactions between the solar thermal plant design, storage sizing and heat pump configurations as well as operational strategy. Overall, it can be shown, that the ST-HP system shows high load flexibility when combined with storages. The results indicate the feasibility of dynamic set-point optimization with black-box optimization approaches using detailed dynamic models. Potentials and challenges for future research are identified. The integration concept as well as the design strategy are crucial decisions to enable the full potential of ST-HP supply systems and further investigations are required in both fields.

Funded by the European Union

Views and opinions expressed are however those of the author(s) only and do not necessarily reflect those of the European Union or CINEA. Neither the European Union nor the granting authority can be held responsible for them.

5. CONCLUSION

This deliverable investigated the use of digital-twin based setpoint optimization for industrial heat pump systems operating under variable source and sink conditions. Three different case studies were analysed, covering batch-wise laminate production, autoclave sterilization, and steam generation for paper drying combined with solar thermal energy. Across the three cases, dynamic simulation models were used to evaluate how heat pump operation, storage behaviour, auxiliary systems, and control setpoints interact under realistic transient operating conditions. The results demonstrate that digital twins are valuable tools for identifying improved control strategies, quantifying performance benefits, and assessing the robustness of industrial heat pump concepts before implementation.

In Case 1, the Mayekawa/TNO cascade heat pump originally designed for shrimp processing was integrated into a high-pressure laminate production process with strongly intermittent hot and cold water flows. The existing digital twin was adapted by modifying the source and sink heat exchangers and by adding stratified hot and cold buffer tanks. The baseline control strategy proved sufficiently robust and operated without trips, achieving an overall COP of 1.54. Based on the simulation results, the ammonia evaporator water outlet temperature and ammonia condenser pressure were identified as the key optimization parameters. A parameter sweep of 38 variants showed that the COP could be increased to 1.84, corresponding to a 19 % improvement compared to the baseline. Alternatively, when optimizing for useful heat delivery, the heat supplied from the hot buffer storage increased by 0.21 GJ per batch, corresponding to a 13 % improvement, while the COP still increased to 1.70. The case demonstrated that even a heat pump designed for another application can be successfully assessed and optimized for a new variable-load process using a digital twin.

In Case 2, the GEA/DTI study considered a heat pump supplying an autoclave process with a cyclic heating, holding, and cooling profile. The system used a steam accumulator on the sink side and a stratified hot water tank on the source side to manage the mismatch between heat demand and heat availability. Due to the computational time of the dynamic model, the optimization was carried out through parameter sweeps. Three main parameters were investigated: steam accumulator size and pressure setpoint, evaporator source-water temperature glide, and cooling-water return bypass temperature. The results showed that larger steam accumulators allowed lower pressure setpoints and improved performance, with the 70 m³ accumulator reaching a COP of 2.51 compared to 2.33 for the 40 m³ case. For the evaporator source-water loop,

Funded by the European Union

Views and opinions expressed are however those of the author(s) only and do not necessarily reflect those of the European Union or CINEA. Neither the European Union nor the granting authority can be held responsible for them.

low temperature glide setpoints of 2.5–5 K gave the best COP, although practical pump energy considerations should be included in future work. For the return-water bypass, a 60 °C setpoint gave the best performance, showing that the temperature level at which recovered heat is stored is as important as the quantity of heat recovered. Overall, the study confirmed that suitable storage and control strategies allow heat pumps to operate effectively in highly cyclic industrial processes.

In Case 3, the Spilling/DLR study investigated an MVR steam compressor system combined with solar thermal direct steam generation, a hot water storage tank, and an auxiliary heat pump. The system was exposed to variable solar availability, fluctuating waste heat temperatures, paper tear-off events, and dynamic electricity prices. A detailed transient Modelica model was exported as an FMU and optimized in Python using black-box optimization approaches. Both a globally initialized SLSQP method and Bayesian optimization were tested for time horizons ranging from 24 hours to 5 days. The optimized control strategies reduced operating costs by approximately 10–16 % compared to the baseline control logic, mainly by charging and discharging the storage tank according to electricity prices, solar availability, and system state. The study also showed that the flash pressure setpoint has a strong influence on auxiliary heat pump demand and steam compressor operation. This highlights that operational optimization and system design are strongly coupled, particularly in hybrid solar thermal and heat pump systems.

Across all three cases, the work confirms that digital-twin based optimization can provide significant benefits for industrial heat pump systems under variable operating conditions. The main improvements were obtained by identifying the most influential setpoints, evaluating their effect through dynamic simulations, and adapting control strategies to the specific interaction between heat pump, process load, and thermal storage. The studies also show that thermal storage is a key enabler for flexible operation, allowing heat pumps to decouple heat production from process demand and to exploit favourable operating conditions such as higher source temperatures, lower sink temperatures, available solar energy, or lower electricity prices.

The results further show that the most suitable optimization method depends on model complexity, simulation time, and the number of decision variables. Parameter sweeps were effective for cases with a limited number of setpoints and relatively expensive simulations. For dynamic operational optimization over longer time horizons, black-box optimization using FMUs and Python was shown to be feasible, especially when combined with dimensionality reduction techniques such as spline-based

Funded by the European Union

Views and opinions expressed are however those of the author(s) only and do not necessarily reflect those of the European Union or CINEA. Neither the European Union nor the granting authority can be held responsible for them.

control trajectories. However, computational cost remains an important limitation, particularly for high-dimensional optimization problems or very detailed transient models.

In conclusion, the three case studies demonstrate that digital twins can be used effectively to analyse, optimize, and de-risk industrial heat pump operation under variable loads. The achieved improvements in COP, useful heat delivery, and operating costs show that optimized control strategies can unlock substantial performance gains without necessarily requiring major hardware changes. Digital-twin based set-point optimization therefore represents a promising approach for improving the efficiency, flexibility, and economic viability of industrial heat pump systems in future decarbonized heat supply concepts.

Funded by the European Union

Views and opinions expressed are however those of the author(s) only and do not necessarily reflect those of the European Union or CINEA. Neither the European Union nor the granting authority can be held responsible for them.

6. REFERENCES

Gollasch, J. et al., 2025. Numerical investigation of a heat pump demonstrator for partial electrification of the steam supply for paper drying. *Applied Thermal Engineering.*

SWEP International AB, 2025. *SWEP SSP G8,* Landskrona, Sweden: SWEP International AB.

Trespa, 2023. *TRESPA METEON METALLICS AND FOCUS.* [Online] Available at: https://www.trespa.com/dam/jcr:5d965cb7-6762-49b4-96d6-46817f1b6163/139089_BROCHURE_Meteon_Metallics_Focus_UK_LR.pdf [Accessed 2025].

Funded by the European Union

Views and opinions expressed are however those of the author(s) only and do not necessarily reflect those of the European Union or CINEA. Neither the European Union nor the granting authority can be held responsible for them.